Abstract

A finite element based numerical method for the two-dimensional elliptic interface problems is presented. Due to presence of these interfaces the problem will contain discontinuities in the coefficients and singularities in the right hand side that are represented by delta functionals along the interface. As a result, the solution to the interface problem and its derivatives may have jump discontinuities. The introduced method is specifically designed to handle this features of the solution using non-body fitted grids, i.e. the grids are not aligned with the interfaces.

The main idea is to modify the standard basis function in the vicinity of the interface such that the jump conditions are well approximated. The resulting finite element space is, in general, non-conforming. The interface itself is represented by a set of Lagrangian markers together with a parametric description connecting them. To illustrate the abilities of the method, numerical tests are presented. For all the considered test problems, the introduced method has been shown to have super-linear or second order of convergence. Our approach is also compared with the standard finite element method.

Finally, the method is applied to the interface Stokes problem, where the interface represents an elastic stretched band immersed in fluid. Since we assume the fluid to be homogeneous, the Stokes equations are reduced to a sequence of three Poisson problems that are solved with our method. The numerical results agree well with those found in the literature.

ISBN 91-7178-292-3 • TRITA-NA-0545 • ISSN 0348-2952 • ISRN KTH/NA/R--05/45--SE

Acknowledgments

First of all I would like to thank my advisor, Prof. Björn Engquist, for his guidance and support through my research. His wide knowledge and intuition have always been a great source of inspiration and new ideas for me.

A very special thanks goes to Michael Hanke for providing invaluable help during all my time at NADA. His assistance, involvement and infinite patience made this thesis a reality and I deeply appreciate that. I also would like to express my gratitude to Prof. Jesper Oppelstrup. He has always given encouraging help and showed a never failing enthusiasm for my and everybody's work. Furthermore, I would like to thank Prof. Gunilla Kreiss for her encouragements and support, especially on the last stages of this thesis.

A big thanks to all my colleagues and friends, present and former, at NADA with whom I had a true privilege to work with. I have benefited greatly from all of you and I look forward to the continuation of my work at NADA.

I want to extend a warm thanks to my mother for helping me become who I am and for her constant support and encouragement over these years. Finally, I would like to thank my wife, Margarita, from the depths of my heart, for her never ending love, for her endless support in times of doubt and despair and for choosing to share her life with me.

Financial support has been provided by NADA and Royal Institute of Technology (excellenstjänst). All financial supporters are greatfully acknowledged.

Contents

Chapter 1

Introduction

Many important physical and industrial applications involve flows with very complicated structure that is characterized by free moving surfaces inside the fluid domain and by discontinuous or even singular material properties. Examples include composite materials, multi-phase flows, crystal growth, solidification and many others. This type of problems, which we refer to as interface problems, has attracted a lot of attention over the past years. These interface problems can be classified into the following categories:

- Free surface problems: These problems involve fluid interfaces with no separating material, just a contact discontinuity between different fluids. Examples of this kind of problems include bubbly flow, motion of vortex sheets with surface tension, multicomponent fluids with surface tension and generation of capillary waves on the free surface.

- Fluid-structure interaction and multiphase material: These interface problems concern the interactions between solid structures and fluid or the solid-solid interactions. Examples include acoustic media, gas/liquid storage tanks, pipeline systems and others.

- Material interface problems: For this kind of problems the interface represents a real material. The interaction between fluid and material interfaces creates rich and complex dynamics that is an interesting subject to many scientists and mathematicians.

In this thesis we will mainly study material interface problems. A good example of a two dimensional material interface problem is a thin elastic rubber band immersed in the fluid and moving along with it. Furthermore, this band can separate two immiscible fluids, that have different viscosity and density and thus experience a jump in a value across the band. One has also to account for singular forces, such as an elastic or surface tension forces, that act on the interface with strength that depends on the shape of the interface itself. Any numerical method designed for the material interface problem has to include an accurate description of the moving and deforming interface and has to account for the complex dynamics and the properties of the flow.

1.1 Problem Formulation

This work was motivated was by the need in the robust numerical method for the interface Stokes problem that models moving inner boundaries in the incompressible flow of a highly

viscous fluid. These equations are a limit case of Navier-Stokes equations where the Reynolds number tends to zero and both the convective and the inertial terms are dropped. We will concentrate on the two-dimensional problems in which the interface exerts a singular force on the fluid, e.g. elastic force or surface tension, across the interface. The interface is a surface of codimension one, that may represent a region separating different fluids or an elastic boundary immersed in the fluid. A good example is a closed curve that represent an elastic band immersed in a fluid for a two-dimensional problem.

Consider the two-dimensional Stokes equations

$$\begin{aligned} \nabla p &= \mu \Delta \mathbf{u} + \mathbf{F} \\ \nabla \cdot \mathbf{u} &= 0 \end{aligned} \tag{1.1}$$

where $\mathbf{u} = (u, v)$ is the velocity vector, p is the pressure and $\mathbf{F} = (F_1, F_2)$ is an external singular force exerted by the interface Γ and that can be written as

$$\mathbf{F}(\mathbf{x}) = \mathbf{f}(\mathbf{x}, t)\delta_\Gamma$$

where $\mathbf{f}(\mathbf{x}, t) = (f_1, f_2)$ is the force strength in this point and δ_Γ is a two-dimensional delta functional with the support along the interface Γ. This singular force is best viewed as a distribution whose action on any smooth test function $\psi(\mathbf{x})$ is

$$\big\langle F_i(\mathbf{x}), \psi(\mathbf{x}) \big\rangle = \int_\Omega f_i(\mathbf{x}, t)\delta_\Gamma \psi(\mathbf{x}) d\mathbf{x} = \int_{s_0}^{s_1} f_i(\mathbf{X}(s), t)\psi(\mathbf{X}(s))|\nabla \mathbf{X}(s)| ds$$

where $\mathbf{X}(s)$ is the location of the interface at time t with some parameterization s for $s_0 \le s \le s_1$. We also use the notation $\mathbf{x} = (x, y)$. A short review of the distributions is given in Chapter 3. Note that the evolution of the flow with time comes entirely from the time-dependence of the force $\mathbf{F}$. This is a reflection of the fact that there is no inertia in the system.

The velocity field $\mathbf{u}$ is continuous but has a jump in the first derivatives which is due to the singularity of the force terms. As it will be shown later the equation for pressure p involves divergence of $\mathbf{F}$ and hence a dipole source. As a result, pressure will be discontinuous along with its derivatives. For more details on the derivation of the jump conditions see Chapters 4 and 5.

In practice we eliminate the singular source from the right hand side of (1.1) and solve instead

$$\begin{aligned} \nabla p &= \mu \Delta \mathbf{u} \\ \nabla \cdot \mathbf{u} &= 0 \end{aligned} \tag{1.2}$$

with the specified jump conditions. We first define and apply our method for one and two-dimensional elliptic model problems that contain both singular source terms and discontinuous coefficients. Finally, we apply our method to an interface Stokes problem. As an example of the interface Stokes problem we consider the model problem introduced by Tu and Peskin [9], an elastic band immersed in a homogeneous fluid.

This model problem is a two-dimensional analog of an elastic balloon in a highly viscous homogeneous fluid. In equilibrium, an ideal balloon would take a spherical shape, with zero velocity everywhere, pressure jump across the elastic membrane and uniform pressure both inside and outside. The magnitude of this jump depends on how far the membrane is stretched from its resting configuration. In two space dimensions the analog is an elastic band which contains an incompressible fluid and is stretched to a diameter greater than its resting diameter. The equilibrium configuration is a circle with jump in pressure that balances the elastic force exerted by the stretched membrane. This is described in more detail in Chapter 5.

1.2 The Present Work

In this thesis, a new finite element based numerical method for the two-dimensional elliptic interface problems with the inner boundaries is presented. We show that the introduced method can handle well both the jumps in the coefficients that in general occur across the interface and the singular forces acting along the interface. The method has also been successfully applied to the incompressible Stokes equations with moving inner boundary.

Our method is based on the Immersed Interface Method (IIM) that was first introduced by LeVeque and Li in [31] as a second order accurate finite difference type method for solving elliptic equation whose solution is not smooth across the interface, due to discontinuous coefficients or singular source terms in the equation. The main idea of the original IIM was to incorporate the known jumps in the solution or its derivatives into the finite difference scheme, obtaining a scheme with the modified stencil whose solution is second order accurate at all points on the uniform Cartesian mesh even for arbitrary interfaces. This approach has been extended to parabolic and hyperbolic equations, and successfully applied to many applications, see Chapter 2 for a brief review. Most important for us are Li's papers [46] and [50] where he presented a finite element immersed interface method for one and two-dimensional elliptic problems involving discontinuities in the coefficients. As a consequence of the discontinuity in the coefficients, the solution to those problems is a continuous function that has a jump in the flux. To account for this discontinuity, Li proposed to construct specific basis functions such that the interface jump conditions for the solution and its flux are satisfied either exactly or approximately.

However, in the case of most general elliptic interface problem with both discontinuities in the coefficients and singularities in the source terms, i.e. delta functionals and its derivatives, the solution itself is discontinuous. Thus the original finite element IIM proposed by Li cannot be applied. To improve the capabilities of the method, we use the fact that the problems we are dealing with are linear and that we can always identify the source of the discontinuity in the solution or its derivative. Namely, presence of a delta functional in the right hand side causes the solution to have discontinuous derivatives, while a dipole is responsible for the jump in the solution itself. Having this in mind, we apply the superposition principle. That is, we break the original problem into a set of simpler problems, with the source term to each of the problems being either an L^2 function, a delta functional or a dipole. As a result, the corresponding solution will satisfy one of three alternatives: solution and its flux have homogeneous jumps, the solution itself is continuous while the flux is subject to a non-homogeneous jump condition and finally, the solution is discontinuous while the flux is continuous.

All information that is needed to evaluate the jump conditions is extracted from the position of the interface together with the equations itself. Using these explicitly known values of the jumps we can calculate the solutions to the simple problems and thus the solution to the original problem, see Chapter 4 for more details. The discretization of the method is based on a simple piecewise-linear polynomials on a uniformly triangulated domain. Note that the mesh is not aligned with the interfaces. Thus there is almost no cost for such grid generation, which is very significant for moving interface problems. This simple modification allows us to extend Li's approach to a much broader class of interface problems. Numerical results are presented, showing that the method is capable of second order convergence in L^2 and L^∞ norms.

The modified method has also been applied to the Stokes interface problem, modeling an elastic band immersed in the homogeneous fluid. We rewrite Stokes equations as a sequence of three Poisson problems, one for each variable. Namely, by applying the divergence operator to the momentum equations, adding them together and using the incompressibility

condition we get the Poisson equation for the pressure p. Once the pressure is known, the momentum equations become independent Poisson problems for u and v. Thus the techniques developed for the elliptic interface problems can be applied directly.

Since the flow is considered to be homogeneous, the jumps in the solution result only from the singularity of the source function, which represent an elastic force along the interface. This singular force leads to jumps in derivatives of u and v. The Poisson problem for pressure involves derivatives of this source term, and hence a dipole. As a result, the pressure will be discontinuous along with its derivatives. Similar to the model problems, the magnitude of the jump conditions is derived solely from the equations and the location of the interface, without a-priori knowledge of the solution.

The interface is described by a given set of discrete control points $\{\mathbf{X}_i(s,t)\}$, together with a parametric description connecting them. Time evolution of the interface is accomplished by moving these control points using an additional constraint that the interface must move with the fluid. The velocity $\mathbf{u}$ is continuous across the interface and the following differential equation is valid

$$\frac{\partial}{\partial t}\mathbf{X}(s,t) = \mathbf{u}(\mathbf{X}(s,t),t)$$

The velocities computed on a uniform Cartesian mesh by solving the interface Stokes problem (1.2) are interpolated to the marker positions, which are then moved with this velocity over a time step Δt. In practice one has to use an implicit or semi-implicit method in order to take reasonable time steps.

Our approach differs from that of Li in several ways. The fundamental difference is our treatment of the interface problem via the superposition principle. This improves the applicability of the method greatly by allowing to treat both singular source terms and discontinuous coefficients at the same time. There are other differences as well. Our derivation of the jump conditions is based on comparing the variational formulation obtained from the classical formulation of the problem with the one obtained from the distributional formulation. To our knowledge, it is also first time that finite element IIM was applied to interface Stokes problem.

1.3 Outline of the thesis

In Chapter 2, we review the existing methods for the interface problems. We also give some historical background on the Immersed Boundary (IBM) and Immersed Interface methods (IIM). Chapter 3 contains some basic notations from the distribution theory and definitions of some spaces that are important for us. In Chapter 4 we introduce our new finite element based immersed interface method and apply it to several one and two-dimensional model problems. Numerical results are presented and some conclusion are drawn. The next chapter contains the application of our method to the interface Stokes problem (Chapter 5). The derivation of the jump conditions is covered in both Chapter 4 and Chapter 5. Finally, we summarize current results and give an outlook for the future work.

Chapter 2

Existing numerical methods for the interface problems

In this chapter we review some of the existing numerical methods for interface problems and discuss in particular the immersed interface (IIM) method since it had inspired our work.

One of the main difficulties arising when dealing with interface problems is the fact that the solution itself is usually non-smooth or discontinuous across the moving inner boundaries. Due to this fact many classical numerical methods designed for smooth solutions perform poorly or do not work at all for interface problems. One has also to take care of the topological changes in the moving free surfaces. To summarize, a numerical scheme developed particularly for the interface problems should be able to handle the following:

- Discontinuity in the coefficients of the differential equation/system;
- Singularity of the source terms of differential equation/system (Dirac delta function as an example);
- One or several internal moving boundaries, with a changing topology.

There are two different approaches to the design of a method for interface problems. The first is to construct the methods on the body fitted grids. That is to solve the interface problem on the mesh that is aligned with the internal boundaries using some appropriate method (for example Galerkin finite element method with the standard linear basis functions [21], [42]). However, it is difficult and time consuming to generate this kind of body fitted grids. Such difficulties becomes even more severe for moving interface problems with topological changes.

Much effort has been put into the development of the alternative approach, where a fixed computational grid is used over the global spatial domain. This fixed grid typically does not align with any internal interfaces. The interfaces are then represented by some additional structure that is then continuously updated using some information from the background mesh.

Those numerical methods that follow the second approach can be further classified as interface tracking or an interface capturing methods. In interface tracking (examples include the immersed boundary method, the immersed interface method, the boundary integral method, the volume-of-fluid method and the front tracking method) the interfaces are then represented as codimension 1 surfaces moving relative to the fixed grid. In interface capturing methods, such as level-set and phase-field methods, the interface is implicitly represented by a contour of a particular scalar function, defined over the computational

domain. The evolution of the interface is governed by the level set PDE's discretized on fixed, uniform grids. Recently, a large number of hybrid methods that combine interface tracking and interface capturing methods together have appeared as well.

2.1 Interface tracking methods

The boundary integral method

The boundary integral method (BIM) is highly accurate for modeling interface problems with non-changing topologies. BIM was first introduced by Rosehead [26] to study vortex sheet roll-up. In this approach, the flow equations are mapped from the immiscible fluid domains to the sharp interfaces separating them thus reducing the dimension of the problem (the computational mesh discretizes only the interfaces). The flow solution is than deduced only from the information available on the interfaces.

This approach has been used for both inviscid and Stokes flows. A complete review of Stokes computations is given by Pozrikidis [6], and for computations of inviscid flows, see Hou [40]. For flows with both inertia and viscosity, surface integrals must be incorporated into the formulation.

The main advantage of the boundary integral method is the reduction of the problem by one dimension since the formulation involve quantities defined on the interface only. There is also a potential for highly accurate solutions if the flow doesn't have topological changes. In addition, highly efficient adaptive surface mesh refinement algorithms have recently been developed to improve the accuracy and the performance of the methods. On the other hand, the main disadvantage of the boundary integral method is the difficulty in modeling topological changes (such as merges or break-ups of the interfaces).

The volume-of-fluid method

The volume-of-fluid (VOF) method was first reported in Nichols and Hirt [5] and [10] (for a recent review see Scardovelli and Zaleski [36]). In this approach the location of the interface is determined by the volume fraction c_{ij} of fluid 1 in the computational cell Ω_{ij}, see Figure 2.1. The interface is contained in the cells where $0 < c_{ij} < 1$, fluid 1 if $c_{ij} = 1$ and fluid 2 if $c_{ij} = 0$.

Generally, the VOF algorithm consists of two parts: a reconstruction step and propagation step. A typical reconstruction step is a piecewise linear interface construction method (PLIC), where in every cell Ω_{ij} the true interface is approximated by a surface perpendicular to the interface normal vector n_{ij}. The normal vector n_{ij} is determined from the volume fraction gradient using data from neighboring cells. Once the interface has been reconstructed, its motion by the flow field must be modeled by a suitable advection algorithm (for example, the projection method originally developed by Chorin in [22] for single phase flows). VOF methods are popular and have been used in commercial multiphase flow codes. The principal advantage of VOF methods is their inherent volume conserving property. Unfortunately, spurious bubbles or drops may be created. The computation of geometric quantities such as curvature and reconstruction of the interfaces from the volume fractions tends to be less accurate compared to other methods.

The immersed boundary method

The immersed boundary method (IBM) was introduced to study flow patterns around heart valves [8] and has evolved into a generally useful method for interface problems. It has been

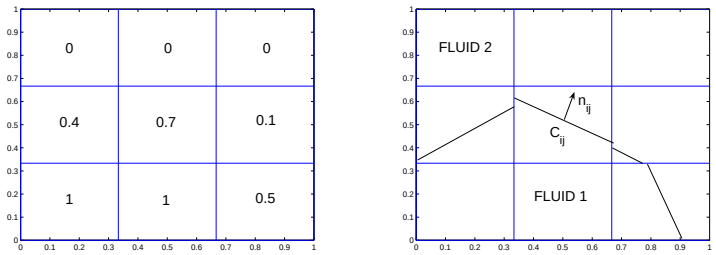

(a) Volume fraction function c_{ij} (b) Reconstructed interface using piecewise linear approximation

Figure 2.1: Volume of fluid representation of interface

used for many applications, examples include modeling of swimming organisms, platelet aggregation in blood clotting, cochlea dynamics, wood pulp fiber dynamics and many more. See a recent paper of Peskin [7] for a thorough review on the immersed boundary method.

The key idea is to employ a mixture of Eulerian and Lagrangian variables. These are related by interaction equations in which the Dirac delta function plays a prominent role. Numerically, the Eulerian variables are defined on a fixed Cartesian mesh, and the Lagrangian variables are defined on a curvilinear mesh, represented by a set of discrete control points $\{\mathbf{X}_k^n\}$ for $1 \le k \le N$ and $t = t^n$. These points move freely through the fixed Cartesian mesh without being constrained to adapt to it in any way at all. The interaction between two meshes comes from the singular force that is exerted by the interface. Namely, the singular force of each control point $\mathbf{F}_k^n$ is spread to the nearby Cartesian grid points near the interface by a discrete delta function so that it yields nonzero force term $\mathbf{F}_k^n$ at grid points near the interface. A typical example of the discrete one-dimensional delta function is

$$\delta_h(x) = \begin{cases} (h - |x|)/h^2, & \text{if} \quad |x| \le h \\ 0, & \text{otherwise} \end{cases} \tag{2.1}$$

or Peskin's original discrete cosine delta function

$$\delta_h(x) = \begin{cases} (1 + \cos(\pi x/2h)/4h, & \text{if} \quad |x| \le 2h \\ 0, & \text{otherwise} \end{cases} \tag{2.2}$$

where h is a grid size parameter. The first one is not smooth but the solution obtained using it gives second order accuracy for some one-dimensional problems [35]. The discrete cosine delta function is smooth but the solution is only first order accurate. In higher dimensions, the discrete delta function is often taken as a product of one dimensional discrete delta functions. Then, the numerical approximation of the singular force is given in the form of a sum over the interface elements

$$\mathbf{F}_{ij}(\mathbf{x}) = \sum_k \mathbf{f}_k(t)\delta_h(\mathbf{x}_{ij} - \mathbf{X}_k^n) \tag{2.3}$$

where $\mathbf{f}_k$ is the discrete force density at the point $\mathbf{X}_k^n$ and $\mathbf{x}_{ij}$ is an Eulerian mesh grid point.

After the singular force is approximated the fluid equations can be solved on the cartesian mesh by a simple finite difference method. The same discrete delta function is used to

interpolate the resulting velocity to the control points

$$\mathbf{U}_k^n = \sum_{ij} \mathbf{u}_{ij}(\mathbf{x})\delta_h(\mathbf{x}_{ij} - \mathbf{X}_k^n) \tag{2.4}$$

Finally, the control points are advected by solving

$$\frac{\partial \mathbf{X}_k}{\partial t} = \mathbf{U}_k(\mathbf{X}_k, t) \tag{2.5}$$

by an appropriate method. To summarize, the immersed boundary method involves the following steps

- Given the location of the interface $\mathbf{X}_k^n$ at time t^n compute the force densities $\mathbf{f}_k^n$ at the immersed points.
- Spread the forces $\mathbf{f}_k^n$ to values $\mathbf{F}_{ij}(\mathbf{x})$ on the background grid using (2.3).
- Solve the fluid equations on the regular grid with appropriate boundary conditions to obtain $\mathbf{u}_{ij}^{n+1}$.
- Interpolate the resulting velocities $\mathbf{u}_{ij}^{n+1}$ to the immersed boundary using (2.4) to obtain $\mathbf{U}_k^{n+1}$.
- Move the boundary points $\mathbf{X}_k^n$ to $\mathbf{X}_k^{n+1}$ using the velocities $\mathbf{U}_k^n$ and/or $\mathbf{U}_k^n$ and some discrete approximation to the ODE (2.5).
- Repeat all the steps for next timestep.

The immersed boundary method is fast and simple to implement. Additionally, it is a flexible method that can deal with complex geometries. However, as a trade off the original method is at most first-order accurate (except for a few special cases), due to the smearing effect of the discrete delta function [35] (though some recent work [3] uses adaptive gridding to overcome this limitations). Immersed boundary computations have also been demonstrated to suffer from a high degree of stiffness. In [9] Tu and Peskin recognized the necessity of handling the singular force calculation implicitly and several implicit and semi-implicit schemes were proposed. Unfortunately, in practice, scheme based on the fully implicit equations are extremely expensive since it requires the solution of the nonlinear coupled interface-fluid equations at each time step. Due to their simplicity, the semi-explicit and "approximate implicit" schemes perform much better than the implicit ones, but the time-step restrictions are still severe.

The front-tracking method

This method was introduced by Richtmyer and Morton [30] and further developed by Glimm [23]. For most recent advances see Unverdi and Tryggvason [17] and [38]. The front-tracking method has its roots in the immersed boundary method of Peskin and McQueen [8] and marker-and-cell (MAC) method [16]. The basic idea is very similar to Peskin's approach, that is to use of two grids, see Figure 2.2. One standard, Eulerian finite difference mesh is used to solve the fluid equations. The other is a set of Lagrangian markers, the disretized interface mesh, that is used to explicitly track the interface and compute the singular force which is then transferred to the finite difference mesh via discrete delta-functions. Similar to the immersed boundary method, the interface is represented by a given ordered list of

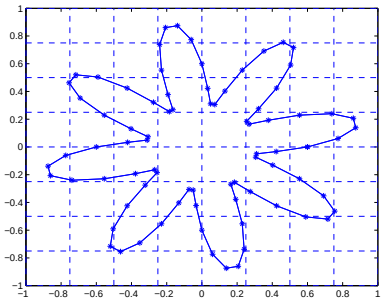

Figure 2.2: Example of the stationary and moving meshes for the front-tracking method. Here the stationary mesh is showed with the dashed lines. The stars mark the positions of the markers and the solid line represents the piecewise linear reconstruction of the interface.

marker particles $\{\mathbf{X}_k^n\}$. The first step in this algorithm is to reconstruct the interface by a list of connected polynomials using the marker list. This gives a parametric representation of the interface. Since both lists are ordered the topology of the interface is uniquely identified. Next, one computes the singular forces defined only along the interfaces. This is done using Peskin's immersed boundary technique. That is, one uses discrete function (2.1) or (2.2) to distribute the singular forces over the grid points nearest to the interface via (2.3). The same discrete delta functions are used to interpolate the velocity field from the stationary grid to the interface using (2.4).

The major novelty in the front-tracking method is the construction of the indicator function $I(\mathbf{x})$ which enables computations with discontinuous material properties. This is done by solving the Poisson equation

$$\Delta I = \nabla \cdot \mathbf{G}$$

where $\mathbf{G}(\mathbf{x})$ is a grid-gradient field generated by spreading the jump in the indicator function by the discrete delta function to the stationary grid. The indicator function is constant within each material region. The primary advantage of this approach is that closed interfaces can interact in a natural way since the gradients simply add or cancel as the grid distribution is constructed from the information carried by the tracked front. Then the fluid properties are easily determined via $\rho(\mathbf{x}) = \rho_1 + (\rho_2 - \rho_1)I(\mathbf{x})$, etc.

The next step is to solve the resulting fluid equations on the Eulerian mesh and interpolate the velocity field on the marker positions. Finally, the advection of the particles is performed by solving equation (2.5).

Front-tracking methods give the precise location and geometry of the interfaces. These algorithms are considered to be very accurate since they can use a large number of grid points on the interface. In addition, front-tracking permits more than one interface to be present in one computational cell without coalescence, which can be important in some applications. Another crucial property of the front tracking method is the ability to handle topological changes. During the computations the interface usually moves and deforms, thus markers tend to deplete in some regions and cluster in other regions. Thus, one has to add or delete some of these markers to maintain regularity. Namely, the distance between the adjacent points, d, is maintained on the order of the stationary grid spacing, h (for example $0.4 < d/h < 0.6$). To accommodate topology changes, interfaces are allowed to

reconnect when either parts of the same interface or parts of two separate interfaces come close together. The instantaneous change in topology is, of course, only an approximation of what happens in reality. Since it is not well known at what distance the interfaces will merge, we artificially reconnect the interface when two points come closer than some small distance, l. This distance is chosen rather arbitrarily for lack of a better physical model. But here the advantage of front-tracking is evident since we can control the distance at which the interfaces merge and study the effect of varying l, unlike in some other methods where there is no control over topology changes.

The major disadvantages of front-tracking methods is the difficulty in handling topological changes for three-dimensional simulations and the relative complexity in implementation.

2.2 Interface capturing methods

The level set method

The level set method was first introduced by Osher and Sethian [37] and is a popular computational technique for tracking moving interfaces. The main idea is to rely on a implicit representation of the interface as the zero set of an auxiliary function (level-set function). The first application of this method to incompressible multiphase flows was done by Sussman [29] and Chang [41].

The level set function $\phi(\mathbf{x}, t)$ is defined as follows

$$\phi(\mathbf{x},t) = \begin{cases} > 0, & \text{if } \mathbf{x} \in \text{ fluid 1} \\ = 0, & \text{if } \mathbf{x} \in \Gamma \text{ (the interface between fluids)} \\ < 0, & \text{if } \mathbf{x} \in \text{ fluid 2} \end{cases}$$

and the evolution of ϕ is given by the level set PDE

$$\phi_t + \mathbf{u} \cdot \nabla \phi = 0,$$

meaning that the interface moves with the fluid (see Figure 2.3 for an example of the level set function). To keep the interface geometry well resolved, the level-set function is required to

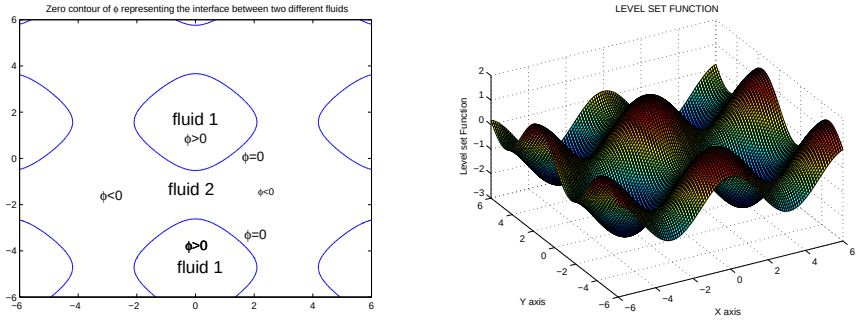

(a) Zero contour of ϕ representing the interfaces. (b) Level set function $\phi = \cos(x) + \sin(y) - 0.5$

Figure 2.3: Example of the level set function

be a distance function near the interface. However, under the evolution ϕ will not necessary remain as such. Typically, a reinitilization step (solving a Hamilton-Jacobi type equation) is performed to keep ϕ as a distance function near the interface while keeping the original zero level set unchanged. Namely, given ϕ at time t, the contours are redistributed by finding the steady state solution of the equation

$$\frac{\partial d}{\partial \tau} = S_\epsilon(\phi)(1 - |\nabla d|), \quad \dot{(}\mathbf{x}, 0) = \phi(\mathbf{x})$$

where S_ϵ is the smoothed sign function defined as

$$S_\epsilon(\phi) = \frac{\phi}{\sqrt{\phi^2 + \epsilon^2}},$$

where ϵ is usually equal to one or two grids lengths. After solving the above equations to steady state $\phi(\mathbf{x}, t)$is then replaced by $d(\mathbf{x}, \tau_{\text{steady}})$. The density and viscosity are defined as

$$\rho(\phi) = \rho_2 + (\rho_1 - \rho_2)H_\epsilon(\phi) \quad \text{and} \quad \mu(\phi) = \mu_2 + (\mu_1 - \mu_2)H_\epsilon(\phi)$$

where $H_\epsilon(\phi)$ is the smoothed Heaviside function given by

$$H_\epsilon(\phi) = \begin{cases} 0 & \text{if } \phi < -\epsilon \\ 0.5(1 + \phi/\epsilon + \sin(\pi\phi/\epsilon)) & \text{if } |\phi| \leq \epsilon \\ 1 & \text{if } \phi > -\epsilon \end{cases}$$

The mollified delta function is $\delta_\epsilon(\phi) = dH_\epsilon/d\phi$. The surface tension force is given as

$$\mathbf{F}_{\text{sing}} = -\tau\nabla \cdot \Big(\frac{\nabla\phi}{|\nabla\phi|}\Big)\delta_\epsilon(\phi)\frac{\nabla\phi}{|\nabla\phi|}$$

Finally, the fluid equations are solved with some appropriate method.

Advantages of the level-set algorithm include the simplicity of implementation, the inherited ability to capture topological changes of interfaces and ease with which the intrinsic properties of the interface (such as curvature, normal, etc.) can be obtained from the level-set function. The main disadvantage of the level set method is that mass is not conserved.

The phase-field method

Phase field, or diffuse-interface, models are another popular technique that belongs to the family of interface capturing methods. For a recent review see [15]. The main idea is to replace sharp fluid interfaces by thin but nonzero thickness transition regions where the interfacial forces are smoothly distributed. The idea is to introduce a conserved order parameter, for example mass concentration, that varies continuously over thin interfacial layers and is mostly uniform in the bulk phases.

The phase field is governed by the following advective Cahn-Hilliard equation

$$\begin{aligned} \frac{\partial c}{\partial t} + \mathbf{u} \cdot \nabla c = \nabla \cdot \Big(M(c)\nabla\mu\Big), \\ \mu = F'(c) - \epsilon^2\Delta c \end{aligned} \tag{2.6}$$

where $M(c) = c(1-c)$ is the mobility, $F(c) = 0.25c^2(1-c)^2$ is a Helmholtz free energy that describe the coexistence of immiscible phases, and ϵ is a measure of interface thickness. It

can be shown that in the sharp interface limit $\epsilon \Rightarrow 0$, the classical Navier-Stokes equations and jump conditions are recovered [25]. The singular surface tension force is $\mathbf{F}_{sing} = -6\sqrt{2}\tau\epsilon\nabla \cdot (\nabla c \otimes \nabla c)$, where τ is the surface tension coefficient [25].

The main advantages of the phase-field method are: topological changes are automatically described and the composition field c has a physical meaning both in the bulk phases and near the interface. It is also easy to incorporate complex physics into the framework, thus the phase-field methods are straightforwardly extended to multicomponent systems, where miscible, immiscible and partially miscible phases can be modeled. Unfortunately, for some case the numerical solution can be computationally expensive to obtain.

2.3 Hybrid methods

Recently, a number of hybrid methods that combine good features of each algorithm, have been developed. These include coupled particle level-set methods, level-set VOF algorithms, marker and VOF methods.

In the particle level-set method [13], Lagrangian disconnected marker particles are randomly positioned near the interface and are passively advected by the flow in order to rebuild the level set function in underresolved zones, such as high curvature regions. In these regions, the standard non-adaptive level-set method regularizes excessively the interface structure and mass is lost. The use of the Lagrangian markers significantly decreases these difficulties.

VOF and level-set methods have been combined in [28] and [27]. The level-set function is used to describe the geometry of the interface while VOF is used to maintain volume conservation properties. Both functions are made compatible after every time step. The coupling between the volume fraction function c_{ij} and level-set function ϕ occurs through the normal of the reconstructed interface and through the fact that the level-set function is reset to the exact signed normal distance to the reconstructed interface.

The hybrid method that uses both VOF and marker particles is developed in [1]. As usual, the volume fraction function is used to assure mass conservation while marker particles are used to reconstruct and move the interface. As a result, one achieves a smooth motion of the interface, typical for all marker methods, together with volume conservation, which is standard for VOF methods. Thus, this approach increases both the accuracy of interface tracking, when compared to standard VOF methods, and the conservation of mass, with respect to original marker method.

2.4 Immersed interface method and its extensions

The immersed interface method (IIM) was first introduced by LeVeque and Li in [31] as a finite difference type method for elliptic equations

$$\nabla \cdot (\beta(x,y)\nabla u) + k(x,y)u = f \quad (x,y) \in \Omega$$

with interface Γ being an arbitrary piecewise smooth curve such that $\Omega = \Omega^+ \cup \Omega^- \cup \Gamma$, discontinuous coefficients $\beta(x,y)$, $k(x,y)$ across the interface

$$\beta(x,y) = \begin{cases} \beta^+(x,y) & \in \Omega^+ \quad \text{(outer part)} \\ \beta^-(x,y) & \in \Omega^- \quad \text{(inner part)} \end{cases} \qquad k(x,y) = \begin{cases} k^+(x,y) & \in \Omega^+ \\ k^-(x,y) & \in \Omega^- \end{cases}$$

and a singular force f.

Similar to IBM and front-tracking methods, immersed interface method employs two different meshes: a fixed mesh for the fluid equations and a moving one for the interface representation. However, it seemed unlikely [35] that the discrete delta function approach can achieve second order or higher accuracy in two or three dimensional problems (except for a few special situations when the grid is aligned with the interface). Thus, the key idea of the IIM is to avoid the discretisation of the delta function by introducing the explicitly calculated jump conditions directly into the finite difference stencil. To do that, we modify the finite difference stencil, which uses the grid points on either side of the interface. Namely,

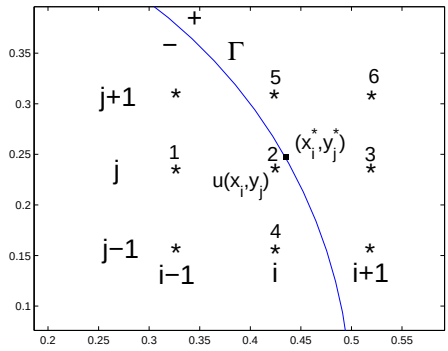

Figure 2.4: The geometry near the modified stencil. The coefficients γ_1 through γ_6 will be determined in the labeled points.

we rewrite the finite difference equation as

$$\sum_k \gamma_k u_{i+i_k,j+j_k} + k_{ij} u_{ij} = f_{ij} + C_{ij}$$

for every grid point (x_i, y_j). The sum over k involves a finite numbers of points neighboring (x_i, y_j) (at most six in the derived formula). So each i_k, j_k will take a value in the set $\{-1, 0, 1\}$. If the interface does not lie between any points in the standard 5-point stencil centered in (x_i, y_j) no modification is needed for γ_k and $C_{ij} = 0$. For the rest of the grid points the modified coefficients γ_k are determined by requiring truncation error at these points to be of order $O(h)$. It turns out to be sufficient to require $O(h)$ truncation error since the interface forms a lower dimensional set.

To obtain γ_k we expand the solution $u_{x_i,y_{j\pm1}}$,$u_{x_{i\pm1},y_j}$ and u_{x_i,y_j} in Taylor series at some point (x_i^*, y_j^*) on the interface (which is usually the closest point to (x_i, y_j)), being careful to use the limiting values of derivatives of u from the correct side of the interface. As an example, in the configuration shown on Figure 2.4, we would expand

$$u(x_i, y_j) = u^- + u_x^-(x_i - x^*) + u_y^-(y_j - y^*) + \frac{1}{2}u_{xx}^-(x_i - x^*)^2 + \frac{1}{2}u_{yy}^-(y_j - y^*)^2 + u_{xy}^-(x_i - x^*)(y_j - y^*) + O(h^3)$$

and

$$u(x_{i+1}, y_j) = u^+ + u_x^+(x_{i+1} - x^*) + u_y^+(y_j - y^*) + \frac{1}{2}u_{xx}^+(x_{i+1} - x^*)^2 + \frac{1}{2}u_{yy}^+(y_j - y^*)^2 + u_{xy}^+(x_{i+1} - x^*)(y_j - y^*) + O(h^3)$$

After inserting this expansions at each point in the difference equation we can express the local truncation error as a linear combination of the values $u^{\pm}$, $u_x^{\pm}$, $u_y^{\pm}$, $u_{xx}^{\pm}$, $u_{yy}^{\pm}$ and $u_{xy}^{\pm}$. We now wish to eliminate all values on one side, say the values on $+$, in terms of the values on the other side, say $-$ side. To do this, we must use the jump conditions across the interface

$$[u] = u^+ - u^- = G(x, y) \quad \text{and} \quad \left[\beta \frac{\partial u}{\partial n}\right] = \beta^+ \frac{\partial u^+}{\partial n} - \beta^- \frac{\partial u^-}{\partial n} = H(x, y)$$

where $\partial/\partial n$ represents a differentiation in normal direction. Differentiating these jump conditions and manipulating the results allows us to perform the desired elimination. In order to do this, it turns out to be very convenient to perform a local coordinate transformation into normal and tangential directions to the interface.

Once the local truncation error is expressed as a linear combination of the values $u^{\pm}$, $u_x^{\pm}$, $u_y^{\pm}$, $u_{xx}^{\pm}$, $u_{yy}^{\pm}$ and $u_{xy}^{\pm}$, we must require that the coefficient of each of these terms vanish in order to achieve an $O(h)$ truncation error. This gives a system of six equations to determine the unknown coefficients γ_k. Thus, we require six points in the stencil: 5-point stencil together with one additional point. To summarize, in order to determine a modified stencil we need to do the following

- Select a point $(x_i^*, y_j^*) \in \Gamma$ near (x_i, y_j).
- Apply a local coordinate transformation in directions normal and tangential to Γ at (x_i^*, y_j^*).
- Derive the jump conditions relating u^+ and u^- (and their derivatives) at (x_i^*, y_j^*) in the local coordinates.
- Choose an additional point to form a 6-point stencil.
- Set up and solve a linear system of six equations for the coefficients γ_k. The value of C_{ij} is also obtained.

Finally, the resulting linear system is solved then with some appropriate method. The method has been successfully used in several applications and extended in different directions, notably to hyperbolic and parabolic problems. Li applied the IIM idea to heat equations in 2D with fixed interfaces, followed by his dissertation [43] where IIM was applied to some 3D partial differential equations. LeVeque and Li used IIM for Stokes interface problem in 2D [31]. In [44] and [4] the method was extended to treat nonlinear problems.

However, the original method suffered from lack of fast solvers and strong dependence of the error on the relative position of interface and grid even for moderate contrast in the coefficients. In the original paper [32], the discontinuities in the coefficient were always "mild" (the quotient between β's on different sides of the interface was always $0.1 \leq \beta^+/\beta^- \leq 10$).

In [45], where Li introduced a Fast Iterative IIM (FIIIM). Li used the observation that for piecewise constant coefficients, the equation can be written as a Poisson equation by dividing through the coefficient, if in addition one observes the jump condition across the

interface. This leads naturally to the idea of splitting the finite differences near the interface into standard differences and corrections to the standard differences, and brings the FIIIM closer to Peskin's immersed boundary method. The jumps in the function and its derivatives (not jumps in the flux $[\beta u_n]$) turn out to be crucial quantities. Given the jumps, the FIIIM needed only corrections to the right hand side. Li chose to do that in the spirit of the original IIM, by selecting a point on the interface and developing Taylor expansions about it on both sides of the interface. Another question was how to find the jumps. To do that, Li used the equations for the jumps based on local properties of the solution derived in [31]. The jumps were computed only at the fixed set of control points and then interpolated.

It was shown in [19] and [2] that stability of the original algorithm depends on the choice of one or more extra grid points in addition to the standard five-point stencil. In other words, it is not always guaranteed that the original IIM will converge and satisfy the maximum principle. To eliminate this problem, Li and Ito proposed a modification to the original approach [48]. The new method was to guarantee that the discrete maximum principle is satisfied.

The original spline representation of the interface was replaced with a level set method by Hou, Li, Osher and Zhao which allowed to compute moving interface problems with topological changes [39]. This formulation was used to study electron migration in [49] and applied to Stefan problems in [47]. IIM was combined with a multigrid approach by Adams in [24]. LeVeque and Zhang used IIM for hyperbolic systems of partial differential equations with discontinuous coefficients arising from acoustic or elastic problems in heterogeneous media [33],[11]. Calhoun [12] and LeVeque and Calhoun [34] extended the IIM to a stream-function vorticity formulation of incompressible flow in 2D.

The most recent advances include a finite element formulation of IIM for 1D and 2D elliptic interface problems with discontinuous coefficients [46], [50].

Chapter 3

Distribution theory preliminaries

It is a common situation for the interface problem to contain singular and discontinuous quantities. A good example of that is a two-phase flow where two different fluids are separated by an elastic membrane. In this case the singularity comes from the forcing term, defined only on the surface of the membrane, while discontinuity is due to inhomogeneity of the fluid. A natural way to model such quantities is the use of distributions or generalized functions.

In this chapter we introduce some basic notation and definitions from the theory of distributions. We begin by giving the physical background of the generalized functions, starting with delta functional, which is considered to be the origin of distributional theory. Next, we lay out basic notation of generalized functions and define operations of algebra and calculus on them. We finalize this chapter with the definition of the jump conditions. For detailed discussion of distributions see [20] and [14].

3.1 Background

The theory of generalized functions was invented in order to give a solid theoretical foundation to the delta functional, which was first introduced by Dirac (1930) as a mathematical tool in quantum mechanics. Dirac's idea of the delta functional can be easily understood in the following way.

Consider a rod of nonuniform thickness and introduce a mass-density function $\rho(x)$ which describes mass distribution along the rod. Physically, this function is defined as mass per unit length of the rod at some point x. The total mass of some section of the rod $(a < x < b)$ is defined as $\int_a^b \rho(x)dx$. But if the mass is concentrated only at a finite number of points instead of being continuously distributed, then the above description is no longer valid. Consider a wire of negligible mass, with a small but heavy load attached to some point $x = \alpha$. Suppose that the load has unit mass and is small enough to be mathematically represented as a point. Then the total mass of the segment of the rod is zero if it doesn't include point α and one otherwise. Unfortunately, there is no continuous function $\rho(x)$ that can represent such mass distribution. If there were, it would be $\rho(x) = 0$ for all $x \neq \alpha$. But if a function vanishes except for a few discrete points, it is easy to show that the integral over the whole rod is zero. Thus the integral including α will not give a correct result, 1. Therefore, Dirac introduced a mathematical tool δ_α, the delta functional, having the properties

$$\delta_\alpha(x) = 0 \quad \text{for } x \neq \alpha \quad \text{and} \quad \int_a^b \delta_\alpha(x)dx = 1 \quad \text{if} \quad a < \alpha < b$$

For some short time, delta functional lacked theoretical foundation and was considered as a technical trick for obtaining results for discrete point particles from the continuous theory. The situation was similar to that of complex numbers in 16th century. It proved useful to pretend that -1 has a square root, since one could then use an algorithm involving complex numbers for obtaining real roots of cubic equations. Any result obtained this way could be directly verified substituting it in the equation and showing that it really was a root. It was only much later that complex numbers were given a solid mathematical foundation, and then with the development of the theory of functions of a complex variable their application was fully discovered.

In the same way, the solid theoretic foundation that was developed by Sobolev (1936) and Schwartz (mid 1950's) went far beyond then justification of the delta functional. The theory of generalized function or distributions can be used to replace ordinary analysis, and is in many ways simpler. For example, any generalized function can be differentiated and integration of series can be perform term by term without worrying about convergence. Naturally, there are limitations as well. For example, multiplication of the delta functional by itself or any discontinuous function is meaningless, [14].

3.2 Definition of the spaces

For the sake of simplicity we restrict ourselves to at most two dimensional problems. The generalization to higher dimensions is obvious. Then, let $\Omega \subset \mathbb{R}^d$ $(d = 1, 2)$ be a bounded domain and assume that the boundary $\partial\Omega$ of Ω is sufficiently smooth such that the divergence theorem applies. Moreover, let $u : \Omega \to \mathbb{R}$ and $x \in \Omega$.

Definition 3.2.1. *The following standard function spaces will be employed in this thesis:*

$$
\begin{aligned}
C^k(\Omega) &= \{u : \Omega \to \mathbb{R}| \quad u \text{ is } k\text{-times continuously differentiable}\}\\
L^p(\Omega) &= \{u : \Omega \to \mathbb{R}| \quad u \text{ is Lebesque measurable}, ||u||_{L^p(\Omega)} < \infty\}\\
L^\infty(\Omega) &= \{u : \Omega \to \mathbb{R}| \quad u \text{ is Lebesque measurable}, ||u||_{L^\infty(\Omega)} < \infty\}\\
L^p_{loc}(\Omega) &= \{u : \Omega \to \mathbb{R}|u|_K \in L^p(K) \text{ for each closed subset } K \subset \Omega\}
\end{aligned}
$$

where k is a non-negative integer and

$$
||u||_{L^\infty(\Omega)} = ess\sup_{\Omega}|u| \quad \text{and} \quad ||u||_{L^p(\Omega)} = \Big(\int_\Omega |u|^p dx\Big)^{1/p} \qquad (1 \le p < \infty)
$$

Definition 3.2.2. *The support of a function $\phi : \Omega \to \mathbb{R}$ is denoted by*

$$
supp(\phi) := \overline{\{x \in \mathbb{R}^d | \phi(x) \neq 0\}}
$$

where the overline denotes the closure.

Remark 1. *The functions with the compact support that belong to $C^k(\Omega)$ are denoted by $C^k_c(\Omega)$.*

In order to introduce the Sobolev spaces we will need the following definitions

Definition 3.2.3. *A vector of the form $\alpha = (\alpha_1, .., \alpha_d)$, where each component α_i is a nonnegative integer, is called a multi-index of order*

$$
|\alpha| = \alpha_1 + ... + \alpha_d
$$

Definition 3.2.4. *Given a multi-index α, define*

$$D^{\alpha}u(x) = \frac{\partial^{|\alpha|}u(x)}{\partial x_1^{\alpha_1}\cdots\partial x_d^{\alpha_d}} = \partial_{x_1}^{\alpha_1}\cdots\partial_{x_d}^{\alpha_d}u(x)$$

Then

Definition 3.2.5. *We define the Sobolev space as follows*

$$W^{k,p}(\Omega) = \{u : \Omega \to \mathbb{R} \quad u \in L^p_{loc}(\Omega) \text{ and } \forall \quad \alpha : |\alpha| \leq k, D^{\alpha}u \in L^p(\Omega)\}$$

Remark 2. *In this thesis we are interested in Sobolev spaces with $p = 2$ which are denoted by*

$$H^k(\Omega) = W^{k,2}(\Omega) \quad k = 0, 1, ..$$

Note, that $H^0(\Omega) = L^2(\Omega)$.

Definition 3.2.6. *If $u \in H^k(\Omega)$, we define its norm to be*

$$||u||_{H^k(\Omega)} = \Big(\sum_{|\alpha|\leq k}\int_{\Omega}|D^{\alpha}u|^2dx\Big)^{1/2}$$

Definition 3.2.7. *We denote by $H_0^k(\Omega)$ the closure of $C_c^{\infty}(\Omega)$ in $H^k(\Omega)$*

3.3 Basic notation and definitions

There are several approaches how to describe a generalized function. We will follow the Schwartz approach, who called generalized functions - distributions. The idea is to define Dirac's delta functional as something which makes sense only under the integral sign, possibly multiplied by some other function ϕ. Namely, we will define distribution as a rule, which, given any function ϕ, provides a number. This number may be thought of as a weighted average, with weight function ϕ, of a corresponding mass-distribution. However, one has to be careful about which function are allowed to be considered as a weight function.

Definition 3.3.1. *A function $\phi : \Omega \to \mathbb{R}$ is said to be smooth if $\phi \in C^{\infty}(\Omega)$.*

Definition 3.3.2. *A smooth function $\phi : \Omega \to \mathbb{R}$ with $supp(\phi) \subset \Omega$ is called a test function. The set of all test functions is denoted by $\mathcal{D}(\Omega)$.*

Definition 3.3.3. *A linear functional on $\mathcal{D}(\Omega)$ is a mapping $F : \mathcal{D}(\Omega) \to \mathbb{R}$ such that $F(a\phi + b\psi) = aF(\phi) + bF(\psi)$ for all $a, b \in \mathbb{R}$ and $\phi, \psi \in \mathcal{D}(\Omega)$.*

For a linear functional F on $\mathcal{D}(\Omega)$ it is convenient to use the following notation

$$\big\langle F, \phi \big\rangle := F(\phi) \qquad \forall \phi \in \mathcal{D}(\Omega)$$

Then we define convergence in the space $\mathcal{D}(\Omega)$ as follows

Definition 3.3.4. *Let $\{\phi_n\}$ be a sequence of test function in $\mathcal{D}(\Omega)$ and ψ some test function. We say that $\{\phi_n\}$ is a convergent sequence and $\phi_n \to \psi$ in $\mathcal{D}(\Omega)$ if*

(i). there is a closed subset $K \subset \Omega$ containing $supp(\phi_n)$ for all n and $supp(\psi)$,

(ii). for any k, $\phi_n^k(x) \to \psi^k(x)$ as $n \to \infty$ uniformly for $x \in K$. Here $\phi^k(x)$ denotes the k-th derivative of $\phi(x)$.

Then a distribution is defined as follows:

Definition 3.3.5. *A functional F on $\mathcal{D}(\Omega)$ is continuous if it maps every convergent sequence in $\mathcal{D}(\Omega)$ into a convergent sequence in $\mathbb{R}$, that is, if $\langle F, \psi_n \rangle \to \langle F, \psi \rangle$ whenever $\phi_n \to \psi$ in $\mathcal{D}(\Omega)$. A continuous linear functional on $\mathcal{D}(\Omega)$ is called a distribution, or generalized function. The set of all distributions on $\mathcal{D}(\Omega)$ is denoted by $\mathcal{D}'(\Omega)$.*

In order to establish the connection between distributions and ordinary functions we need the following definition

Definition 3.3.6. *To every function $f \in L^1_{loc}(\Omega)$ there corresponds a distribution F defined by*

$$\langle F, \phi \rangle := \int_\Omega f(x)\phi(x)dx \tag{3.1}$$

Remark 3. *(i). For $f \in L^1_{loc}(\Omega)$ it is common to identify f and the distribution $F \in \mathcal{D}'(\Omega)$ given in (3.1). Therefore, $L^1_{loc}(\Omega) \subset \mathcal{D}'(\Omega)$.*

(ii). Let F be a distribution. If $F \in L^1_{loc}(\Omega)$, then F is called a regular distribution. Otherwise, F is called a singular distribution.

(iii). If $F \in L^2(\Omega) \subset L^1_{loc}(\Omega)$

$$\langle F, \phi \rangle = \int_\Omega F(x)\phi(x)dx = (F, \phi)$$

where $(\cdot, \cdot)$ denote the usual scalar product in $L^2(\Omega)$.

Thus the class of distributions contains objects that correspond to ordinary functions as well as singular distributions which do not. For later use, the following property is convenient

Definition 3.3.7. *For $F \in \mathcal{D}'(\Omega)$ and $h \in \mathcal{D}(\Omega)$, the product $hF \in \mathcal{D}'(\Omega)$ is defined by*

$$\langle hF, \phi \rangle = \langle F, h\phi \rangle \qquad \forall \phi \in \mathcal{D}(\Omega)$$

We now proceed to the differential calculus of distributions. Partial derivatives with respect to the space variables will be denoted by $\partial_i = \frac{\partial}{\partial x_i}$. If $d = 1$, let $\partial = \partial_1$.

Definition 3.3.8. *Distributions can be differentiated as follows: for $f \in \mathcal{D}'(\Omega)$, $\partial_i f \in \mathcal{D}'(\Omega)$ is the distribution satisfying*

$$\langle \partial_i f, \phi \rangle = -\langle f, \partial_i \phi \rangle \quad \text{for all} \quad \phi \in \mathcal{D}(\Omega)$$

Consequently, the derivative of the product of a distribution F and any smooth function h is given by

$$\langle \partial_i(hF), \phi \rangle = -\langle hF, \partial_i \phi \rangle$$

We will use the following distributions

Definition 3.3.9. *Let $d = 1$ and $\alpha \in \Omega$. The delta function δ_α is the distribution that satisfies*

$$\langle \delta_\alpha, \phi \rangle := \phi(\alpha)$$

for all $\phi \in \mathcal{D}(\Omega)$.

Remark 4. *In view of (3.1) it is common to write*

$$\langle \delta_\alpha, \phi \rangle = \int_\Omega \delta_\alpha(x)\phi(x)dx$$

Definition 3.3.10. *Let $d = 1$ and $\alpha \in \Omega$. The dipole function δ'_α is the distributional derivative of the delta function $\delta'_\alpha = \partial\delta_\alpha$.*

Remark 5. *(i) If $d = 1$, δ_α is a continuous linear functional on $\mathcal{D}(\Omega)$ w.r.t. the Sobolev norm $||.||_1$. Therefore, it can be continuously and uniquely extended onto all of $H_0^1(\Omega)$. For the extension we will continue to use the same notation δ_α.*

(ii) Similarly, for $d = 1$ the dipole function can be continuously extended onto $H_0^2(\Omega)$.

(iii) By definition of the functional derivative, it holds

$$\langle \partial\delta_\alpha, \phi \rangle = -\langle \delta_\alpha, \partial\phi \rangle = -\partial\phi(\alpha)$$

(iv) It is sometimes common to denote the delta function δ_α by

$$\langle \delta(x-\alpha), \phi \rangle = \int_\Omega \delta(x-\alpha)\phi(x)dx = \phi(\alpha)$$

Similarly, the dipole function yields

$$\langle \delta'(x-\alpha), \phi \rangle = \int_\Omega \delta'(x-\alpha)\phi(x)dx = -\phi'(\alpha)$$

For the two-dimensional case, we need a description of the surface. Our guiding picture is that of a bubble in a surrounding medium. The surface of the bubble shall be described by a smooth closed double-point free curve $\Gamma \subset \Omega$: Let there exist a sufficiently smooth one-to-one mapping $X : (s_0, s_1) \to \Gamma$ such that $X(s_0) = X(s_1)$ and $X(s) \neq X(t)$ if $s, t \in (s_0, s_1)$ and $s \neq t$.

Definition 3.3.11. *Let $d = 2$ and Γ be as defined above. The functional $\delta_\Gamma \in \mathcal{D}'(\Omega)$ is defined by*

$$\langle \delta_\Gamma, \phi \rangle = \int_{s_0}^{s_1} \phi(X(s))|\nabla X(s)|ds$$

for all $\phi \in \mathcal{D}(\Omega)$.

Remark 6. *(i) The definition of δ_Γ is independent of its representation.*

(ii) By the trace theorem, δ_Γ can be extended to a continuous linear functional on $H_0^1(\Omega)$.

(iii) Another common notation for the functional δ_Γ is

$$\langle \delta_\Gamma, \phi \rangle = \int_\Omega \phi(x)\delta_\Gamma(x)dx$$

(iv) According to the Def. 3.3.8

$$\langle \partial_i\delta_\Gamma, \phi \rangle = -\langle \delta_\Gamma, \partial_i\phi \rangle = \int_{s_0}^{s_1} \partial_i\phi(X(s))|\nabla X(s)|ds$$

(v) Let $\mathbf{F} = (f_1, f_2)$*. Then the divergence operator applied to the distribution* $\mathbf{F}\delta_\Gamma$ *is given by*

$$\begin{aligned}\big\langle \nabla \cdot (\mathbf{F}\delta_\Gamma), \phi \big\rangle &= \sum_{i=1}^{2} \big\langle \partial_i (f_i \delta_\Gamma), \phi \big\rangle \\ &= -\sum_{i=1}^{2} \big\langle f_i \delta_\Gamma, \partial_i \phi \big\rangle = -\sum_{i=1}^{2} \int_{s_0}^{s_1} f_i(X(s)) \partial_i \phi(X(s)) |\nabla X(s)| ds\end{aligned}$$

where the second equality is obtained by applying Def. 3.3.8.

(vi) For the sake of simplicity, in the rest of this thesis, we will use the following notation

$$\int_\Gamma f(X(s)) ds := \int_{s_0}^{s_1} f(X(s)) |\nabla X(s)| ds$$

When later on deriving classical expressions for partial differential equations containing distributions we must take care of the discontinuities arising in the solutions across the interface Γ. We will use the following notations

Definition 3.3.12. *Let* $d = 1$ *,* $\alpha \in \Omega$ *and* $u : \Omega \to \mathcal{R}$*. The jump of* u *at* α *is denoted by*

$$[u]|_\alpha = \lim_{x \to \alpha^+} u(x) - \lim_{x \to \alpha^-} u(x)$$

whenever the expression on the right-hand side is well defined. The superscripts $-$ *and* $+$ *indicates that we approach the interface point* α *from the left (or right) side, correspondingly.*

Definition 3.3.13. *Let* $d = 2$ *and the assumptions of Def. 3.3.11 be fulfilled. The interface* Γ *splits the domain* Ω *into two parts. The part encircled by the interface* Γ *is denoted by* Ω_- *and the outer part is denoted by* Ω_+*. Let* $u : \Omega \to \mathbb{R}$*. If the traces* u^- *and* u^+ *of* $u|_{\Omega_-}$ *and* $u|_{\Omega_+}$*, respectively, on* Γ *exist, then denote*

$$[u]|_\Gamma = u^+ - u^-$$

Definition 3.3.14. *Let* $d = 2$ *and the assumptions of Def.(3.3.11) be fulfilled and* β *some real-valued function. Moreover, let the traces* ∇u^+ *and* ∇u^- *of* $\nabla u|_{\Omega_+}$ *and* $\nabla u|_{\Omega_-}$*, together with the traces* β^+ *and* β^- *of* $\beta|_{\Omega_+}$ *and* $\beta|_{\Omega_-}$ *, respectively, exist on* Γ*, then denote*

$$\Big[\beta \frac{\partial u}{\partial n}\Big]|_\Gamma = \beta^+ \frac{\partial u^+}{\partial n} - \beta^- \frac{\partial u^-}{\partial n}$$

where n *is the outward normal vector on* Γ*.*

Chapter 4

Finite Element IIM for the elliptic interface problems

In this chapter we describe in detail our finite element formulation of the immersed interface method for the elliptic interface problems. We start with the model problem formulation (both one and two dimensional) and explain the relevance of these problems in the context of solving the interface Stokes problem. Next, we present the weak formulation and discuss the construction of the specific basic functions that accounts for the presence of the jumps in the solution. Finally, the numerical experiments are presented and the conclusions are drawn.

4.1 Model problems formulation

Here, we formulate the model problems which we will use to describe our finite element immersed interface method. As it was stated in the Chapter 1, the motivation for our approach comes from the interface Stokes problem in two dimensions (the generalization to 3D is straightforward but tedious). The solution to that problem consists of the velocity field (u_1, u_2) and the pressure p. Generally, the velocity components are continuous, but not smooth. The pressure is discontinuous itself together with its derivatives. To solve the interface Stokes problem, we intend to reduce the system of equations to three separate Poisson problems. That is one Poisson problem for the pressure and two for the velocity components, see Chapter 5 for more details.

Naturally, we first approach similar problems but in one space dimension where the interface is represented by a single point α. That is, we construct two elliptic model problems: the first one with a continuous but non-smooth solution and the second model problem with the solution that is discontinuous together with its derivatives. For the sake of definiteness, we assume that the computational domain Ω is a simple domain, such as an interval in one dimensional case or a square in two space dimensions. The interface is typically not aligned with the grid but rather intersects the gridlines.

For the first model problem the non smoothness of the solution arises from the presence of the delta functional on the right hand side and the discontinuity of the coefficient β.

Model problem 1

Consider the following problem

$$\begin{aligned} (\beta u_x)_x + ku &= f_c + \nu\delta_\alpha \quad \text{on } \Omega \\ u &= 0 \quad \text{on } \partial\Omega \end{aligned} \tag{4.1}$$

where β is a piecewise continuous function, $f_c \in L^2(\Omega)$, $k \in L^\infty(\Omega)$ and $\nu \in \mathbb{R}$. Here δ_α is a delta functional with the support at α.

Since the second model problem is intended to have a discontinuous solution, we include a dipole functional in the source terms. Thus the problem reads

Model problem 2

Let $\alpha \in \Omega$, $f_c \in L^2(\Omega)$ and $\nu, w \in \mathbb{R}$. Consider

$$\begin{aligned} u_{xx} &= f_c + \nu\delta_\alpha + w\delta'_\alpha \quad \text{on } \Omega \\ u &= 0 \quad \text{on } \partial\Omega \end{aligned} \tag{4.2}$$

where δ_α and δ'_α are the delta and the dipole functionals, respectively.

Next, we define an analog of *Model problem* 1 in two space dimensions. The main difference is that the delta functional has now support along a curve, instead of one single point.

Model problem 3

Let $f_c \in L^2(\Omega)$ and Γ be defined as in Def. 3.3.11 and $\beta \in L^\infty(\Omega)$

$$\begin{aligned} \nabla \cdot (\beta \nabla u) &= f_c + f\delta_\Gamma \quad \text{on } \Omega \\ u &= 0 \quad \text{on } \partial\Omega \end{aligned} \tag{4.3}$$

where $f \in \mathrm{C}(\Gamma)$.

Finally, *Model problem* 4 is defined as follows

Model problem 4

Let $f_c \in L^2(\Omega)$ and Γ be defined as before. Then

$$\begin{aligned} \Delta u &= f_c + \nabla \cdot \mathbf{F} \quad \text{on } \Omega \\ u &= 0 \quad \text{on } \partial\Omega \end{aligned} \tag{4.4}$$

where $\mathbf{F} = (F_1, F_2) = (f_1\delta_\Gamma, f_2\delta_\Gamma)$ with $f_1, f_2 \in \mathrm{C}(\Gamma)$. Later in this Chapter we show that the discontinuities in the solution of eq. (4.4) and its derivatives arise from the presence of the $\nabla \cdot \mathbf{F}$ term.

Remark 7. *As it has been shown in Chapter 3, it is reasonable to consider Dirichlet boundary conditions for model problems* 2 *and* 4.

4.2 Variational formulation of the model problems

In all the cases above, the equations are to be understood in the distributional sense. Thus we will proceed as follows. We first formulate the variational formulations using the properties of the distributions, than, using the extension operators we reformulate the weak formulations in terms of the Sobolev spaces. Finally, we state the equivalent classical formulations of the above model problems.

Model problem 1

Rewrite eq. (4.1) using the test functions $\psi \in \mathcal{D}(\Omega)$. Then, the problem reads: Find $u \in \mathcal{D}'(\Omega)$

$$\langle \partial(\beta\partial u) + ku, \psi \rangle = \langle f_c + \nu\delta_\alpha, \psi \rangle \quad \forall\psi \in \mathcal{D}(\Omega)$$

Using the linearity of distributions and Def. 3.3.8 we get

$$-\langle \beta\partial u, \partial\psi \rangle + \langle ku, \psi \rangle = \langle f_c, \psi \rangle + \langle \nu\delta_\alpha, \psi \rangle \quad \forall\psi \in \mathcal{D}(\Omega)$$

Recall the definition of the delta functional and apply Remark 5 (i), we arrive at the following: Find $u \in H_0^1(\Omega)$

$$\int_\Omega (-\beta u_x\psi_x + ku\psi)dx = \int_\Omega f_c\psi dx + \nu\psi(\alpha) \quad \forall\psi \in H_0^1(\Omega) \tag{4.5}$$

Let

$$\begin{aligned} a(u,\psi) &= \int_\Omega (-\beta u_x\psi_x + ku\psi)dx \\ L_{\text{cont}}(\psi) &= \int_\Omega f_c\psi dx \\ L_{\text{discl}}(\psi) &= \nu\psi(\alpha) \end{aligned}$$

Then, the weak form reads: Find $u \in V_0(\Omega)$

$$a(u,\psi) = L_{\text{cont}}(\psi) + L_{\text{discl}}(\psi) \quad \forall\psi \in V_0(\Omega)$$

Split the solution $u = u^H + u^N$ (admissible due to the linearity of the bilinear form $a(u,\psi)$) such that

$$\begin{aligned} a(u^H,\psi) &= L_{\text{cont}}(\psi) \\ a(u^N,\psi) &= L_{\text{discl}}(\psi) \end{aligned} \tag{4.6}$$

and approximate the discontinuous part of the solution u^N by an explicitly calculated function. Thus, we end up with: Find $u^H \in V_0(\Omega)$

$$a(u^H,\psi) = L_{\text{cont}}(\psi) + L_{\text{discl}}(\psi) - a(u^N,\psi) \quad \forall\psi \in V_0(\Omega) \tag{4.7}$$

For proof of existence and uniqueness of the solution of (4.5) see, for example, [21] and [42]. The following remarks should be done here:

Remark 8.

- *The exact cancellation does not occur during discretisation of (4.7) due to the discrete representation of u^N, explained further in the subsection 4.3.*
- *For the sake of completeness, let us write the classical formulation of the model problem. Let $\Omega = \Omega^+ \cup \Omega^- \cup \alpha$ and define two arbitrary test functions $\psi^+ \in H_0^1(\Omega^+)$ and $\psi^- \in H_0^1(\Omega^-)$. Then eq. (4.5) can be written on two separate domains*

$$\int_{\Omega^\pm} (-\beta u_x\psi_x^\pm + ku\psi^\pm)dx = \int_{\Omega^\pm} f_c\psi^\pm dx \quad \forall\psi^\pm \in H_0^1(\Omega^\pm)$$

since $H_0^1(\Omega^\pm) \subset H_0^1(\Omega)$. Integration by parts of the first term on the left hand side yields the following classical formulation of the problem

$$\begin{aligned} (\beta u_x)_x + ku &= f_c \quad \text{on } \Omega\backslash\alpha \\ u &= 0 \quad \text{on } \partial\Omega \end{aligned} \tag{4.8}$$

For the solution of (4.8) to be uniquely defined two additional boundary conditions are required. The following theorem will supply us with them.

Theorem 4.2.1. *The solution to the model problem* 1 *(4.1) satisfies the following boundary conditions at the interface point α (jump conditions)*

$$[u]|_\alpha = 0, \quad [\beta u_x]|_\alpha = \nu \tag{4.9}$$

Proof. Consider equation (4.8)

$$(\beta u_x)_x + ku = f_c \tag{4.10}$$

defined on the separate intervals $[0, \alpha]$ and $[\alpha, 1]$. The functions $\beta(x)$ and $k(x)$ are continuous on either side of the interface. Namely,

$$\beta = \begin{cases} \beta^-(x) & \text{on} \quad [0, \alpha] \\ \beta^+(x) & \text{on} \quad [\alpha, 1] \end{cases} \qquad \text{and} \qquad k = \begin{cases} k^-(x) & \text{on} \quad [0, \alpha] \\ k^+(x) & \text{on} \quad [\alpha, 1] \end{cases}$$

and f_c is a smooth function as before. Multiply by some test function $\psi \in H_0^1(\Omega)$, integrating by parts on $[0, \alpha]$ and $[\alpha, 1]$ and add the equations together we get

$$\int_0^1 (-\beta u_x \psi_x + ku\psi)dx + (\beta^-(\alpha)u_x^-(\alpha) - \beta^+(\alpha)u_x^+(\alpha))\psi(\alpha) = \int_0^1 f_c \psi dx \quad \forall \psi \in H_0^1(\Omega) \tag{4.11}$$

where the integrals should be understood in the classical sense. Compare with the equation (4.5) and recall Definition 3.3.13, we uniquely identify the jump conditions as

$$[u] = 0 \quad \text{and} \quad [\beta u_x] = \nu$$

□

Remark 9. *We can think of splitting (4.6) as decoupling the original equation (4.1) into two problems*

$$\begin{aligned} (\beta u_x^H)_x + ku^H &= f_c \quad \text{on } \Omega \\ u^H &= 0 \quad \text{on } \partial\Omega \end{aligned} \tag{4.12}$$

and

$$\begin{aligned} (\beta u_x^N)_x + ku^N &= \nu\delta_\alpha \quad \text{on } \Omega \\ u^N &= 0 \quad \text{on } \partial\Omega \end{aligned} \tag{4.13}$$

where the solution to (4.12) satisfies

$$[u^H]|_\alpha = 0 \quad [\beta u_x^H]|_\alpha = 0$$

and the solution to (4.13) fulfills

$$[u^N]|_\alpha = 0 \quad [\beta u_x^N]|_\alpha = \nu$$

Model problem 2

As before, we will proceed in the distributional sense. Find $u \in \mathcal{D}'(\Omega)$

$$\left\langle \partial^2 u, \psi \right\rangle = \left\langle f_c + \nu\delta_\alpha + w\delta'_\alpha, \psi \right\rangle \quad \forall \psi \in \mathcal{D}(\Omega)$$

Using the linearity of distributions and Def. 3.3.8 we get

$$\left\langle u, \partial^2 \psi \right\rangle = \left\langle f_c, \psi \right\rangle + \left\langle \nu\delta_\alpha, \psi \right\rangle + \left\langle w\delta'_\alpha, \psi \right\rangle \quad \forall \psi \in \mathcal{D}(\Omega)$$

Recall the definition of the delta and dipole functionals and apply Remark 5 (ii) we arrive at the following: Find $u \in L^2(\Omega)$

$$\int_\Omega u\psi_{xx} dx = \int_\Omega f_c \psi dx + \nu\psi(\alpha) - w\psi_x(\alpha) \quad \forall \psi \in H_0^2(\Omega) \tag{4.14}$$

Let

$$\begin{aligned} \hat{a}(u, \psi) &= \int_\Omega u\psi_{xx} dx \\ L_{\text{cont}}(\psi) &= \int_\Omega f_c \psi dx \\ L_{\text{disc1}}(\psi) &= \nu\psi(\alpha) \\ L_{\text{disc2}}(\psi) &= w\psi_x(\alpha) \end{aligned}$$

Then, the weak form reads: Find $u \in L^2(\Omega)$

$$\hat{a}(u, \psi) = L_{\text{cont}}(\psi) + L_{\text{disc1}}(\psi) + L_{\text{disc2}}(\psi) \quad \forall \psi \in H_0^2(\Omega)$$

We split the solution using the superposition principle

$$u = u^H + u^N + u^M$$

such that

$$\begin{aligned} \hat{a}(u^H, \psi) &= L_{\text{cont}}(\psi) \\ \hat{a}(u^N, \psi) &= L_{\text{disc1}}(\psi) \\ \hat{a}(u^M, \psi) &= -L_{\text{disc2}}(\psi) \end{aligned} \tag{4.15}$$

and approximate u^N and u^M by an explicitly calculated functions. Thus, we end up with: Find $u^H \in H_0^1(\Omega)$

$$\hat{a}(u^H, \psi) = L_{\text{cont}}(\psi) + L_{\text{disc1}}(\psi) - L_{\text{disc2}}(\psi) - \hat{a}(u^N, \psi) - \hat{a}(u^M, \psi) \quad \forall \psi \in H_0^2(\Omega) \tag{4.16}$$

Remark 10. *Using the same arguments as for the first model problem we get the following classical formulation of (4.2)*

$$\begin{aligned} u_{xx} &= f_c \quad \text{on } \Omega\backslash\alpha \\ u &= 0 \quad \text{on } \partial\Omega \end{aligned} \tag{4.17}$$

To obtain the additional boundary conditions at α we use the following theorem.

Theorem 4.2.2. *The solution to the model problem 2 (4.2) satisfies the following boundary conditions at the interface point α*

$$[u]|_\alpha = w, \quad [\beta u_x]|_\alpha = \nu \tag{4.18}$$

Proof. Consider equation (4.17)

$$u_{xx} = f_c \quad \text{on} \quad [0,\alpha] \cup [\alpha,1] \tag{4.19}$$

where f_c is a smooth function. Multiply by some test function $\psi \in H_0^2(\Omega)$, integrating by parts twice on $[0,\alpha]$ and $[\alpha,1]$ and add the equations together we get

$$\int_0^1 u\psi_{xx}dx + (u_x^-(\alpha) - u_x^+(\alpha))\psi(\alpha) + (u^+(\alpha) - u^-(\alpha))\psi_x(\alpha) = \int_0^1 f_c\psi dx \quad \forall\psi \in H_0^2(\Omega) \tag{4.20}$$

where the integrals should be understood in the classical sense. Compare with the equation (4.14) and recall Definition 3.3.13, we uniquely identify the jump conditions as

$$[u] = w \quad \text{and} \quad [u_x] = \nu$$

□

At this point we should note that

Remark 11. *Similar to the first model problem, the splitting (4.15) can be regarded as decoupling the original equation (4.2) into three separate problems*

$$\begin{aligned} (u_x^H)_x &= f_c \quad \text{on } \Omega \\ u^H &= 0 \quad \text{on } \partial\Omega \end{aligned}$$

$$\begin{aligned} (u_x^N)_x &= \nu\delta_\alpha \quad \text{on } \Omega \\ u^N &= 0 \quad \text{on } \partial\Omega \end{aligned}$$

and

$$\begin{aligned} (u_x^M)_x &= -w\delta'_\alpha \quad \text{on } \Omega \\ u^M &= 0 \quad \text{on } \partial\Omega \end{aligned}$$

with the following jumps for the solutions

$$\begin{aligned} [u^H]|_\alpha &= 0 \quad [u_x^H]|_\alpha = 0 \\ [u^N]|_\alpha &= 0 \quad [u_x^N]|_\alpha = \nu \\ [u^M]|_\alpha &= w \quad [u_x^M]|_\alpha = 0 \end{aligned} \tag{4.21}$$

Integrate by parts $\hat{a}(.,\psi)$ separately on $[0,\alpha]$ and $[\alpha,1]$ intervals we get

$$\begin{aligned} \hat{a}(u^M,\psi) &= -\int_0^\alpha u_x^M\phi_x dx - \int_\alpha^1 u_x^M\phi_x dx - [u^M]|_\alpha\phi_x = -a(u^M,\phi) - L_{\text{disc2}}(\phi) \\ \hat{a}(u^N,\psi) &= -\int_0^\alpha u_x^N\phi_x dx - \int_\alpha^1 u_x^N\phi_x dx - [u^N]|_\alpha\phi_x = -a(u^N,\phi) \\ \hat{a}(u^H,\psi) &= -\int_0^\alpha u_x^H\phi_x dx - \int_\alpha^1 u_x^H\phi_x dx - [u^H]|_\alpha\phi_x = -a(u^H,\phi) \end{aligned} \tag{4.22}$$

where

$$a(u,\phi)=\int_{\Omega\setminus\alpha}u_x\phi_x dx \tag{4.23}$$

and we have used (4.21). Substitute (4.22) in (4.16) we get: Find $u^H\in H_0^1(\Omega)$

$$-a(u^H,\phi)=L_{\text{cont}}(\phi)+L_{\text{disc1}}(\phi)+a(u^N,\phi)+a(u^M,\phi)\quad\forall\phi\in H_0^1(\Omega) \tag{4.24}$$

note, that the test function ψ belongs to $H_0^1(\Omega)$. This is due to fact that we have changed the bilinear form from $\hat{a}(.,.)$ to $a(.,.)$ such that we require only H^1 regularity of the test functions.

Model problem 3

Consider (4.3). This is a two-dimensional analog of (4.1) thus we will proceed in the similar way. Find $u\in\mathcal{D}'(\Omega)$

$$\left\langle\nabla\cdot(\beta\nabla u),\psi\right\rangle=\left\langle f_c+f\delta_\Gamma,\psi\right\rangle\quad\forall\psi\in\mathcal{D}(\Omega)$$

By linearity of distributions and Definition 3.3.8 we get

$$\begin{aligned}\left\langle\partial_1(\beta\partial_1 u),\psi\right\rangle+\left\langle\partial_2(\beta\partial_2 u),\psi\right\rangle&=\left\langle f_c,\psi\right\rangle+\left\langle f\delta_\Gamma,\psi\right\rangle\quad\forall\psi\in\mathcal{D}(\Omega)\\ -\left\langle\beta\partial_1 u,\partial_1\psi\right\rangle-\left\langle\beta\partial_2 u,\partial_2\psi\right\rangle&=\left\langle f_c,\psi\right\rangle+\left\langle f\delta_\Gamma,\psi\right\rangle\quad\forall\psi\in\mathcal{D}(\Omega)\end{aligned}$$

Recall the Definition 3.3.11 and Remark 6 (iv) we arrive at the following: Find $u\in V_0(\Omega)$

$$-\iint_\Omega\beta\nabla u\cdot\nabla\psi d\mathbf{x}=\iint_\Omega f_c\psi d\mathbf{x}+\int_\Gamma f(X(s))\psi(X(s))ds\quad\forall\psi\in V_0(\Omega) \tag{4.25}$$

Let

$$\begin{aligned}a(u,\psi)&=-\iint_\Omega\beta\nabla u\cdot\nabla\psi d\mathbf{x}\\ L_{\text{cont}}(\psi)&=\iint_\Omega f_c\psi d\mathbf{x}\\ L_{\text{disc1}}(\psi)&=\int_\Gamma f(X(s))\psi(X(s))ds\end{aligned}$$

Thus, the weak form reads: Find $u\in V_0(\Omega)$

$$a(u,\psi)=L_{\text{cont}}(\psi)+L_{\text{disc1}}(\psi)\quad\forall\psi\in V_0(\Omega)$$

Split the solution $u=u^H+u^N$ such that

$$\begin{aligned}a(u^H,\psi)&=L_{\text{cont}}(\psi)\\ a(u^N,\psi)&=L_{\text{disc1}}(\psi)\end{aligned} \tag{4.26}$$

approximate the discontinuous part of the solution u^N explicitly. Thus, we end up with: Find $u^H\in V_0(\Omega)$

$$a(u^H,\psi)=L_{\text{cont}}(\psi)+L_{\text{disc1}}(\psi)-a(u^N,\psi)\quad\forall\psi\in V_0(\Omega) \tag{4.27}$$

subject to homogeneous Dirichlet boundary conditions.

Remark 12. *Let $\Omega = \Omega^+ \cup \Omega^- \cup \Gamma$ and define two arbitrary test functions $\psi^+ \in H_0^1(\Omega^+)$ and $\psi^- \in H_0^1(\Omega^-)$. Since $H_0^1(\Omega^\pm) \subset H_0^1(\Omega)$ we can rewrite eq. (4.25) for two separate domains*

$$-\iint_\Omega \beta \nabla u \cdot \nabla \psi^\pm d\mathbf{x} = \iint_\Omega f_c \psi^\pm d\mathbf{x} \quad \forall \psi \pm \in V_0(\Omega^\pm) \tag{4.28}$$

Applying the Greens theorem to the left hand side yields the following classical formulation of the problem

$$\begin{aligned} \nabla \cdot (\beta \nabla u) &= f_c \quad \text{on } \Omega \backslash \Gamma \\ u &= 0 \quad \text{on } \partial\Omega \end{aligned} \tag{4.29}$$

The additional boundary conditions are obtained with the help of following theorem

Theorem 4.2.3. *The solution to the model problem 3 (4.3) satisfies the following boundary conditions at the interface Γ*

$$[u]|_\Gamma = 0, \quad \left[\beta \frac{\partial u}{\partial n}\right]\Big|_\Gamma = f \tag{4.30}$$

Proof. Consider equation (4.29)

$$\nabla \cdot (\beta \nabla u) = f_c \tag{4.31}$$

defined on the separate domains Ω^+ and Ω^-. Here β is

$$\beta = \begin{cases} \beta^-(x,y) & \text{on} \quad \Omega^+ \\ \beta^+(x,y) & \text{on} \quad \Omega^- \end{cases}$$

and f_c is a smooth function. Multiply by some test function $\psi \in H_0^1(\Omega)$, apply Greens theorem separately on Ω^+ and Ω^- and add the equations together we get

$$-\int_\Omega \beta \nabla u \cdot \nabla \psi d\mathbf{x} + (\beta^-(\alpha)\frac{\partial}{\partial n}u^-(\alpha) - \beta^+(\alpha)\frac{\partial}{\partial n}u^+(\alpha))\psi(\alpha) = \int_\Omega f_c \psi d\mathbf{x} \quad \forall \psi \in H_0^1(\Omega) \tag{4.32}$$

where the integrals should be understood in the classical sense. Compare with the equation (4.25) and recall Definition 3.3.14, we uniquely identify the jump conditions as

$$[u]|_\Gamma = 0 \quad \text{and} \quad \left[\beta \frac{\partial u}{\partial n}\right]\Big|_\Gamma = f$$

□

Remark 13. *In the same fashion as for the previous model problems, we think of (4.26) as solving*

$$\begin{aligned} \nabla \cdot (\beta \nabla u^H) &= f_c \quad \text{on } \Omega \\ u^H &= 0 \quad \text{on } \partial\Omega \end{aligned} \tag{4.33}$$

and

$$\begin{aligned} \nabla \cdot (\beta \nabla u^N) &= f\delta_\Gamma \quad \text{on } \Omega \\ u^N &= 0 \quad \text{on } \partial\Omega \end{aligned} \tag{4.34}$$

where the corresponding solutions satisfy

$$\begin{aligned} [u^H]|_\Gamma = 0 \quad \left[\beta \frac{\partial u^H}{\partial n}\right]\Big|_\Gamma = 0 \\ [u^N]|_\Gamma = 0 \quad \left[\beta \frac{\partial u^N}{\partial n}\right]\Big|_\Gamma = f \end{aligned} \tag{4.35}$$

Model problem 4

Similar to *model problem* 2: Find $u \in \mathcal{D}'(\Omega)$

$$\langle \Delta u, \psi \rangle = \langle f_c + \nabla \cdot \mathbf{F}, \psi \rangle \quad \forall \psi \in \mathcal{D}(\Omega)$$

where $\mathbf{F} = (F_1, F_2)^T = (f_1 \delta_\Gamma, f_2 \delta_\Gamma)^T$ and $f_c \in L^2(\Omega)$. Due to linearity and Definition 3.3.8 we get

$$\langle u, \Delta \psi \rangle = \langle f_c, \psi \rangle + \langle \partial_1 F_1, \psi \rangle + \langle \partial_2 F_2, \psi \rangle \quad \forall \psi \in \mathcal{D}(\Omega)$$

Recall Definition 3.3.11 and apply the Remark 6 (v) we end up with: Find $u \in L^2(\Omega)$

$$\iint_\Omega u \Delta \psi d\mathbf{x} = \iint_\Omega f_c \psi d\mathbf{x} - \int_\Gamma f_1(X(s)) \frac{\partial}{\partial x} \psi(X(s)) ds - \int_\Gamma f_2(X(s)) \frac{\partial}{\partial y} \psi(X(s)) ds \quad \forall \psi \in H_0^2(\Omega) \quad (4.36)$$

In order to split the solution in smooth/discontinuous parts, as we did previously, we have to identify discontinuous parts of the solution with the corresponding parts of the right hand side. We express $\frac{\partial \psi}{\partial x}$ and $\frac{\partial \psi}{\partial y}$ in terms of the normal and tangential derivatives along the interface

$$\begin{aligned} \frac{\partial \psi}{\partial x} &= \frac{\partial}{\partial n} \psi \cos(\Theta) - \frac{\partial}{\partial \tau} \psi \sin(\Theta) \\ \frac{\partial \psi}{\partial y} &= \frac{\partial}{\partial n} \psi \sin(\Theta) + \frac{\partial}{\partial \tau} \psi \cos(\Theta) \end{aligned}$$

where τ is a tangent vector, Θ is the angle between x-axis and outward normal vector n. Then

$$\begin{aligned} \int_\Gamma (f_1(X(s)) \frac{\partial}{\partial x} \psi(X(s)) + f_2(X(s)) \frac{\partial}{\partial y} \psi(X(s))) ds \\ = \int_\Gamma \Big(\big(f_1(X(s)) \cos(\Theta) + f_2(X(s)) \sin(\Theta) \big) \frac{\partial}{\partial n} \psi(X(s)) \\ + \big(f_2(X(s)) \cos(\Theta) - f_1(X(s)) \sin(\Theta) \big) \frac{\partial}{\partial \tau} \psi(X(s)) \Big) ds = \\ = \int_\Gamma (\hat{f}_1(X(s)) \frac{\partial}{\partial n} \psi(X(s)) + \hat{f}_2(X(s)) \frac{\partial}{\partial \tau} \psi(X(s))) ds \end{aligned}$$

where $\hat{f}_1(X(s))$ and $\hat{f}_2(X(s))$ are correspondingly the normal and tangential components of the force density $\mathbf{f}(X(s))$

$$\begin{aligned} \hat{f}_1(X(s)) &= f_1(X(s)) \cos(\Theta) + f_2(X(s)) \sin(\Theta) \\ \hat{f}_2(X(s)) &= -f_1(X(s)) \sin(\Theta) + f_2(X(s)) \cos(\Theta) \end{aligned} \quad (4.37)$$

Integrating the second term by parts and using the fact that the interface Γ is a closed curve

$$\begin{aligned} \int_\Gamma \hat{f}_2(X(s)) \frac{\partial}{\partial \tau} \psi(X(s))) ds = \hat{f}_2 \psi|_{s=s_1} - \hat{f}_2 \psi|_{s=s_0} - \\ \int_\Gamma \frac{\partial \hat{f}_2(X(s))}{\partial \tau} \psi(X(s)) ds = - \int_\Gamma \frac{\partial \hat{f}_2(X(s))}{\partial \tau} \psi(X(s)) ds \end{aligned}$$

Then

$$\iint_\Omega u\Delta\psi d\mathbf{x} = \iint_\Omega f_c\psi d\mathbf{x} + \int_\Gamma \frac{\partial}{\partial\tau}\hat{f}_2(X(s))\psi(X(s)) - \hat{f}_1(X(s))\frac{\partial}{\partial n}\psi(X(s))ds \tag{4.38}$$

and let

$$\begin{aligned}
\hat{a}(u,\psi) &= \iint_\Omega u\Delta\psi d\mathbf{x} \\
L_{\text{cont}}(\psi) &= \iint_\Omega f_c\psi d\mathbf{x} \\
L_{\text{disc1}}(\psi) &= \int_\Gamma \frac{\partial}{\partial\tau}\hat{f}_2(X(s))\psi(X(s))ds \\
L_{\text{disc2}}(\psi) &= \int_\Gamma \hat{f}_1(X(s))\frac{\partial}{\partial n}\psi(X(s))ds
\end{aligned}$$

Then, the weak form reads: Find $u \in L^2(\Omega)$

$$\hat{a}(u,\psi) = L_{\text{cont}}(\psi) + L_{\text{disc1}}(\psi) - L_{\text{disc2}}(\psi) \quad \forall\psi \in H_0^2(\Omega)$$

Similarly to model problem 2, represent the solution as

$$u = u^H + u^N + u^M \tag{4.39}$$

such that

$$\begin{aligned}
\hat{a}(u^H,\psi) &= L_{\text{cont}}(\psi) \\
\hat{a}(u^N,\psi) &= L_{\text{disc1}}(\psi) \\
\hat{a}(u^M,\psi) &= -L_{\text{disc2}}(\psi)
\end{aligned} \tag{4.40}$$

and approximate u^N and u^M explicitly. Thus our weak formulation reads: Find $u^H \in H_0^1(\Omega)$

$$\hat{a}(\tilde{u},\psi) = L_{\text{cont}}(\psi) + L_{\text{disc1}}(\psi) - L_{\text{disc2}}(\psi) - \hat{a}(u^N,\psi) - \hat{a}(u^M,\psi) \quad \forall\phi \in H_0^2(\Omega)$$

Remark 14. *Similar to the previous model problems, we derive the equivalent classical formulation*

$$\begin{aligned}
\Delta u &= f_c \quad \text{on } \Omega\backslash\Gamma \\
u &= 0 \quad \text{on } \partial\Omega
\end{aligned} \tag{4.41}$$

where the additional boundary conditions at the position of the interface Γ are given by the following theorem.

Theorem 4.2.4. *The solution to the model problem 4 (4.4) satisfies the following boundary conditions at the interface* Γ

$$[u]|_\Gamma = \hat{f}_1, \quad \left[\frac{\partial u}{\partial n}\right]\Big|_\Gamma = \frac{\partial}{\partial\tau}\hat{f}_2 \tag{4.42}$$

Proof. Consider (4.41)

$$\Delta u = f_c \quad \text{on} \quad \Omega_+ \cup \Omega_-$$

Apply Greens formula twice to the left hand side we get

$$\begin{aligned}\iint_{\Omega_+} \Delta u\psi d\mathbf{x} &= \iint_{\Omega_+} u\Delta\psi d\mathbf{x} - \int_\Gamma \frac{\partial}{\partial n}u^+\psi ds + \int_\Gamma u^+\frac{\partial}{\partial n}\psi ds \\ \iint_{\Omega_-} \Delta u\psi d\mathbf{x} &= \iint_{\Omega_-} u\Delta\psi d\mathbf{x} + \int_\Gamma \frac{\partial}{\partial n}u^-\psi ds - \int_\Gamma u^-\frac{\partial}{\partial n}\psi ds\end{aligned} \tag{4.43}$$

where $u_n^{\pm}$ is a derivative with respect to outward normal vector to the interface Γ and the superscripts $\pm$ indicate that solution approaches the interface from Ω_+ or Ω_- side, respectively. Add equations (4.43) together and recall the Definition 3.3.14 we obtain Find $u \in H_0^2(\Omega)$

$$\iint_\Omega u\Delta\psi d\mathbf{x} - \int_\Gamma \Big[\frac{\partial}{\partial n}u\Big]\psi ds + \int_\Gamma [u]\frac{\partial}{\partial n}\psi ds = \iint_\Omega f_c\psi d\mathbf{x} \quad \forall\psi \in H_0^2(\Omega) \tag{4.44}$$

Compare this equation with (4.38) and use the fact that ψ is arbitrary we get the following jump conditions

$$[u]|_\Gamma = \hat{f}_1 \quad \text{and} \quad [u_n]\Big|_\Gamma = (\nabla\hat{f}_2 \cdot \tau)$$

□

Remark 15. *By this time it should be evident that the splitting (4.40) can be regarded as solving three problems instead of the original (4.4). The first problem is*

$$\begin{aligned}\Delta u^H &= f_c \quad \text{on } \Omega \\ u^H &= 0 \quad \text{on } \partial\Omega\end{aligned} \tag{4.45}$$

the second one is given by

$$\begin{aligned}\Delta u^N &= \frac{\partial\hat{f}_2}{\partial\tau}\delta_\Gamma \quad \text{on } \Omega \\ u^N &= 0 \quad \text{on } \partial\Omega\end{aligned} \tag{4.46}$$

and the last one is defined as

$$\begin{aligned}\Delta u^M &= \nabla\cdot(n\hat{f}_1\delta_\Gamma) \quad \text{on } \Omega \\ u^M &= 0 \quad \text{on } \partial\Omega\end{aligned} \tag{4.47}$$

Here, $\hat{f}_1$ and $\hat{f}_2$ are defined in (4.37), and s is some parameterization parameter for the interface Γ. Additionally, the corresponding solutions must satisfy the following jump conditions

$$\begin{aligned}[u^H]|_\Gamma &= 0 \quad \Big[\frac{\partial u^H}{\partial n}\Big]\Big|_\Gamma = 0 \\ [u^N]|_\Gamma &= 0 \quad \Big[\frac{\partial u^N}{\partial n}\Big]\Big|_\Gamma = \frac{\partial\hat{f}_2}{\partial\tau} \\ [u^M]|_\Gamma &= \hat{f}_1 \quad \Big[\frac{\partial u^M}{\partial n}\Big]\Big|_\Gamma = 0\end{aligned} \tag{4.48}$$

Integrate by parts $\hat{a}(.,\psi)$ separately on Ω^+ and Ω^-

$$\begin{aligned}
\hat{a}(u^M,\psi) &= -\iint_{\Omega\setminus\Gamma} \nabla u^M \cdot \nabla\phi d\mathbf{x} - [u^M]|_\Gamma \phi_n = -a(u^M,\phi) - L_{\text{disc2}}(\phi) \\
\hat{a}(u^N,\psi) &= -\iint_{\Omega\setminus\Gamma} \nabla u^N \cdot \nabla\phi d\mathbf{x} - [u^N]|_\Gamma \phi_n = -a(u^N,\phi) \\
\hat{a}(u^H,\psi) &= -\iint_{\Omega\setminus\Gamma} \nabla u^H \cdot \nabla\phi d\mathbf{x} - [u^H]|_\Gamma \phi_n = -a(u^H,\phi)
\end{aligned} \tag{4.49}$$

where

$$a(u,\phi) = \iint_{\Omega\setminus\Gamma} \nabla u \cdot \nabla\phi d\mathbf{x} \tag{4.50}$$

and we have used (4.48). Substitute (4.49) in (4.38) we rewrite the weak form as follows: Find $u^H \in H_0^1(\Omega)$

$$-a(u^H,\phi) = L_{\text{cont}}(\psi) + L_{\text{disc1}}(\phi) + a(u^N,\phi) + a(u^M,\phi) \quad \forall\phi \in H_0^1(\Omega) \tag{4.51}$$

as for model problem 2, we note that we relax the regularity requirement on the test function ψ by applying the divergence theorem to bilinear form $\hat{a}(.,.)$ constrained to the separate regions Ω_+ and Ω_- only.

4.3 Finite Element Formulation of the 1-dimensional IIM

We now turn our attention to the construction of the discrete finite element spaces in one space dimension whose basis functions satisfy (or approximate) the jump conditions. Introduce a Cartesian uniform mesh $\Lambda_h = \{x_i = ih, \quad i = 1,2,...,n\}$ with the stepsize h and T being an element of the mesh. The interface reduces to one or several discrete points α_i that are not aligned with Λ_h.

Definition 4.3.1. *An element $T = [x_k, x_{k+1}]$ is called an* interface element *if the interface Γ passes through interior of T, otherwise we call T a non-interface element.*

In the next subsection, we introduce a finite element space on each element T of the partition Λ_h denoted by $\mathcal{F}_h(T)$. On the non-interface elements, the standard piecewise linear (hat) basis functions are used. Thus the modification to the hat functions is only needed on the interface elements. For the sake of completeness let us also define the following finite-dimensional spaces

$$\begin{aligned}
V^h &= \{v_h | v_h \in H^1(\Omega), v_h|_T \in P_1, \forall T \in \Lambda_h\} \\
V_0^h &= \{v_h | v_h \in V_0, v_h|_T \in P_1, \forall T \in \Lambda_h, v_h|\partial\Omega = 0\}
\end{aligned}$$

where P_1 is the space of polynomials of degree ≤ 1.

Model Problem 1

For the sake of simplicity assume that the interface is represented by a single point α and recall the solution of (4.7)

$$u = u^H + u^N$$

where u^H is subject to

$$[u^H]|_\alpha = 0 \quad \text{and } [\beta u_x^H]|_\alpha = 0 \tag{4.52}$$

and u^N satisfies

$$[u^N]|_\alpha = 0 \quad \text{and } [\beta u_x^N]|_\alpha = \nu \tag{4.53}$$

The discrete representation of u^H is a linear combination of the modified basis functions $\phi_i(x)$

$$u_h^H = \sum_{i=1}^{N-1} U_i^H \phi_i(x)$$

The need to modify the basis functions comes from the fact that jump conditions (4.52) won't be satisfied by the standard piecewise-linear basis. Thus, in general, the solution u_h^H will only be first order accurate in the L^∞ norm. To avoid the problem, we redefine the basis function on the interface elements using the jump conditions as external constraint

$$\phi_i(x_k) = \begin{cases} 1, & \text{if} \quad i = k \\ 0, & \text{otherwise} \end{cases}$$
$$[\phi_i(x)]|_\alpha = 0,$$
$$[\beta(\phi_i(x))_x]|_\alpha = 0$$

This modification to the basis functions was proposed by Li in [46]. Calculating the coefficients for the modified basis we end up with the following expressions

$$\phi_i(x_k) = \begin{cases} 0, & \text{if} \quad 0 \le x \le x_{j-1} \\ \dfrac{x - x_{j-1}}{h}, & \text{if} \quad x_{j-1} \le x \le x_j \\ \dfrac{x_j - x}{D} + 1, & \text{if} \quad x_j \le x \le \alpha \\ \rho\dfrac{x_{j+1} - x}{D}, & \text{if} \quad \alpha \le x \le x_{j+1} \\ 0, & \text{if} \quad x_{j+1} \le x \le 1 \end{cases} \tag{4.54}$$

and

$$\phi_{i+1}(x_k) = \begin{cases} 0, & \text{if} \quad 0 \le x \le x_j \\ \dfrac{x - x_j}{D}, & \text{if} \quad x_j \le x \le \alpha \\ \rho\dfrac{x - x_{j+1}}{D} + 1, & \text{if} \quad \alpha \le x \le x_{j+1} \\ \dfrac{x_{j+2} - x}{h}, & \text{if} \quad x_{j+1} \le x \le x_{j+2} \\ 0, & \text{if} \quad x_{j+2} \le x \le 1 \end{cases} \tag{4.55}$$

where

$$\rho = \frac{\beta^-}{\beta^+}, \quad D = h - \frac{\beta^+ - \beta^-}{\beta^+}(x_{j+1} - \alpha) = \rho(x_{j+1} - \alpha) + (\alpha - x_j)$$

In Figure 4.1, we can clearly see the kink in the basis function at the interface point α which reflects the jump condition in the derivative. Furthermore, define the local finite element space $\mathcal{F}_h(T)$ as follows:

$$\mathcal{F}^h(T) = \begin{cases} \{\phi_i(x) \quad | \quad \text{standard piecewise linear hat basis on the non-interface element} \quad T\} \\ \{\phi_i(x) \quad | \quad \text{given by (4.54) and (4.55) on the interface element} \quad T\} \end{cases} \tag{4.56}$$

Then the finite element space over all of Ω is given by

$$\mathcal{F}_0^h(\Omega) = \{\phi(x) \quad | \quad \forall T \in \Lambda_h, \quad \phi|_T \in \mathcal{F}^h(T), \quad \phi|_{\partial\Omega} = 0\} \tag{4.57}$$

Remark 16. *At this point we should point out that $\mathcal{F}_0^h(\Omega)$ is in many ways similar to the space of standard piecewise linear basis functions. Namely:*

- *On the non-interface elements the basis functions are equal to the usual hat functions.*
- *From (4.54) and (4.55) we also conclude that the modified basis functions are equal to the standard ones for the case when $\beta_+ = \beta_-$. Thus the space $\mathcal{F}_0^h(\Omega)$ reduces to the standard one $V_0^h(\Omega)$.*

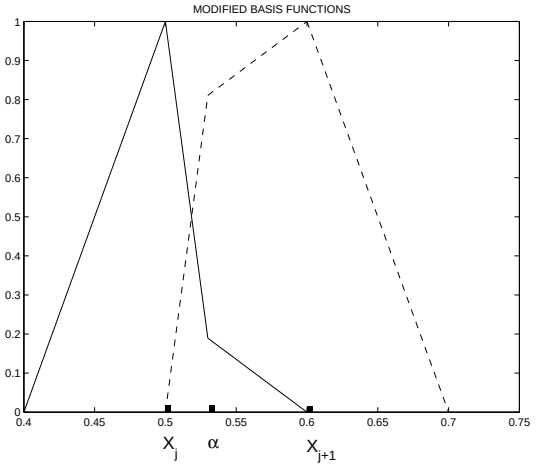

Figure 4.1: An example of the modified basis functions ϕ, satisfying $[\phi_i]|_\alpha = 0$ and $[\beta(\phi_i)_x]|_\alpha = 0$.

The discrete representation of u^N is a linear combination

$$u_h^N = u_h^{N,1} + u_h^{N,2}$$

where $u_h^{N,1}$ is defined over the entire computational domain, $u_h^{N,2}$ has support only on the interface element and they satisfy the following jump conditions

$$\begin{aligned} [u_h^{N,1}]|_\alpha = 0 \qquad & [u_h^{N,2}]|_\alpha = 0, \\ [\beta(u_h^{N,1})_x]|_\alpha = 0 \qquad & [\beta(u_h^{N,2})_x]|_\alpha = \nu \end{aligned}$$

The sole purpose of this additional splitting is to enforce the already known jump conditions in the solution of (4.7). As we can see (Figure 4.2) all irregularity of u_h^N is inherited by $u_h^{N,2}$, while $u_h^{N,1}$ is a function that belongs to $\mathcal{F}_0^h(\Omega)$. Thus to approximate $u_h^{N,1}$ we use the same modified basis functions as for u_h^H. That is

$$u_h^{N,1} = \sum_{i=1}^{N-1} U_i^N \phi_i(x) \in \mathcal{F}_0^h(\Omega)$$

while $u_h^{N,2}$ is approximated by

$$u_h^{N,2} = \begin{cases} 0, & \text{if} \quad 0 \le x \le x_j \\ \eta(x - x_j), & \text{if} \quad x_j \le x \le \alpha \\ (\rho\eta + \xi)(x - x_{j+1}), & \text{if} \quad \alpha \le x \le x_{j+1} \\ 0, & \text{if} \quad x_{j+1} \le x \le 1 \end{cases} \tag{4.58}$$

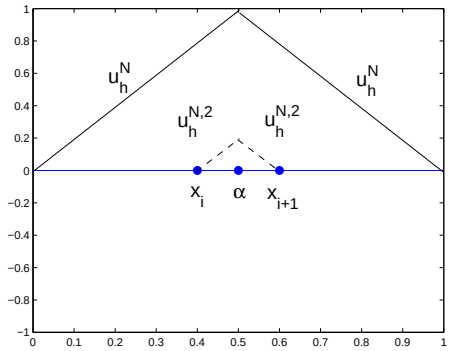

Figure 4.2: Discrete representation of the u^N part of the solution u. The solid line represents u_h^N and $u_h^{N,2}$ is shown as a dashed line.

where

$$\xi = \frac{\nu}{\beta^+}, \quad \eta = \frac{\xi(\alpha - x_{j+1})}{D}.$$

The coefficients of $u_h^{N,2}$ are obtained in the similar way as we did for $\phi_i(x)$. Since $u_h^H, u_h^{N,1} \in \mathcal{F}_0^h(\Omega)$, denote $\tilde{u}_h = u_h^H + u_h^{N,1} \in \mathcal{F}_0^h(\Omega)$. Then $u_h = \tilde{u}_h + u_h^{N,2}$, where $u_h^{N,2}$ is a approximated explicitly by (4.58) and

$$\tilde{u}_h = \sum_{i=1}^{N-1} U_i \phi_i(x)$$

Thus, the resulting discretisation of (4.7) reads: Find $\tilde{u}_h \in \mathcal{F}_0^h(\Omega)$

$$a(\tilde{u}_h, \psi) = L_{\text{cont}}(\psi) + L_{\text{disc1}}(\psi) - a(u_h^{N,2}, \psi) \quad \forall \psi \in \mathcal{F}_0^h(\Omega)$$

Model Problem 2

Similar to model problem 1, we represent the discrete solution as a linear combination

$$u_h = u_h^H + u_h^{N,1} + u_h^{N,2} + u_h^{M,1} + u_h^{M,2} = \tilde{u}_h + u_h^{N,2} + u_h^{M,2} \tag{4.59}$$

where $\tilde{u}_h \in \mathcal{F}_0^h(\Omega)$ is given by

$$\tilde{u}_h = u_h^H + u_h^{N,1} + u_h^{M,1} = \sum_{i=1}^{N-1} U_i \phi_i(x)$$

with ϕ_i defined by (4.57). The discrete linear functions $u_h^{N,2}$ and $u_h^{M,2}$ have support only on the interface element and satisfy

$$u_h^{N,2}(x_j) = u_h^{N,2}(x_{j+1}) = u_h^{M,2}(x_j) = u_h^{M,2}(x_{j+1}) = 0,$$
$$[u_h^{N,2}]|_\alpha = 0 \qquad [u_h^{M,2}]|_\alpha = w,$$
$$[(u_h^{N,2})_x]|_\alpha = \nu \qquad [(u_h^{M,2})_x]|_\alpha = 0$$

Here, $u_h^{N,2}$ is approximated by (4.58) and $u_h^{M,2}$ is given by

$$u_h^{M,2} = \begin{cases} 0, & \text{if} \quad 0 \le x \le x_j \\ \sigma(x_j - x), & \text{if} \quad x_j \le x \le \alpha \\ \rho\sigma(x_{j+1} - x), & \text{if} \quad \alpha \le x \le x_{j+1} \\ 0, & \text{if} \quad x_{j+1} \le x \le 1 \end{cases} \tag{4.60}$$

where $\sigma = w/D$.

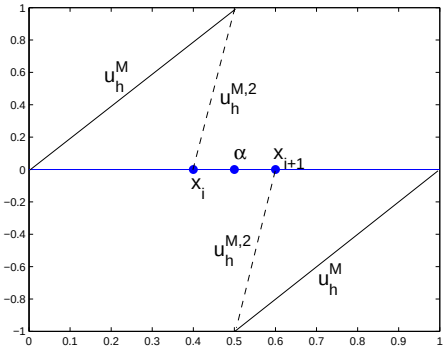

Figure 4.3: Discrete representation of the u^M part of the solution u. As before, the jump in u^M (solid line) is enforced through the explicitly calculated function $u_h^{M,2}$ (dashed line).

Substitute the discrete solution (4.59) in (4.24): Find $\tilde{u}_h \in \mathcal{F}_0^h(\Omega)$

$$-a(\tilde{u}_h, \psi) = L_{\text{cont}}(\psi) + L_{\text{disc1}}(\psi) + a(u_h^{N,2}, \psi) + a(u_h^{M,2}, \psi) \quad \forall \psi \in \mathcal{F}_0^h(\Omega)$$

4.4 Finite Element Formulation of the 2-dimensional IIM

Here, we introduce a non-conforming finite element space satisfying (approximating) the jump conditions and discuss the treatment of these jump conditions. Consider a rectangular domain Ω subdivided by the interface Γ (that is represented by a closed curve) in two subdomains Ω^+ and Ω^- such that $\Omega = \Omega^+ \cup \Omega^- \cup \Gamma$. An uniform triangulation $\mathcal{T}_h$ that is not aligned with the interface Γ is introduced with the stepsize h and T being an element of this triangulation.

Definition 4.4.1. *An element $T \in \mathcal{T}_h$ is called an* interface element *if the interface Γ passes through interior of T (we consider only the cases when interface Γ can cut at most two edges of the element T), otherwise we call T a* non-interface element.

Inside the interface element T the interface is approximated by a line segment that connects the intersections of the Γ with the edges of T (for example line segment $\overline{ED}$ in Figure 4.4) and separates the element in

$$T = T^+ \cup T^- \cup \overline{ED}$$

parts. At this point we should also mention that this particular representation of the interface introduces a $O(h^2)$ error in the solution. Namely, for every interface element T there is an area

$$T_r = T \backslash ((T^+ \cap \Omega^+) \cup (T^- \cap \Omega^-))$$

of order $O(h^3)$. The sum of this areas over all interface elements contribute to the perturbation in the interface position of $O(h^2)$ magnitude. From [42] and discussions in [50] we know that this perturbation will only affect the solution up to $O(h^2)$.

As is common practice, we introduce a finite element space on each element T of the partition $\mathcal{T}_h$ denoted by $\mathcal{S}_h(T)$. On the non-interface elements, the standard piecewise linear (pyramid) basis functions are used. The modification to the basis function is only required on the interface elements. We construct the modified basis function in the similar way as we did in the one-dimensional case, as it is described in the following subsections.

Model Problem 3

Similar to the one dimensional case, we represent the discrete solution as a combination

$$u_h = u_h^H + u_h^{N,1} + u_h^{N,2} = \tilde{u}_h + u_h^{N,2}$$

where $\tilde{u}_h = \sum_{i=1}^{N-1} U_i \phi_i(\mathbf{x})$ and $u_h^{N,2}$ is defined only on the interface elements and they satisfy

$$[\tilde{u}_h]|_\Gamma = 0 \qquad [u_h^{N,2}]|_\Gamma = 0,$$
$$\left[\beta \frac{\partial \tilde{u}_h}{\partial n}\right]\Big|_\Gamma = 0 \quad \left[\beta \frac{\partial u_h^{N,2}}{\partial n}\right]\Big|_\Gamma = f$$

Consequently, the linear basis functions $\phi_i(\mathbf{x})$ must satisfy the same jump conditions as $\tilde{u}_h$

$$[\phi_i(\mathbf{x})]|_\Gamma = 0 \quad \text{and} \quad \left[\beta \frac{\partial \phi_i}{\partial n}\right]\Big|_\Gamma = 0 \tag{4.61}$$

To introduce the appropriate modification to the basis functions $\phi_i(\mathbf{x})$, without loss of generality, we consider a general interface element showed in Figure 4.4

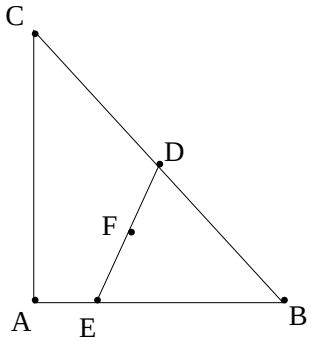

Figure 4.4: One of the three possible cases for the interface element. The line segment ED represents the approximated interface that cuts the triangle in T_+ and T_- parts. Here F is a middle point of the segment $\overline{ED}$.

We define the modified basis functions $\phi_i(\mathbf{x})$ as follows

$$\phi_i(\mathbf{x}) = \begin{cases} \phi_i^+ = C_1 + C_2 x + C_3 y \\ \phi_i^- = C_4 + C_5 x + C_6 y \end{cases}$$

where the $+$ or $-$ signs indicate if the function lies on plus or minus side of the interface. Additionally, let $\mathbf{x}_k$ be the coordinates of one of the nodes in the interface triangle (for example A,B or C in the Figure 4.4). Then the jump conditions (4.61) on the element T are approximated by

$$\begin{aligned} [\phi_i]|_\Gamma &= \begin{cases} \phi_i^+(D) - \phi_i^-(D) = 0, \\ \phi_i^+(E) - \phi_i^-(E) = 0, \end{cases} \\ \left[\beta \frac{\partial \phi_i}{\partial n}\right]\Big|_\Gamma &= \beta^+ \frac{\partial \phi_i^+(F)}{\partial n} - \beta^- \frac{\partial \phi_i^-(F)}{\partial n} = 0 \end{aligned} \tag{4.62}$$

where E and D are the points where the interface intersects with the element and F is the middle point of the line segment $\overline{ED}$. This approximation to the jumps together with the usual requirement that the basis function is unity in one of the nodes and zero in others

$$\phi_i(\mathbf{x}_k) = \begin{cases} 1, & \text{if} \quad i = k \\ 0, & \text{otherwise} \end{cases} \tag{4.63}$$

constitutes a 6×6 system of equations (with a small variation depending on where Γ cuts the element), see Figure 4.5 for a typical example of such modified piecewise linear basis function. As it was shown in [50] the solution of such system exists and is unique. Thus the local finite element space on each element T is given by

$$\mathcal{S}^h(T) = \begin{cases} \{\phi_i(\mathbf{x}) \quad | \quad \text{standard piecewise linear basis on the non-interface element} \quad T\} \\ \{\phi_i(\mathbf{x}) \quad | \quad \text{given by (4.62) and (4.63) on the interface element} \quad T\} \end{cases} \tag{4.64}$$

Then the finite element space over the entire computational domain Ω is defined as follows

$$\mathcal{S}_0^h(\Omega) = \{\phi(\mathbf{x}) \quad | \quad \forall T \in \mathcal{T}_h, \quad \phi|_T \in S^h(T), \quad \phi|_{\partial\Omega} = 0\} \tag{4.65}$$

At this point we should note:

Remark 17.
- *$\mathcal{S}_0^h(\Omega)$ is very similar to the usual linear finite element space defined on the $\mathcal{T}_h$. That is, on the non-interface elements they are the same. For the cases when there is no discontinuity present in the coefficient β the $\mathcal{S}_0^h(\Omega)$ space reduces the the standard one.*
- *Generally, $\mathcal{S}_0^h(\Omega)$ will be a non-conforming finite element space, since the basis function are not constrained to be continuous across the edges of the interface elements (see Figure 4.5 for a typical example).*
- *The approximation capability of $\mathcal{S}_0^h(\Omega)$ has been discussed in [50].*

Analogically to one-dimensional case we also introduce a piecewise linear function $u_h^{N,2}(\mathbf{x})$ (defined only on the interface elements) that satisfies the following conditions:

$$\begin{aligned} & u_h^{N,2}(A) = u_h^{N,2}(B) = u_h^{N,2}(C) = 0, \\ & [u_h^{N,2}]|_\Gamma = \begin{cases} (u_h^{N,2})^+(D) - (u_h^{N,2})^-(D) = 0, \\ (u_h^{N,2})^+(E) - (u_h^{N,2})^-(E) = 0, \end{cases} \\ & \left[\beta \frac{\partial u_h^{N,2}}{\partial n}\right]\Big|_\Gamma = \beta^+ \frac{\partial (u_h^{N,2})^+(F)}{\partial n} - \beta^- \frac{\partial (u_h^{N,2})^-(F)}{\partial n} = f(F) \end{aligned} \tag{4.66}$$

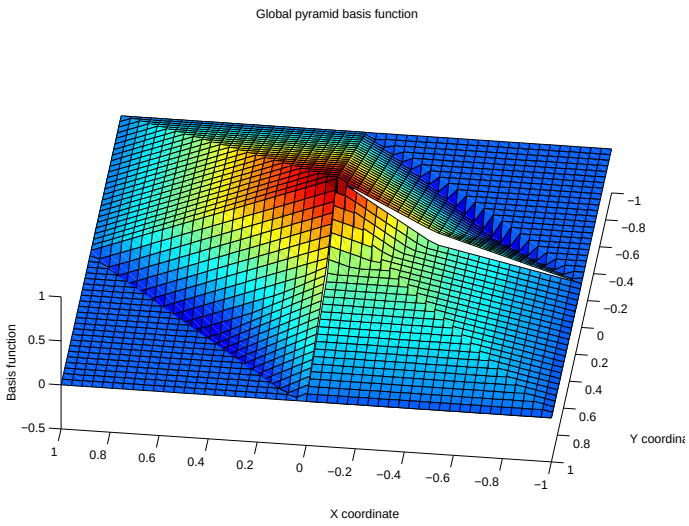

Figure 4.5: An example of the modified basis functions, satisfying $[\phi_i]|_\Gamma = 0$ and $[\beta(n \cdot \nabla\phi_i)]|_\Gamma = 0$. The discontinuity over the edges of interface elements are clearly seen.

with the coefficients of $u_h^{N,2}(\mathbf{x})$ obtained in the same manner (from a 6×6 system) as we did for $\phi_i(\mathbf{x})$. Substitute the discrete solution in the equation (4.27) we get: Find $\tilde{u}_h \in \mathcal{S}_0^h(\Omega)$

$$a(\tilde{u}_h, \psi) = L_{\text{cont}}(\psi) + L_{\text{disc1}}(\psi) - a(u_h^{N,2}, \psi) \quad \forall\psi \in \mathcal{S}_0^h(\Omega) \tag{4.67}$$

Model Problem 4

Finally, we consider the two dimensional model problem where the jump is imposed on both solution and its derivative. Here, the discrete representation of the solution (4.39) is given by

$$u_h = u_h^H + u_h^{N,1} + u_h^{N,2} + u_h^{M,1} + u_h^{M,2} = \tilde{u}_h + u_h^{N,2} + u_h^{M,2}$$

where $\tilde{u}_h \in \mathcal{S}_0^h(\Omega)$ is given by

$$\tilde{u}_h = \sum_{i=1}^{N-1} U_i\phi_i(x)$$

with $\phi_i \in \mathcal{S}_0^h(\Omega)$ defined by (4.65). The discrete linear functions $u_h^{N,2}$ and $u_h^{M,2}$ have support only on the interface element and satisfy

$$[u_h^{N,2}]|_\Gamma = 0 \qquad \left[\frac{\partial u_h^{N,2}}{\partial n}\right]\Big|_\Gamma = \partial\hat{f}_2/\partial\tau,$$
$$[(u_h^{M,2})_x]|_\Gamma = \hat{f}_1 \qquad \left[\frac{\partial u_h^{M,2}}{\partial n}\right]\Big|_\Gamma = 0$$

Here $u_h^{N,2}$ is approximated as before (by solving a 6×6 system originating from (4.66) with the appropriate value of the jump in the normal derivative of $u_h^{N,2}$) and $u_h^{M,2}$ is computed

by using the following conditions:

$$\begin{aligned} &u_h^{M,2}(A) = u_h^{M,2}(B) = u_h^{M,2}(C) = 0, \\ &[u_h^{M,2}]|_\Gamma = \begin{cases} (u_h^{M,2})^+(D) - (u_h^{M,2})^-(D) = \partial \hat{f}_2(D)/\tau, \\ (u_h^{M,2})^+(E) - (u_h^{M,2})^-(E) = \partial \hat{f}_2(E)/\tau, \end{cases} \\ &[n \cdot \nabla u_h^{M,2}]|_\Gamma = n \cdot \nabla (u_h^{M,2})^+(F) - n \cdot \nabla (u_h^{M,2})^-(F) = 0 \end{aligned} \tag{4.68}$$

Finally, we arrive at the following: Find $\tilde{u}_h \in \mathcal{S}_h$

$$-a(\tilde{u}_h, \psi) = L_{\text{cont}}(\psi) + L_{\text{disc1}}(\psi) + a(u_h^{N,2}, \psi) + a(u_h^{M,2}, \psi) \quad \forall \psi \in \mathcal{S}_0^h(\Omega) \tag{4.69}$$

4.5 Numerical Results

Here, we present the numerical results for both one and two dimensional problems. The main emphasis is to check how well our method can perform for various elliptic problems with discontinuous coefficients and singular distributions on the right hand side. For every test problem, we also compare the results from our approach with the ones obtained using the standard finite element method.

One-dimensional case

We begin by considering the one-dimensional test problems. For simplicity the computational domain is always an interval $\Omega = [a, b]$ and the interface is represented by one or several points α_i. Moreover, the solution satisfies homogeneous Dirichlet boundary conditions and is approximated on the uniform grid

$$x_i = a + ih \quad i = 0, 1, .., n \quad \text{with} \quad h = (b - a)/n$$

that is not aligned with the interface points. We will employ the discrete L^∞ and L^2 norms defined by

$$||E_n||_{L^\infty} = \max_j\{|e_j|\} \quad \text{and} \quad ||E_n||_{L^2} = \sqrt{h \sum_j e_j^2}$$

respectively. Here $e_j = u(x_j) - u_j$ is the error in the grid point x_j between the exact solution $u(x_j)$ and the approximate solution u_j. Note, that the grid $\{x_j\}$ is typically finer then $\{x_i\}$. We also display the ratios between the successive errors

$$ratio = ||E_n||_{L^\infty}/||E_{2n}||_{L^\infty}, \quad \text{or} \quad ||E_n||_{L^2}/||E_{2n}||_{L^2}$$

A ratio of 2 corresponds to first order accuracy, while a ratio of 4 indicates second order of accuracy.

Test problem 1

In this example we apply our method to a problem where there is both a delta functional and discontinuous coefficients. Let β be a piecewise constant function with a jump at some point α

$$\beta = \begin{cases} \beta_+, & \text{if } x \ \geq \alpha \\ \beta_-, & \text{if } x < \alpha \end{cases}$$

and define $\gamma_+ = \sqrt{1/\beta_+}$ and $\gamma_- = \sqrt{1/\beta_-}$. Then the differential equation is given by

$$(\beta u_x)_x + u = 1 + \delta_\alpha \quad \text{for} \quad x \in [0, 2/(\pi\gamma_+)]$$
$$u(0) = u(2/(\pi\gamma_+)) = 0$$

where $\alpha = \pi/(6\gamma_+)$, $\beta^- = 10$ and $\beta^+ = 100$. The exact solution to this problem is

$$u(x) = \begin{cases} C_1 \cos(x\gamma_-) + C_2 \sin(x\gamma_-) + 1, & \text{if} \quad 0 \le x < \alpha \\ C_3 \cos(x\gamma_+) + C_4 \sin(x\gamma_+) + 1, & \text{if} \quad \alpha \le x \le \pi/(2\gamma_+). \end{cases}$$

where the constants C_i's are chosen such that both the boundary and jump conditions are fulfilled, see Appendix A. The plots of the exact solution and its approximation are done for the resolution up to 2560 discretisation points (Figure 4.6). From the results we see that our method accurately gives the jump in the derivative. Table 4.1 shows the results of a grid refinement study for our method.

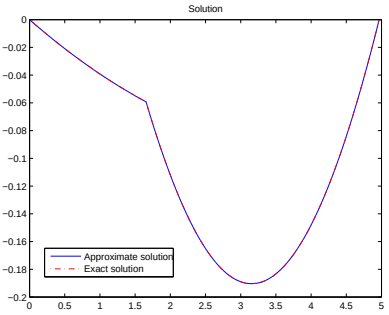

(a) The numerical and exact solutions.

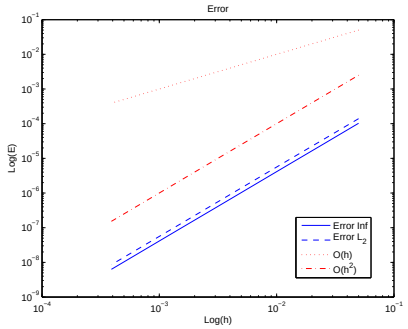

(b) The dot and the dash-dot lines represents the slope for first and second order accurate methods, respectively. The solid and the dashed lines show the error of our method in the L^∞ and L^2, correspondingly.

Figure 4.6: The solution and the error plots for test problem 1.

n	$\|\|E_n\|\|_\infty$	ratio	$\|\|E_n\|\|_{L^2}$	ratio
20	1.0274e-04	-	1.3948e-04	-
40	2.5714e-05	3.9954	3.4913e-05	3.9951
80	6.4418e-06	3.9917	8.7502e-06	3.9899
160	1.6106e-06	3.9996	2.1878e-06	3.9995
320	4.0282e-07	3.9984	5.4722e-07	3.9980
640	1.0070e-07	4.0000	1.3681e-07	4.0000

Table 4.1: Grid refinement study for the test problem 1 using FEM IIM.

Note that second order accuracy is obtained which is consistent with our expectations. The approximate solution obtained with the standard finite element method is expected to be of the first order accuracy, see Table 4.2. Though, if the interface points are aligned

n	$\|\|E_n\|\|_\infty$	ratio	$\|\|E_n\|\|_{L^2}$	ratio
20	1.2462e-02	-	1.4718e-02	-
40	6.0878e-03	2.0470	7.0033e-03	2.1016
80	3.1830e-03	1.9126	3.6570e-03	1.9151
160	1.5770e-03	2.0184	1.7995e-03	2.0322
320	7.9997e-04	1.9713	9.1262e-04	1.9718
640	3.9768e-04	2.0116	4.5291e-04	2.0150

Table 4.2: Grid refinement study for the test problem 1 using standard FEM.

with the grid points, the common finite element method will regain second order accuracy. Unfortunately in two or higher dimensions it can be very costly to create these sort of body-fitting grids.

Test problem 2

In this example we impose a jump on the solution itself but not on the derivative of the solution. That is we consider a problem with continuous part $f_c(x) = 0$, dipole as a source function and the interface represented by two points $\alpha_1 = 1/3$ and $\alpha_2 = 2/3$

$$u_{xx} = \delta'_{\alpha_1} - \delta'_{\alpha_2} \quad \text{for} \quad x \in [0,1]$$
$$u(0) = u(1) = 0$$

with the known jump conditions

$$[u]|_{\alpha_1} = 1, \quad [u]|_{\alpha_2} = -1, \quad [u_x]|_{\alpha_1} = [u_x]|_{\alpha_2} = 0$$

The exact solution in this case is

$$u(x) = \begin{cases} 0, & \text{for} \quad x \in [0, \alpha_1) \cup (\alpha_2, 1] \\ 1, & \text{for} \quad x \in (\alpha_1, \alpha_2) \end{cases}$$

n	$\|\|E_n\|\|_{L^2}$ standard FEM	ratio	$\|\|E_n\|\|_{L^2}$ IIM FEM	ratio
20	2.2212e-02	-	5.8934e-32	-
40	1.1131e-02	1.9955	8.7204e-31	-
80	5.5123e-03	2.0193	1.4784e-29	-
160	2.7787e-03	1.9838	8.2754e-30	-
320	1.3669e-03	2.0328	4.9155e-30	-
640	6.9444e-04	1.9683	1.1097e-28	-

Table 4.3: Grid refinement study for the test problem 2. The first column represents the results obtained with standard FEM, the second column corresponds to FEM IIM.

As we can see from the Figure 4.8, the actual error in the solution obtained with the standard FEM occurs only at those intervals that contain the interface points. Away from the interface points the solution is captured exactly since it is a a piecewise constant function. Our modified approach captures the piecewise linear discontinuous solution exactly

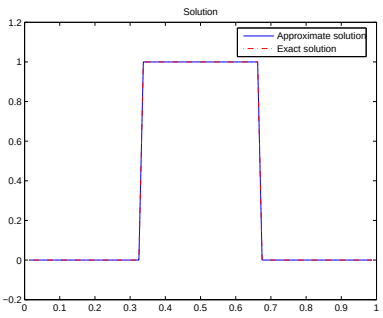

(a) The plot of the numerical solution with $n = 80$.

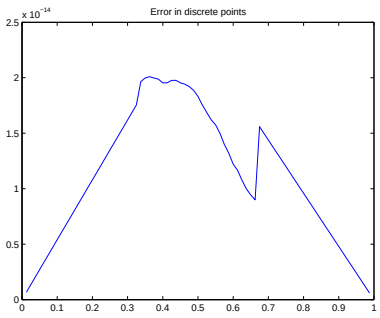

(b) The error in the solution.

Figure 4.7: The solution and the error plots for the test problem 2 for $n = 80$ using IIM FEM. Note that we obtain an error in the order of magnitude of a roundoff error for for other values of n as well.

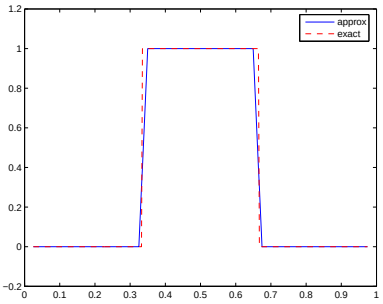

(a) The plot of the numerical solution with $n = 80$.

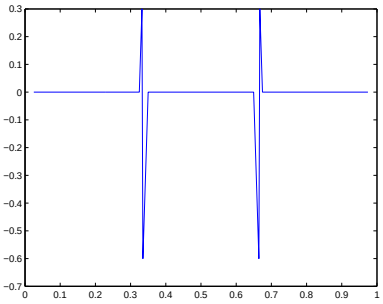

(b) The error in the solution.

Figure 4.8: The solution and the error plots for the test problem 2 for $n = 80$ using standard FEM.

up to roundoff, see Figure 4.7. Since the standard FEM always provides a continuous approximation, we expect the error to be of $O(1)$ in the L^∞ norm and $O(h)$ in the L^2 norm. For the IIM FEM we expect the error to be up to roundoff. In the Table 4.3 we present the grid refinement study for both methods using the L^2 norm. The standard FEM solution is only first order accurate while IIM FEM solution is exact up to roundoff.

Test problem 3

Finally, we impose the jump on both the solution and its derivative. Namely, the right hand side of the problem consists of both the dipole and delta functionals, $f_c(x) = 0$ and $\alpha = 1/3$

$$u_{xx} = \delta_\alpha + \delta'_\alpha, \quad \text{for} \quad x \in [0, 1]$$
$$u(0) = u(1) = 0$$

and the jump conditions given by

$$[u] = 1, \quad [u_x] = 1.$$

The exact solution is

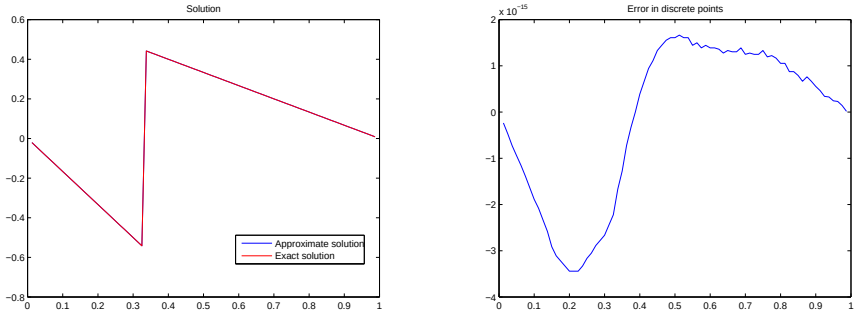

(a) The plot of the numerical solution with $n = 80$.

(b) The error in the solution

Figure 4.9: The solution and the error plot for the test problem 3 for $n = 80$ using IIM FEM. Again, note that the solution is exact up to roundoff.

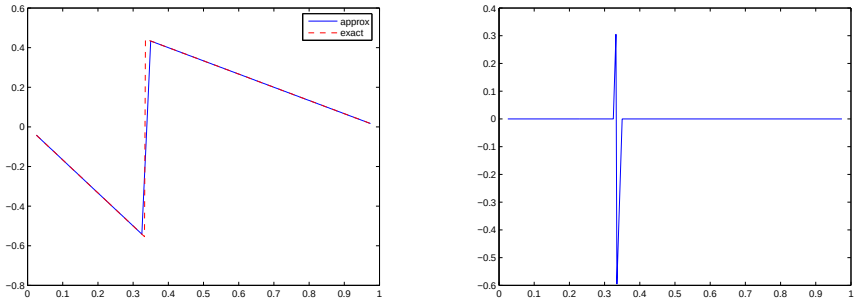

(a) The plot of the numerical solution with $n = 80$.

(b) The error in the solution

Figure 4.10: The solution and the error plot for the test problem 3 for $n = 80$ using standard FEM.

$$u(x) = \begin{cases} x(\alpha - 2), & \text{for} \quad x \in [0, \alpha) \\ (\alpha - 1)(x - 1) & \text{for} \quad x \in (\alpha, 1] \end{cases}$$

Similar to the test problem 2 the IIM FEM solution is exact up to roundoff, see Figure 4.9. The standard FEM delivers a solution that is first order accurate in the L^2 norm and produces $O(1)$ error in the L^∞ norm, Figure 4.10. See Table 4.4 for the tabulated results.

n	$\|\|E_n\|\|_{L^2}$ standard FEM	ratio	$\|\|E_n\|\|_{L^2}$ IIM FEM	ratio
20	5.6811e-03	-	9.5014e-32	-
40	2.7472e-03	2.0680	3.9825e-32	-
80	1.3966e-03	1.9671	5.6323e-32	-
160	6.9252e-04	2.0167	1.1149e-31	-
320	3.4771e-04	1.9917	5.7921e-30	-
640	1.7349e-04	2.0042	3.1085e-31	-

Table 4.4: Grid refinement study for the test problem 3. The first column represents the results obtained with standard FEM, the second column corresponds to FEM IIM.

Two-dimensional case

Here, we the investigate the performance of our modified finite element method for the two-dimensional elliptic problems. For the sake of simplicity, for all the test cases the computational domain Ω is the rectangle $-1 \leq x, y \leq 1$ and the interface Γ is represented by a circle with the center at the origin and with some radius r_0. For every problem the source term and the Dirichlet boundary conditions are determined from the exact solution. Once again, the main concern will be to investigate the performance of our modified approach and compare it to the results obtained with the standard finite element method, that is a standard conforming Galerkin finite element whose piecewise linear basis functions has not been modified. In all the test problems, the solution is approximated on the uniform $n \times n$ Cartesian mesh with m discrete points, representing the interface Γ. For the performance analysis we employ the discrete L^∞ and L^2 norms defined by

$$||E_n||_{L^\infty} = \max_{i,j}\{|e_{ij}|\} \quad \text{and} \quad ||E_n||_{L^2} = h\sqrt{\sum_{i,j} e_{ij}^2}$$

where $e_{ij} = u(x_i, y_j) - u_{ij}$ is the error in the grid point (x_i, y_j) between the exact solution $u(x_i, y_j)$ and the approximate solution u_{ij}. As in the one dimensional case, we display the ratios between the successive errors

$$ratio = ||E_n||_{L^\infty}/||E_{2n}||_{L^\infty}, \quad \text{or} \quad ||E_n||_{L^2}/||E_{2n}||_{L^2}$$

A ratio of 2 corresponds to first order accuracy, while a ratio of 4 indicates second order of accuracy.

Test problem 4

In this example we compare the results from our method and the standard FEM for a problem where there is a two-dimensional delta functional with the support on the interface Γ on the right hand side of the equation. Then the problem reads

$$\Delta u = 2\delta_\Gamma \quad \text{on} \quad \Omega$$

with the Dirichlet boundary conditions which are determined from the exact solution

$$u(\mathbf{x}) = \begin{cases} 1, & \text{if} \quad r \leq 1/2 \\ 1 + \log(2r), & \text{if} \quad r \geq 1/2. \end{cases} \tag{4.70}$$

where $r = \sqrt{x^2 + y^2}$ and the jump conditions

$$[u]|_\Gamma = 0 \quad \text{and} \quad [\partial u/\partial n]|_\Gamma = 2$$

Figure 4.11 shows the numerical solution obtained with the IIM FEM. As we can see, the jump in the normal derivative of the solution is captured sharply. In Tables 4.5 and 4.6 we present the grid refinement study for the IIM FEM. In Table 4.5 we fix $m = 400$ points on the interface and sequentially increase the resolution of the fixed background mesh while in Table 4.6 we do the opposite. That is, we fix 400×400 Cartesian mesh and refine the resolution of the interface.

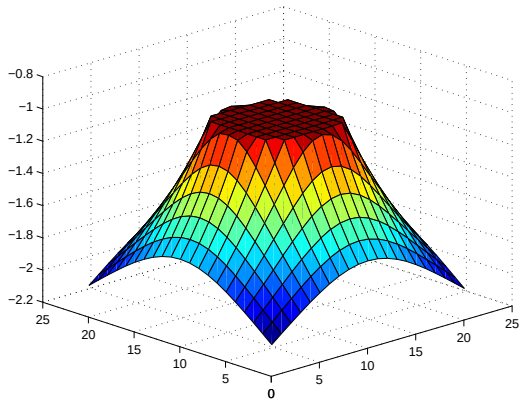

Figure 4.11: The inverse of the solution obtained by FEM IIM for the test problem 4 using 20×20 mesh.

$n \times n$	$\|\|E_n\|\|_\infty$	ratio	$\|\|E_n\|\|_{L^2}$	ratio
20	1.0727e-02	-	3.0438e-03	-
40	2.9084e-03	3.6883	6.2860e-04	5.4149
80	7.6542e-04	3.7998	1.4938e-04	4.2081
160	2.1134e-04	3.6217	3.8007e-05	3.9303

Table 4.5: Grid refinement study for the test problem 4 using the FEM IIM for $n \times n$ grids with 400 points on the interface.

In both cases second order convergence is obtained in L^∞ and L^2 norms. With the fixed resolution of the interface, we perform similar grid refinement study for the standard conforming FEM.

As we see from Table 4.7, the standard FEM has at most $p \approx 1.6$ order of convergence in the L^2 norm and first order convergence in the L^∞ norm. Notice, that since $\beta_- = \beta_+$ the modified basis is equal to the standard one. Thus the main difference from the usual FEM is the presence of

$$a(u_h^{N,2}, \psi) = \iint_{\Omega\setminus\Gamma} \beta \nabla u_h^{N,2} \cdot \nabla \psi d\mathbf{x}$$

on the right hand side of the variational formulation (4.67).

m	$\|\|E_n\|\|_\infty$	ratio	$\|\|E_n\|\|_{L^2}$	ratio
20	6.6108e-03	-	5.0629e-03	-
40	1.6681e-03	3.9631	1.2604e-03	4.0169
80	4.0783e-04	4.0902	3.0743e-04	4.0998
160	9.9335e-05	4.1056	7.3802e-05	4.1656

Table 4.6: Grid refinement study of the interface discretisation for the test problem 4 using the FEM IIM with the fixed 400×400 background mesh.

n	$\|\|E_n\|\|_\infty$	ratio	$\|\|E_n\|\|_{L^2}$	ratio
20	3.0096e-02	-	7.5408e-03	-
40	1.6072e-02	1.8725	2.3363e-03	3.2277
80	8.3142e-03	1.9331	7.3416e-04	3.1823
160	4.2287e-03	1.9661	2.4100e-04	3.0462

Table 4.7: Grid refinement study for the test problem 4 using the standard FEM for $n \times n$ grids with 400 points on the interface.

Test problem 5

We now consider a problem with the piecewise constant coefficient β. The equations are

$$\nabla \cdot (\beta \nabla u) = 9\sqrt{x^2 + y^2} \quad \text{on} \quad \Omega$$
$$\beta(\mathbf{x}) = \begin{cases} \beta^- & \text{if} \quad r \leq r0 \\ \beta^+ & \text{otherwise} \end{cases}$$

where the interface radius $r0 = \pi/6.28$ and the Dirichlet boundary conditions are given by the exact solution

$$u(\mathbf{x}) = \begin{cases} r^3/\beta^-, & \text{if} \quad r \leq r0 \\ r^3/\beta^+ + (1/\beta^- - 1/\beta^+) r_0^3, & \text{otherwise} \end{cases}$$

It is easy to check that in this case the solution and its flux are continuous ($[u]|_\Gamma = 0$ and $[\beta \partial u/\partial n]|_\Gamma = 0$). In this test problem, the emphasis is to investigate how well the modified and the standard schemes can handle the jump in the β coefficient. The FEM IIM solution for the case when $\beta_+ = 1000, \beta_- = 1$ is presented in Figures 4.12. Note, that the jump in the normal derivative of the solution caused by the large difference in the coefficients is captured sharply.

The convergence studies for the case when $\beta_+ = 1000$ and $\beta_- = 1$ for IIM FEM are presented in Tables 4.8 and 4.9. For the second case with $\beta_+ = 1$ and $\beta_- = 1000$ the results are shown in Table 4.11.

Note, that for both ratios the modified approach exhibits second order convergence in the L^2. The standard FEM is atmost first order accurate in both norms, see Tables 4.10 and 4.12.

n	$\|\|E_n\|\|_\infty$	ratio	$\|\|E_n\|\|_{L^2}$	ratio
20	4.0595e-03	-	1.4868e-03	-
40	1.5311e-03	2.6514	4.8463e-04	3.0679
80	5.5109e-04	2.7783	1.0785e-04	4.4936
160	1.5760e-04	3.5079	2.4501e-05	4.4019

Table 4.8: Grid refinement study for the test problem 5 with $\beta_+ = 1000$ and $\beta_- = 1$ using the FEM IIM for $n \times n$ grids with 400 points on the interface.

m	$\|\|E_n\|\|_\infty$	ratio	$\|\|E_n\|\|_{L^2}$	ratio
20	4.5810e-03	-	2.7894e-03	-
40	1.1719e-03	3.9090	7.0470e-04	3.9583
80	3.4362e-04	3.4105	1.7423e-04	4.0447
160	1.0021e-04	3.4290	4.2478e-05	4.1017

Table 4.9: Grid refinement study of the interface discretisation for the test problem 5 with $\beta_+ = 1000$ and $\beta_- = 1$ using the FEM IIM with the fixed 400×400 background mesh.

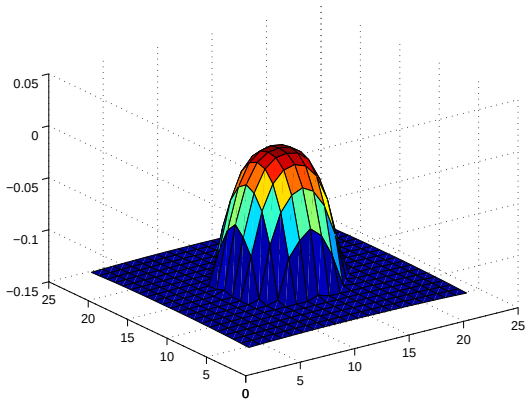

Figure 4.12: The inverse of the solution for the test problem 5 with piecewise constant coefficients $\beta_+ = 1000$ and $\beta_- = 1$ using 20×20 mesh.

n	$\|\|E_n\|\|_\infty$	ratio	$\|\|E_n\|\|_{L^2}$	ratio
20	6.1865e-02	-	3.9485e-02	-
40	3.6550e-02	1.6926	2.0004e-02	1.9739
80	1.9453e-02	1.8789	9.7176e-03	2.0585
160	9.3965e-03	2.0702	4.3156e-03	2.2517

Table 4.10: Grid refinement study of the interface discretisation for the test problem 5 with $\beta_+ = 1000$ and $\beta_- = 1$ using the standard FEM.

n	$\|\|E_n\|\|_\infty$	ratio	$\|\|E_n\|\|_{L^2}$	ratio
20	2.2484e-03	-	1.6318e-03	-
40	1.2201e-03	1.8428	4.3821e-04	3.7238
80	2.6801e-04	4.5524	1.0410e-04	4.2095
160	8.5229e-05	3.1446	2.4940e-05	4.1740

Table 4.11: Grid refinement study for the test problem 5 with $\beta_+ = 1$ and $\beta_- = 1000$ using the FEM IIM for $n \times n$ grids with 400 points on the interface.

n	$\|\|E_n\|\|_\infty$	ratio	$\|\|E_n\|\|_{L^2}$	ratio
20	3.9971e-02	-	3.2445e-02	-
40	2.1669e-02	1.8446	2.0443e-02	1.5871
80	1.1219e-02	1.9315	1.0352e-02	1.9748
160	6.1210e-03	1.8328	5.6070e-03	1.8462

Table 4.12: Grid refinement study for the test problem 5 with $\beta_+ = 1$ and $\beta_- = 1000$ using standard FEM.

Test problem 6

Here, we consider more elaborate problem with both discontinuous coefficients and a singular source function

$$\nabla \cdot (\beta \nabla u) = f_c(\mathbf{x}) + C\delta_\Gamma \quad \text{on} \quad \Omega$$
$$f_c(\mathbf{x}) = 8(x^2 + y^2) + 4$$
$$\beta(\mathbf{x}) = \begin{cases} x^2 + y^2 + 1, & \text{if} \quad r \le 0.5 \\ b, & \text{otherwise} \end{cases}$$

with $C = 0.1$, $b = 10$ and the boundary conditions given by the exact solution

$$u(\mathbf{x}) = \begin{cases} r^2, & \text{if} \quad r \le 0.5 \\ (1 - 1/(8b) - 1/b)/4 + (r^4/2 + r^2)/b + C\log(2r)/b, & \text{otherwise} \end{cases}$$

n	$\|\|E_n\|\|_\infty$	ratio	$\|\|E_n\|\|_{L^2}$	ratio
20	5.4989e-02	-	1.5642e-02	-
40	2.6735e-02	2.0568	4.2840e-03	3.6511
80	1.3026e-02	2.0524	1.1375e-03	3.7662
160	6.4181e-03	2.0296	2.6921e-04	4.2253

Table 4.13: Grid refinement study for the test problem 6 with $\beta = 10$ and $C = 0.1$ using IIM FEM for $n \times n$ grids with 400 points on the interface.

Tables 4.13 and 4.14 gives the numerical results for the IIM FEM and the standard FEM, respectively. The computed solution is presented in Figure 4.13. In this case the error in L^∞ norm is of first order, while the solution is still second order accurate in the L^2 norm.

n	$\|\|E_n\|\|_\infty$	ratio	$\|\|E_n\|\|_{L^2}$	ratio
20	4.0315e-02	-	2.6917e-02	-
40	2.2166e-02	1.8188	1.4601e-02	1.8436
80	1.1606e-02	1.9099	6.8580e-03	2.1290
180	6.2381e-03	1.8605	3.7439e-03	1.8318

Table 4.14: Grid refinement study for the test problem 6 with $\beta = 10$, $C = 0.1$ and with 400 points on the interface using standard FEM.

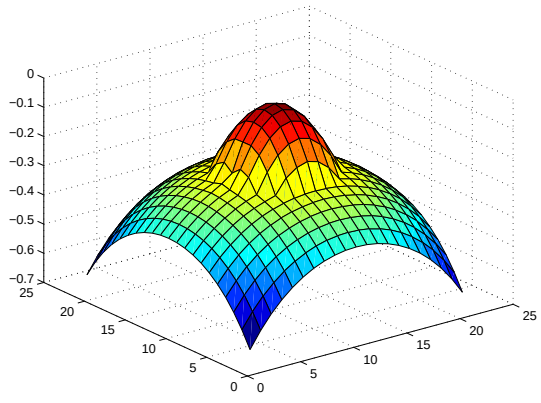

Figure 4.13: The inverse of the solution for the test problem 6 using 20×20 mesh.

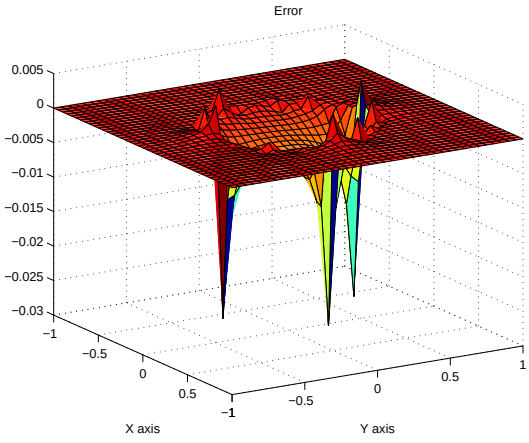

Figure 4.14: The error plot for the test problem 6 computed on the 41×41 mesh.

This is due to the fact that the jump in the normal flux of the solution is approximated only at one single point per element. Thus, in the cases when the magnitude of the jump is non-constant or the coefficient β is a function of x and y (on either side of the interface)

the L^∞ norm will only capture the spikes in error (see Figure 4.14).

Test problem 7

Finally, we impose a jump on both the solution and its normal derivative. The differential equation on each side of the interface Γ is just a Laplace equation

$$\Delta u = 0 \quad \text{on } \Omega \backslash \Gamma$$

The jumps

$$[u]|_\Gamma = e^x cos(y), \quad \text{and} \quad [\partial u/\partial n]|_\Gamma = n \cdot [e^x cos(y), -e^x sin(y)]^T$$

and the boundary conditions are found from the exact solution

$$u(\mathbf{x}) = \begin{cases} e^x cos(y), & \text{if } r \leq 1/2 \\ 0, & \text{if } r \geq 1/2. \end{cases}$$

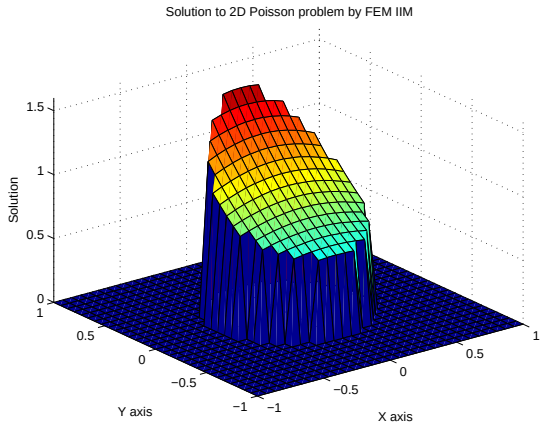

Figure 4.15: The solution for the test problem 7 using 40×40 mesh.

n	$\|\|E_n\|\|_{L^2}$ standard FEM	ratio	$\|\|E_n\|\|_{L^2}$ IIM FEM	ratio
20	2.2488e-01	-	2.3973e-04	-
40	1.2820e-01	1.7541	6.2697e-05	3.8236
80	8.2396e-02	1.5559	1.9771e-05	3.1711
160	5.3091e-02	1.5520	6.2049e-06	3.1864

Table 4.15: Grid refinement study for the test problem 7 with 400 points on the interface. The first column corresponds to the standard FEM, the second represents the results of the IIM FEM.

Table 4.15 shows that IIM FEM has $p \approx 1.6$ order of convergence in the L^2 norm while standard FEM is at most first order accurate. Since the standard FEM provides the continuous approximation to the solution the L^∞ norm of the error is expected to be of $O(1)$ and thus is not presented.

4.6 Conclusions

We have proposed and tested a relatively simple modification of the standard finite element method based on the immersed interface method. It has been shown that the modified approach can handle well both one and two-dimensional elliptic problems with severe discontinuities in the coefficients and singularities represented by the delta and/or dipole functionals. Moreover the new approach proved to be higher then first order accurate in both the L^2 and the L^∞ norms for the considered elliptic interface problems. Additionally, we should remind that our method uses meshes that are not aligned with the interface.

Potentially, our approach can be applied to other type of problems containing discontinuous coefficients or singular forces. All that is required is the explicit knowledge of the jump conditions of the solution and its flux. In the next Chapter we will show that our approach can be successfully applied to even more sophisticated problems, such as an incompressible Stokes equation with a moving immersed interface.

Chapter 5

Finite Element Formulation of the IIM for the interface Stokes problem

5.1 Overview

In this chapter we apply our modified finite element IIM to the interface Stokes problem, modeling an incompressible, viscous flow at low Reynolds numbers with some moving inner boundaries within it. This moving boundary may represent a contact discontinuity between two different fluids without any separating material or some material immersed in a fluid. In this thesis, we will concentrate on a two-dimensional material interface problems.

In two space dimensions Stokes equations take the form

$$\begin{aligned} \nabla p &= \mu \Delta \mathbf{u} + \mathbf{F} \\ \nabla \cdot \mathbf{u} &= 0 \end{aligned} \tag{5.1}$$

where p is the pressure, $\mathbf{u} = (u_1, u_2)$ is the velocity vector and $\mathbf{F} = (F_1, F_2)^T$ is an external singular force exerted by the immersed interface Γ on the fluid. The necessary boundary conditions will be discussed later. The source term $\mathbf{F}$ can be written as

$$\mathbf{F}(\mathbf{x}, t) = \mathbf{f}(\mathbf{x}, t)\delta_\Gamma$$

where $\mathbf{f}(\mathbf{x}, t) = (f_1(\mathbf{x}, t), f_2(\mathbf{x}, t))^T$ is the force density in this point and δ_Γ is a two-dimensional delta functional. This force is best viewed as a generalized function, or distribution. That is for any suffiently smooth test function $\psi(\mathbf{x})$ we have

$$\big\langle F_i(\mathbf{x}, t), \psi(\mathbf{x}) \big\rangle = \int_\Omega f_i(\mathbf{x}, t)\delta_\Gamma \psi(\mathbf{x}) d\mathbf{x} = \int_\Gamma f_i(\mathbf{X}(s), t)\psi(\mathbf{X}(s)) ds$$

where $\mathbf{X}(s, t)$ gives the location of the interface at time t with some parameterization s for $s_0 \le s \le s_1$. Moreover, the equation (5.1) should also be understood in the distributional sense.

To solve (5.1), we first reduce it to a sequence of three separate Poisson problems, one for the pressure and two for the velocity vector. That is, we multiply the equations (5.1) by some test function $\psi \in \mathcal{D}(\Omega)$ and differentiate the first momentum equation with respect to x and the second one with respect to y in the distributional sense and use the linearity of the distributions

$$\begin{aligned} \big\langle \partial_1^2 p, \psi \big\rangle &= \mu(\big\langle \partial_1^3 u_1, \psi \big\rangle + \big\langle \partial_1 \partial_2^2 u_1, \psi \big\rangle) + \big\langle \partial_1 F_1, \psi \big\rangle \\ \big\langle \partial_2^2 p, \psi \big\rangle &= \mu(\big\langle \partial_2 \partial_1^2 u_2, \psi \big\rangle + \big\langle \partial_2^3 u_2, \psi \big\rangle) + \big\langle \partial_2 F_2, \psi \big\rangle \end{aligned} \tag{5.2}$$

Add the equations (5.2) together to get

$$\langle \partial_1^2 p + \partial_2^2 p, \psi \rangle = \mu(\langle \partial_1^2(\partial_1 u_1 + \partial_2 u_2), \psi \rangle + \langle \partial_2^2(\partial_1 u_1 + \partial_2 u_2), \psi \rangle) + \langle \partial_1 F_1 + \partial_2 F_2, \psi \rangle \quad \forall \psi \in \mathcal{D}(\Omega) \quad (5.3)$$

Use the incompressibility condition

$$\langle \partial_1 u_1 + \partial_2 u_2, \zeta \rangle = 0 \quad \forall \zeta \in \mathcal{D}(\Omega)$$

together with the Definition 3.3.8 in (5.3) we get the pressure equation that reads

$$\langle \partial_1^2 p + \partial_2^2 p, \psi \rangle = \langle \partial_1 F_1 + \partial_2 F_2, \psi \rangle \quad \forall \psi \in \mathcal{D}(\Omega)$$

or

$$\langle \Delta p, \psi \rangle = \langle \nabla \cdot \mathbf{F}, \psi \rangle \quad \forall \psi \in \mathcal{D}(\Omega) \quad (5.4)$$

with the appropriate boundary conditions. Since $\mathbf{F}$ is a known function we can obtain the pressure directly. Once the pressure is known, we can separately solve both momentum equations to obtain the velocity components. We note that time-dependence of the flow comes entirely from the right hand side $\mathbf{F}$, but since $\mathbf{F}$ is explicitly known at every particular instance of time the system becomes elliptic and the solution $(\mathbf{u}, p)$ can be determined independently of the previous time.

We will consider a model problem introduced by Tu and Peskin [9], and later used by Leveque and Li in [32]. In this problem the interface represents an immersed elastic band in a fluid and the properties of the fluid are the same on both sides of the interface. This problem can be regarded as a two-dimensional analog of a elastic balloon in a homogeneous highly viscous fluid. In equilibrium configuration, this elastic band will take a circular shape, with piecewise constant pressure (experiencing a jump along the band) and zero velocity everywhere. The magnitude of the pressure jump depends on how much the band is stretched from its resting configuration.

By the *equilibrium configuration* we always mean the steady state solution with a given quantity of fluid inside the encircled area. In this configuration, the band will be stretched since the fluid inside it cannot escape. In contrast, the *resting configuration* is obtained if we allow a small leak of the fluid from the encircled area, until the exerted elastic force vanishes, together with the pressure difference. Since the flow is incompressible, the band perturbed from its equilibrium position should return to it after some time.

The force densities $\mathbf{f}(\mathbf{X}(s), t)$ are established solely from the position of the interface. Namely, we start from Newton's Second Law stating the equivalence of mass times acceleration to a sum of all forces, which in our case are the tension force and force exerted from the fluid to the interface

$$m(s)\frac{\partial^2 \mathbf{X}}{\partial t^2} = \mathbf{F}_T(s,t) + \mathbf{F}_R(s,t), \quad (5.5)$$

The tension force $\mathbf{F}_T(s,t)$ is represented by

$$\mathbf{F}_T(s,t) = \frac{\partial}{\partial s}(T\tau)$$

where τ is the interface tangent vector at $\mathbf{X}(s,t)$

$$\tau(s,t) = \frac{\partial \mathbf{X}}{\partial s} \Big/ \Big|\frac{\partial \mathbf{X}}{\partial s}\Big|$$

and $T(s,t)$ is the tension at the same point defined by the Hooke's Law

$$T(s,t) = T_0\Big(\Big|\frac{\partial \mathbf{X}(s,t)}{\partial s}\Big| - 1\Big)$$

The elastic properties of the band are represented by the scalar T_0 (which we assume uniform for our problem).

The force $\mathbf{F}_R(s)$ is measured in terms of the jumps in pressure and in the derivative of the velocity in the fluid

$$\mathbf{F}_R(s,t) = \Big[-p(s,t)n + \mu\frac{\partial \mathbf{u}(s,t)}{\partial n}\Big]$$

The quantity $-p(s,t)n + \mu\frac{\partial \mathbf{u}(s,t)}{\partial n}$ is known as the normal stress of the fluid element, in terms of the fluid stress tensor. These jumps are what we need for our method. However, it is not possible to compute these jumps directly from the fluid equations. Instead we obtain the jumps by subtracting the inertial terms on the left hand side of equation (5.5) from the tension force

$$\mathbf{f}(s,t) = -\Big[-p(s,t)n + \mu\frac{\partial \mathbf{u}(s,t)}{\partial n}\Big] = \frac{\partial}{\partial s}(T\tau) - m(s)\frac{\partial^2 \mathbf{X}}{\partial t^2}$$

In this thesis, we consider an important special case of a massless interface $m(s) = 0$. Thus the expression for the force densities reduces to

$$\mathbf{f}(s,t) = \frac{\partial}{\partial s}(T\tau) \tag{5.6}$$

Note that when s is an arclength parameter, the density of the elastic force $\mathbf{f}(s,t) = 0$ for a relaxed state, since $\Big|\frac{\partial}{\partial s}\mathbf{X}(s,t)\Big| = 1$.

To apply our finite element IIM discussed earlier we need an explicit expressions for jump conditions for each of the three Poisson problems (for pressure p and velocity components u_1, u_2). Namely, we have to know both the jump in the function and in its normal derivative at any point along the interface. The idea of derivation of the jump condition is the same as used in the model problems. In the next subsections we show that the velocity vector $\mathbf{u} = (u_1, u_2)$ is continuous across the inner boundary, while its normal derivatives are discontinuous. We also prove that the pressure is discontinuous itself together with its normal derivative.

5.2 Variational formulation of the interface Stokes problem

In this section, we present the variational formulation of the interface Stokes problem and derive the necessary jump conditions. This is done in the following way: We start with the the pressure Poisson problem (5.4), derive the appropriate jump conditions and present the corresponding weak formulation. Next, we proceed to the velocity components. With the known right hand side and computed pressure, the momentum equations in (5.1) decouples in two separate Poisson problem. Since they are essentially identical we will explain the procedure in detail only for one of them, say to obtain u_1. For u_2 we will simply state the weak formulation and the corresponding jump conditions.

Pressure Poisson problem

With the location of the interface fixed at some moment of time, we wish to solve the Poisson problem for pressure (5.4) with the force densities of $\mathbf{F}$ given by (5.6) and appropriate boundary conditions.

This problem is similar to the Model problem 4 discussed in the Chapter 4. Thus, we will treat this problem in a same fashion. By Definition 3.3.8 we get

$$\langle p, \Delta\psi \rangle = \langle \partial_1 F_1, \psi \rangle + \langle \partial_2 F_2, \psi \rangle \quad \forall \psi \in \mathcal{D}(\Omega)$$

From Definition 3.3.11 and Remark 6 (v) we have: Find $p \in L^2(\Omega)$

$$\iint_\Omega p\Delta\psi d\mathbf{x} = -\int_\Gamma f_1(\mathbf{X}(s,t),t)\frac{\partial}{\partial x}\psi(\mathbf{X}(s,t),t)ds - \int_\Gamma f_2(\mathbf{X}(s,t),t)\frac{\partial}{\partial y}\psi(\mathbf{X}(s,t),t)ds \quad \forall \psi \in H_0^2(\Omega) \quad (5.7)$$

In order to apply the superposition principle, we have to identify discontinuous parts of the solution with the corresponding parts of the right hand side. We express $\frac{\partial\psi}{\partial x}$ and $\frac{\partial\psi}{\partial y}$ in terms of the normal and tangential derivatives along the interface

$$\begin{aligned}\frac{\partial\psi}{\partial x} &= \frac{\partial}{\partial n}\psi\cos(\Theta) - \frac{\partial}{\partial\tau}\psi\sin(\Theta)\\ \frac{\partial\psi}{\partial y} &= \frac{\partial}{\partial n}\psi\sin(\Theta) + \frac{\partial}{\partial\tau}\psi\cos(\Theta)\end{aligned}$$

where Θ is the angle between an outward normal vector n and x-axis and τ is the tangent vector. Then

$$\begin{aligned}&\int_\Gamma (f_1(\mathbf{X}(s,t),t)\frac{\partial}{\partial x}\psi(\mathbf{X}(s,t),t) + f_2(\mathbf{X}(s,t),t)\frac{\partial}{\partial y}\psi(\mathbf{X}(s,t),t))ds\\ &\quad= \int_\Gamma \Big(\big(f_1(\mathbf{X}(s,t),t)\cos(\Theta) + f_2(\mathbf{X}(s,t),t)\sin(\Theta)\big)\frac{\partial}{\partial n}\psi(\mathbf{X}(s,t),t) +\\ &\qquad \big(f_2(\mathbf{X}(s,t),t)\cos(\Theta) - f_1(\mathbf{X}(s,t),t)\sin(\Theta)\big)\frac{\partial}{\partial\tau}\psi(\mathbf{X}(s,t),t)\Big)ds\\ &\qquad\quad= \int_\Gamma (\hat{f}_1(\mathbf{X}(s,t),t)\frac{\partial}{\partial n}\psi(\mathbf{X}(s,t),t) + \hat{f}_2(\mathbf{X}(s,t),t)\frac{\partial}{\partial\tau}\psi(\mathbf{X}(s,t),t))ds\end{aligned}$$

where $\hat{f}_1(\mathbf{X}(s,t),t)$ and $\hat{f}_2(\mathbf{X}(s,t),t)$ are correspondingly the normal and tangential components of the force density $\mathbf{f}(\mathbf{X}(s,t),t)$

$$\begin{aligned}\hat{f}_1(\mathbf{X}(s,t),t) &= f_1(\mathbf{X}(s,t),t)\cos(\Theta) + f_2(\mathbf{X}(s,t),t)\sin(\Theta)\\ \hat{f}_2(\mathbf{X}(s,t),t) &= -f_1(\mathbf{X}(s,t),t)\sin(\Theta) + f_2(\mathbf{X}(s,t),t)\cos(\Theta)\end{aligned} \quad (5.8)$$

Integrating the second term by parts and using the fact that the interface Γ is a closed curve we get

$$\int_\Gamma \hat{f}_2(\mathbf{X}(s,t),t)\frac{\partial\psi(\mathbf{X}(s,t))}{\partial\tau}ds = \hat{f}_2\psi|_{s=s_1} - \hat{f}_2\psi|_{s=s_0} - \int_\Gamma \frac{\partial\hat{f}_2(\mathbf{X}(s,t),t)}{\partial\tau}\psi(\mathbf{X}(s,t),t)ds = -\int_\Gamma \frac{\partial\hat{f}_2(\mathbf{X}(s,t),t)}{\partial\tau}\psi(\mathbf{X}(s,t),t)ds$$

Then

$$\iint_\Omega p\Delta\psi d\mathbf{x} = \int_\Gamma (\frac{\partial}{\partial\tau}\hat{f}_2(\mathbf{X}(s,t),t)\psi(\mathbf{X}(s,t),t) - \hat{f}_1(\mathbf{X}(s,t),t)\frac{\partial}{\partial n}\psi(\mathbf{X}(s,t),t))ds$$

and let

$$\begin{aligned}\hat{a}(p,\psi) &= \iint_\Omega p\Delta\psi d\mathbf{x}\\ L_{\text{disc1}}(\psi) &= \int_\Gamma \frac{\partial}{\partial\tau}\hat{f}_2(\mathbf{X}(s,t),t)\psi(\mathbf{X}(s,t),t)ds\\ L_{\text{disc2}}(\psi) &= \int_\Gamma \hat{f}_1(\mathbf{X}(s,t),t)\frac{\partial}{\partial n}\psi(\mathbf{X}(s,t),t)ds\end{aligned}$$

Then, the weak form reads: Find $p \in L^2(\Omega)$

$$\hat{a}(p,\psi) = L_{\text{disc1}}(\psi) - L_{\text{disc2}}(\psi) \quad \forall\psi \in H_0^2(\Omega)$$

Due to superposition principle we can represent the solution as

$$p = p^H + p^N + p^M \tag{5.9}$$

such that

$$\begin{aligned}\hat{a}(p^H,\psi) &= 0\\ \hat{a}(p^N,\psi) &= L_{\text{disc1}}(\psi)\\ \hat{a}(p^M,\psi) &= -L_{\text{disc2}}(\psi)\end{aligned} \tag{5.10}$$

and approximate p^N and p^M explicitly in the same fashion as it was done for the Model problem 4. Thus our weak formulation reads: Find $p^H \in H_0^1(\Omega)$

$$\hat{a}(p^H,\psi) = L_{\text{disc1}}(\psi) - L_{\text{disc2}}(\psi) - \hat{a}(p^N,\psi) - \hat{a}(p^M,\psi) \quad \forall\phi \in H_0^2(\Omega) \tag{5.11}$$

Remark 18. *Similar to the model problems, we derive the equivalent classical formulation*

$$\Delta p = 0 \quad \text{on } \Omega\backslash\Gamma \tag{5.12}$$

with some appropriate boundary conditions on $\partial\Omega$ discussed later.

The additional boundary conditions at the position of the interface Γ are given by the following theorem.

Theorem 5.2.1. *The solution to the pressure Poisson problem (5.4) satisfies the following boundary conditions at the interface Γ*

$$[p]|_\Gamma = \hat{f}_1, \quad \left[\frac{\partial p}{\partial n}\right]\Big|_\Gamma = \frac{\partial}{\partial\tau}\hat{f}_2 \tag{5.13}$$

The proof is similar to the one given in Theorem 4.2.4.

Remark 19. *The splitting (5.9) can be understood as decoupling the original problem (5.4) in three separate problems. The first one is*

$$\Delta p^H = 0 \quad \text{on } \Omega \tag{5.14}$$

the second one is given by

$$\Delta p^N = \frac{\partial\hat{f}_2}{\partial\tau}\delta_\Gamma \quad \text{on } \Omega \tag{5.15}$$

and the last one is defined as

$$\Delta p^M = \nabla \cdot (n\hat{f}_1\delta_\Gamma) \quad \text{on } \Omega \tag{5.16}$$

with the appropriate boundary conditions on $\partial\Omega$*. Here,* $\hat{f}_1$ *and* $\hat{f}_2$ *are defined in (5.8), and* s *is some parameterization parameter for the interface* Γ*. Additionally, the corresponding solutions must satisfy the following jump conditions*

$$\begin{aligned} [p^H]|_\Gamma &= 0 \quad \left[\frac{\partial p^H}{\partial n}\right]\Big|_\Gamma = 0 \\ [p^N]|_\Gamma &= 0 \quad \left[\frac{\partial p^N}{\partial n}\right]\Big|_\Gamma = \frac{\partial \hat{f}_2}{\partial \tau} \\ [p^M]|_\Gamma &= \hat{f}_1 \quad \left[\frac{\partial p^M}{\partial n}\right]\Big|_\Gamma = 0 \end{aligned} \tag{5.17}$$

Integrate by parts $\hat{a}(.,\psi)$ separately on Ω^+ and Ω^-

$$\begin{aligned} \hat{a}(p^M,\psi) &= -\iint_{\Omega\setminus\Gamma} \nabla p^M \cdot \nabla\phi d\mathbf{x} - [p^M]|_\Gamma \phi_n = -a(p^M,\phi) - L_{\text{disc2}}(\phi) \\ \hat{a}(p^N,\psi) &= -\iint_{\Omega\setminus\Gamma} \nabla p^N \cdot \nabla\phi d\mathbf{x} - [p^N]|_\Gamma \phi_n = -a(p^N,\phi) \\ \hat{a}(p^H,\psi) &= -\iint_{\Omega\setminus\Gamma} \nabla p^H \cdot \nabla\phi d\mathbf{x} - [p^H]|_\Gamma \phi_n = -a(p^H,\phi) \end{aligned} \tag{5.18}$$

where $a(p,\phi)$ is defined in (4.50) and the jumps in p^H, p^N and p^M are given by (5.17). Substitute (5.18) in (5.11) we rewrite the weak form as follows: Find $p^H \in H_0^1(\Omega)$

$$-a(p^H,\phi) = L_{\text{disc1}}(\phi) + a(p^N,\phi) + a(p^M,\phi) \quad \forall\phi \in H_0^1(\Omega) \tag{5.19}$$

as for model problem 2 and 4, we relaxed the regularity requirement on the test function ψ by applying the divergence theorem to bilinear form $\hat{a}(.,.)$ constrained to the separate regions Ω_+ and Ω_- only.

Remark 20. *Since the pressure is unique only up to a constant, it is appropriate to take Neumann boundary conditions for the pressure. After discretization, this results in a singular linear system of equations. Deflation algorithm is used to obtain the solution of such system, as described in Appendix B (see Stewart [18] for more details).*

Velocity Poisson problems

Here, we explain the solution procedure for the velocity components. Since they are almost identical we will describe only the algorithm to obtain u_1. In this case we have two sources of discontinuity: the forcing term F_1, which represents a delta functional singularity along the interface Γ and a partial derivative of the discontinuous pressure that also contains a delta functional. Both of them lead to a jump in the normal derivative of u_1.

Consider first eq. (5.1). Multiplying by a sufficiently smooth test function $\phi \in \mathcal{D}(\Omega)$ we obtain the following distributional formulation: Find $u_1 \in \mathcal{D}'(\Omega)$

$$\langle \mu\Delta u_1, \phi\rangle = \langle \partial p/\partial x, \phi\rangle - \langle f_1\delta_\Gamma, \phi\rangle \quad \forall\phi \in \mathcal{D}(\Omega) \tag{5.20}$$

integrating by parts we get

$$\mu\langle \nabla u_1, \nabla\phi\rangle = \langle p, \partial\phi/\partial x\rangle + \langle f_1\delta_\Gamma, \phi\rangle \quad \forall\phi \in \mathcal{D}(\Omega)$$

Recalling Definition 3.3.11 and Remark 6 (v) we arrive at the following: Find $u_1 \in H_0^1(\Omega)$

$$\iint_\Omega \mu \nabla u_1 \cdot \nabla \phi d\mathbf{x} = \iint_\Omega p \partial\phi/\partial x d\mathbf{x} + \int_\Gamma f_1(\mathbf{X}(s,t),t)\phi(\mathbf{X}(s,t),t)ds \quad \forall \phi \in H_0^1(\Omega) \tag{5.21}$$

Let

$$\begin{aligned} a(u_1,\phi) &= \iint_\Omega \mu \nabla u_1 \cdot \nabla \phi d\mathbf{x} \\ L_{\text{cont}}(\phi) &= \iint_\Omega p \frac{\partial \phi}{\partial x} d\mathbf{x} \\ L_{\text{disc1}}(\phi) &= \int_\Gamma f_1(\mathbf{X}(s,t),t)\phi(\mathbf{X}(s,t),t)ds \end{aligned}$$

Then, the weak form reads: Find $u_1 \in H_0^1(\Omega)$

$$a(u_1,\phi) = L_{\text{cont}}(\phi) + L_{\text{disc1}}(\phi) \quad \forall \phi \in H_0^1(\Omega)$$

By the superposition principle the solution u_1 is represented as

$$u_1 = u_1^H + u_1^N \tag{5.22}$$

such that

$$\begin{aligned} a(u_1^H,\phi) &= L_{\text{cont}}(\phi) \\ a(u_1^N,\phi) &= L_{\text{disc1}}(\phi) \end{aligned} \tag{5.23}$$

Approximate the discontinuous part of the solution u^N explicitly. Thus, we end up with: Find $u_1^H \in H_0^1(\Omega)$

$$a(u_1^H,\phi) = L_{\text{cont}}(\phi) + L_{\text{disc1}}(\phi) - a(u_1^N,\phi) \quad \forall \phi \in H_0^1(\Omega) \tag{5.24}$$

subject to appropriate boundary conditions.

Remark 21. *The following classical formulation of the problem is valid*

$$\mu \Delta u_1 = p_x \quad \text{on } \Omega \backslash \Gamma \tag{5.25}$$

with the additional boundary conditions obtained with the help of following theorem

Theorem 5.2.2. *The solution to (5.20) satisfies the following boundary conditions at the interface* Γ

$$[u_1]|_\Gamma = 0, \quad \left[\mu \frac{\partial u_1}{\partial n}\right]\Big|_\Gamma = \hat{f}_2 \sin\Theta \tag{5.26}$$

Proof. From the equivalent form (5.25) we have

$$\iint_{\Omega_\pm} \mu \Delta u_1 \phi d\mathbf{x} - \iint_{\Omega_\pm} \frac{\partial p}{\partial x} \phi d\mathbf{x} = 0 \tag{5.27}$$

Apply Greens theorem to the first term of the left hand side for each of the domains

$$\begin{aligned} \iint_{\Omega_+} \mu \Delta u_1 \phi d\mathbf{x} &= -\int_\Gamma \mu(\nabla u_1^+ \cdot n)\phi ds - \iint_{\Omega_+} \mu(\nabla u_1 \cdot \nabla \phi) d\mathbf{x} \\ \iint_{\Omega_-} \mu \Delta u_1 \phi d\mathbf{x} &= \int_\Gamma \mu(\nabla u_1^- \cdot n)\phi ds - \iint_{\Omega_-} \mu(\nabla u_1 \cdot \nabla \phi) d\mathbf{x} \end{aligned} \tag{5.28}$$

The second term of (5.27) is

$$\begin{aligned}\iint_{\Omega_+} \frac{\partial p}{\partial x}\phi d\mathbf{x} &= -\int_\Gamma \phi([p^+,0]^T\cdot n)ds + \iint_{\Omega_+}\Big[\frac{\partial \phi}{\partial x},\frac{\partial \phi}{\partial y}\Big]^T\cdot[p,0]^T d\mathbf{x}\\ \iint_{\Omega_-} \frac{\partial p}{\partial x}\phi d\mathbf{x} &= \int_\Gamma \phi([p^-,0]^T\cdot n)ds + \iint_{\Omega_-}\Big[\frac{\partial \phi}{\partial x},\frac{\partial \phi}{\partial y}\Big]^T\cdot[p,0]^T d\mathbf{x}\end{aligned} \tag{5.29}$$

Insert (5.29) and (5.28) in (5.27) to get an alternative variational formulation

$$\iint_\Omega(-\mu\nabla u_1\nabla\phi + p\frac{\partial\phi}{\partial x})d\mathbf{x} + \int_\Gamma [p]\cos(\theta)\phi ds - \int_\Gamma[\mu\frac{\partial u_1}{\partial n}]\phi ds = 0$$

Comparing this with (5.21) and using the fact that ϕ is arbitrary, we get

$$[u_1]|_\Gamma = 0 \quad \text{and} \quad \Big[\mu\frac{\partial u_1}{\partial n}\Big]\Big|_\Gamma = [p]\cos(\Theta) - f_1 = \hat{f}_2\sin\Theta$$

In the last equality we used pressure jump conditions (5.13). □

Naturally, similar results apply to the u_2 component of the velocity. For both velocity components we use homogeneous Dirichlet boundary conditions.

Remark 22. *Similar to Theorem 5.2.2, we derive the jump conditions for u_2*

$$[u_2]|_\Gamma = 0 \quad \textit{and} \quad \Big[\mu\frac{\partial u_2}{\partial n}\Big]\Big|_\Gamma = [p]\sin\Theta - f_2 = -\hat{f}_2\cos(\Theta) \tag{5.30}$$

Remark 23. *Insert (5.6) in (5.8). Then the jump conditions (5.26) and (5.30) can be expresses as*

$$\Big[\mu\frac{\partial u_1}{\partial n}\Big]\Big|_\Gamma = -\frac{\partial T}{\partial s}\sin(\Theta) \qquad \Big[\mu\frac{\partial u_2}{\partial n}\Big]\Big|_\Gamma = \frac{\partial T}{\partial s}\cos(\Theta) \tag{5.31}$$

5.3 Discrete formulation of the interface Stokes problem

In this section, we introduce our finite element method for the interface Stokes problem. Here, we use the same non-conforming finite element space (4.65) defined in Chapter 4 for the two-dimensional model problems. We also discuss the interface representation and its propagation with the flow.

Finite element formulation of the pressure Poisson equation

We represent the discrete solution (5.9) as a linear combination given by

$$p_h = p_h^H + p_h^{N,1} + p_h^{N,2} + p_h^{M,1} + p_h^{M,2} = \tilde{p}_h + p_h^{N,2} + p_h^{M,2}$$

where $\tilde{p}_h \in \mathcal{S}_0^h(\Omega)$ is given by

$$\tilde{p}_h = \sum_{i=1}^{N-1} P_i\phi_i(x)$$

with $\phi_i \in \mathcal{S}_0^h(\Omega)$ defined by (4.65). The discrete linear functions $p_h^{N,2}$ and $p_h^{M,2}$ have support only on the interface element, satisfy

$$\begin{aligned}[p_h^{N,2}]|_\Gamma = 0 \qquad & \Big[\frac{\partial p_h^{N,2}}{\partial n}\Big]\Big|_\Gamma = \partial\hat{f}_2/\partial\tau,\\ [(p_h^{M,2})_x]|_\Gamma = \hat{f}_1 \qquad & \Big[\frac{\partial p_h^{M,2}}{\partial n}\Big]\Big|_\Gamma = 0\end{aligned}$$

and are approximated as before (by solving a 6×6 system originating from (4.66) and (4.68) with the appropriate value of the jumps). Thus, we arrive at the following finite element formulation of the pressure equation: Find $\tilde{p}_h \in \mathcal{S}_0^h(\Omega)$

$$-a(\tilde{p}_h,\psi) = L_{\text{disc1}}(\psi) + a(p_h^{N,2},\psi) + a(p_h^{M,2},\psi) \quad \forall \psi \in \mathcal{S}_0^h(\Omega) \tag{5.32}$$

Finite element formulation of the velocity Poisson equation

To simplify the notation, denote the discretisation of u_1 by u_h. Then, the discrete solution is represented by a combination

$$u_h = u_h^H + u_h^{N,1} + u_h^{N,2} = \tilde{u}_h + u_h^{N,2}$$

Here $\tilde{u}_h \in \mathcal{S}_0^h(\Omega)$ is given by

$$\tilde{u}_h = \sum_{i=1}^{N-1} U_i \phi_i(x)$$

where $\phi_i \in \mathcal{S}_0^h(\Omega)$ defined by (4.65). The discrete linear function $u_h^{N,2}$ is defined only on the interface element and satisfies

$$[u_h^{N,2}]|_\Gamma = 0 \qquad \Big[\frac{\partial u_h^{N,2}}{\partial n}\Big]\Big|_\Gamma = \hat{f}_2 \sin\Theta$$

We compute $u_h^{N,2}$ by solving a 6×6 system originating from (4.66) with the appropriate value of the jump in the normal derivative of $u_h^{N,2}$. Consequently, we arrive at the following finite element formulation: Find $\tilde{u}_h \in \mathcal{S}_0^h(\Omega)$

$$-a(\tilde{u}_h,\psi) = L_{\text{cont}}(\psi) + L_{\text{disc1}}(\psi) + a(u_h^{N,2},\psi) + a(u_h^{M,2},\psi) \quad \forall \psi \in \mathcal{S}_0^h(\Omega) \tag{5.33}$$

The interface propagation

At any moment in time t_n, the interface is described by a given finite set of control points $\{X_k^n, Y_k^n\}$ for $k = 0, 1, .., N_{\text{Int}}$ and some parametrisation through these points. Here, kth control point gives an approximation to $(X(s_k,t_n), Y(s_k,t_n))$ where s is an arclength parametrisation of the interface. To reconstruct the interface between the control points, we compute piecewise linear interpolants $X^n(s)$ and $Y^n(s)$.

To calculate the force acting along the interface, we first compute $\partial\mathbf{X}/\partial s$ in every control point and hence the tension $T(s,t^n)$. By multiplying the tension with the tangent vector and differentiating again, we obtain an approximation to the force densities (5.6). These densities are then spread all along the interface by constructing another linear interpolant $\mathbf{f}^n(s)$.

To evolve the interface we chose to use the simplest explicit method, namely, the forward Euler scheme

$$X_k^{n+1} = X_k^n + \Delta t U_k^n$$
$$Y_k^{n+1} = Y_k^n + \Delta t V_k^n$$

where the local velocities $\{U_k^n, V_k^n\}$ are obtained by interpolating the velocity field $\{u_1^n, u_2^n\}$ at the control points $\{X_k^n, Y_k^n\}$. This interpolation is complicated by the fact that the velocity field $\{u_1^n, u_2^n\}$ has jumps in the normal derivatives across the interface. Thus the usual bilinear interpolation scheme cannot be applied in this case. A modified interpolation

scheme is required such that the jump conditions for velocity field (5.26) and (5.30) are accounted for. There are different ways to do that. We follow an idea of LeVeque and Li [32] where they used a modified linear interpolation based on three nearby points such that the jump conditions are incorporated.

To obtain local velocities $\{U_k^n, V_k^n\}$ at control point $\{X_k^n, Y_k^n\}$ choose the three closest grid points (x_1, y_1), (x_2, y_2) and (x_3, y_3) (which will typically be the nodes of the triangular element containing the control point $\{X_k^n, Y_k^n\}$). Form a linear combination of these values to obtain, say U_k^n

$$U_k^n = \gamma_1 u(x_1, y_1) + \gamma_2 u(x_2, y_2) + \gamma_3 u(x_3, y_3) + C \tag{5.34}$$

where $u(x_i, y_i)$ is the grid velocity corresponding to the point (x_i, y_i). The coefficients γ_i and the correction term C are chosen such that a second order approximation is achieved. Use Taylor approximation around $\{X_k^n, Y_k^n\}$ to get the values of γ_i's and C

$$u(x_i, y_i) = u^{\pm} + (x_i - X_k^n)u_x^{\pm} + (y_i - Y_k^n)u_y^{\pm} + O(h^2)$$

where h is the stepsize and $+$ or $-$ sign indicates whether we approach $\{X_k^n, Y_k^n\}$ from inside or outside of the interface Γ. Insert this Taylor expansion in eq. (5.34) we get

$$\begin{aligned} U_k^n &= a_1 u^- + a_2 u^+ + a_3 u_x^- + a_4 u_x^+ + a_5 u_y^- + a_6 u_y^+ + C + O(h^2) \\ &= (a_1 + a_2)u^- + (a_3 + a_4)u_x^- + (a_5 + a_6)u_y^- + (a_2[u] + a_4[u_x] + a_6[u_y]) + C + O(h^2) \end{aligned}$$

where the jump condition for $[u_x]$ and $[u_y]$ are obtained from (5.26), $[u] = 0$ since the velocities are continuous across the interface and a_i's are the linear combination of the γ_i's such that

$$\begin{aligned} a_1 &= \sum_{i \in K^-} \gamma_i & a_2 &= \sum_{i \in K^+} \gamma_i \\ a_3 &= \sum_{i \in K^-} (x_i - X_k^n)\gamma_i & a_4 &= \sum_{i \in K^+} (x_i - X_k^n)\gamma_i \\ a_5 &= \sum_{i \in K^-} (y_i - Y_k^n)\gamma_i & a_6 &= \sum_{i \in K^+} (y_i - Y_k^n)\gamma_i \end{aligned}$$

with the index sets $K^{\pm}$ defined as

$$K^{\pm} = \{i : (x_i, y_i) \text{ is on the } \pm \text{ side of the interface } \Gamma\}$$

Finally, we desire

$$\begin{aligned} a_1 + a_2 &= 1 \\ a_3 + a_4 &= 0 \\ a_5 + a_6 &= 0 \end{aligned}$$

Solving this system of linear equations we obtain the expression for the γ_i's

$$\begin{aligned} \gamma_1 &= 1 - \gamma_2 - \gamma_3 \\ \gamma_2 &= \frac{(y_1 - Y_k^n)(x_3 - x_1) - (x_1 - X_k^n)(y_3 - y_1)}{(x_2 - x_1)(y_3 - y_1) - (x_3 - x_2)(y_2 - y_1)} \\ \gamma_3 &= \frac{(y_2 - y_1)(x_1 - X_k^n) - (x_2 - x_1)(y_1 - Y_k^n)}{(x_2 - x_1)(y_3 - y_1) - (x_3 - x_2)(y_2 - y_1)} \end{aligned}$$

while the correction term C is given by

$$C = -(a_4[u_x] + a_6[u_y])$$

The same coefficients are used to compute U_k^n but the correction term will be based on $[v_x]$ and $[v_y]$ instead.

To review, the numerical solution of the interface Stokes problem is obtained by the following procedure:

- Use the location of the interface given by the set of the control points $\{X_k^n, Y_k^n\}$ to compute the forces (5.6) and jump conditions (5.26), (5.30) and (5.13).
- Obtain the background grid velocities u_1 and u_2 by solving three Poisson problem with the known jump conditions.
- Interpolate u_1 and u_2 to compute the local velocities $\{U_k^n, V_k^n\}$ at every control point $\{X_k^n, Y_k^n\}$.
- Advect the interface with these velocities for time Δt.

The procedure is repeated for every time step Δt. This concludes our description of the finite element IIM for the Stokes interface problem.

5.4 Numerical Results

In this section we present the numerical solution of the interface Stokes problem obtained with our approach. The test problem modeling an elastic band immersed in a fluid was described earlier in this Chapter. The computational domain Ω is the rectangle $-1 \leq x, y \leq 1$ and the interface Γ is represented by a closed curve that is, initially, an ellipse with the major and minor axis $a = 0.75$ and $b = 0.5$, respectively.

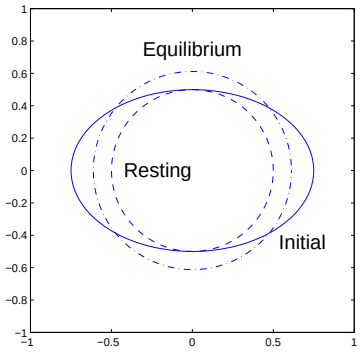

Figure 5.1: Different configuration of the interface. Here, the solid line represents the initial position, the resting configuarion is the the dashed circle and the equilibrium configuration is depicted by dash-dot circle.

Due to the restoration force, that is applied only along the interface, the ellipse will converge to the equilibrium position, that is a circle with radius $r_e = \sqrt{ab} \approx 0.61237$,

[32]. Note, that the equilibrium radius r_e is larger than the resting radius r_0 due to the incompressibility of the encircled fluid. Thus, in the equilibrium position, the interface is still stretched, with the pressure balancing the non-zero boundary force. The solution is approximated on the uniform $n \times n$ Cartesian mesh with m discrete points, representing the interface Γ. Since the exact solution is unknown we measure the accuracy of our method by using the extrapolation principle. That is, we investigate the error between two successive solutions $e = u_n - u_{2n}$ for every resolution n. To measure the error we employ the discrete L^∞ and the L^2 norms defined by

$$||E_n||_{L^\infty} = \max_{i,j}\{|e_{ij}|\} \quad \text{and} \quad ||E_n||_{L^2} = h\sqrt{\sum_{i,j} e_{ij}^2}$$

We also display the ratios between the successive errors

$$ratio = ||E_n||_{L^\infty}/||E_{2n}||_{L^\infty}, \quad \text{or} \quad ||E_n||_{L^2}/||E_{2n}||_{L^2}$$

As usual, a ratio of 2 corresponds to first order accuracy, while a ratio of 4 indicates second order of accuracy.

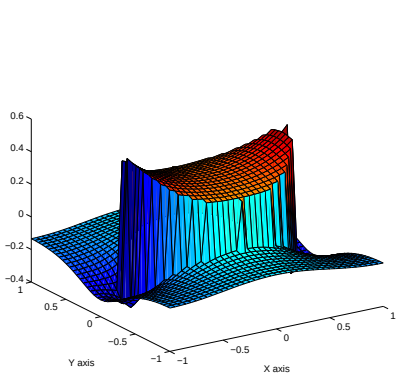

(a) Pressure is discontinuous across the interface at $t = 0$.

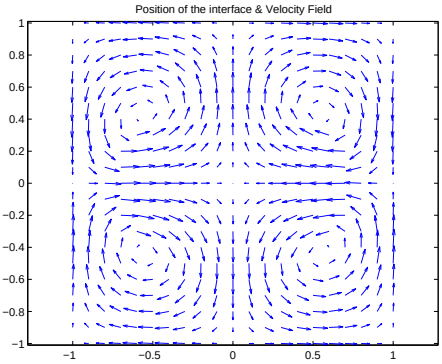

(b) The the velocity field at $t = 0$.

Figure 5.2: The solution to the Stokes interface problem at $t = 0$.

First, we compute the solution at $t = 0$, when the interface has not moved. Pressure p and one of the velocity field are shown in Figure 5.2. As expected, the pressure is discontinuous and the flow goes from the regions with high pressure to the regions with low pressure. In Figure 5.3 we present cross sections of p and u_1 at $t = 0$.

To explain the smooth behavior of the the normal derivative of u_1 in Figure 5.3 we recall Remark 23 which states that the magnitude of the jump in the normal derivative of u_1 is proportional to the change in the tension T which does not vary a lot along the band in our model.

Next, a grid refinement study is performed to measure the order of accuracy of our method. The solution (p, u_1 and u_2) was computed on four different $n \times n$ grids with $n = 40$, 80, 160 and 320 and $m = 400$ points on the interface.

Tables (5.4) and (5.4) shows the ratios in both norms to be around 4 which is a clear indication of second order accuracy.

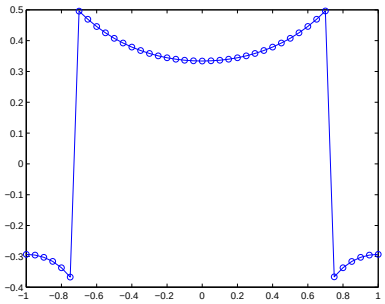

(a) A cross section of the pressure at $t = 0$ and $y = 0$. Note, that there is no smoothing of the pressure. The jump is captured sharply.

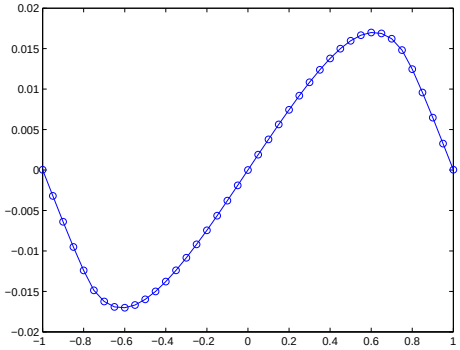

(b) A cross section ($y = 0$) of the u_1 velocity component at $t = 0$.

Figure 5.3: The cross section of the pressure and u_1 velocity at $t = 0$.

n	p ratio in L^∞ norm	u_1 ratio in L^∞ norm
40	3.2821	3.9166
80	3.4858	4.0552

Table 5.1: The ratio in the error between the successive solutions, i.e. $e = p_n - p_{2n}$ and $e = u_n - u_{2n}$ at $t = 0$ in L^∞ norm.

n	p ratio in L^2 norm	u_1 ratio in L^2 norm
40	3.9903	4.2687
80	4.0112	4.1602

Table 5.2: The ratio in the error between the successive solutions, i.e. $e = p_n - p_{2n}$ and $e = u_n - u_{2n}$ at $t = 0$ in L^2 norm.

We now consider the error at later times, when the interface has moved. The main difficulty in comparing the solution at all the points on the fixed grid comes from the fact that the interface may lie on one side of certain fixed grid point in one calculation, but slightly to the other side in a different calculation.

Since the area enclosed by the interface should be conserved we can use the mass conservation as a measure of the convergence of our method. Namely, for the fixed values of the time step $\Delta t = 0.01$ and the background grid $n = 80$, we refine the resolution of the interface m and consider the error

$$E_m = A_0 - A_m$$

where $A_0 = \pi ab$ is the initial area of the ellipse and A_m is the area at some moment in time $t = T$ with m points on the interface.

m	$\lvert E_m\rvert$ at $t = 0.1$	ratio	$\lvert E_m\rvert$ at $t = 1.0$	ratio
20	0.0192513	-	0.0189312	-
40	0.0048583	3.9626	0.0050331	3.7613
80	0.0012161	3.9950	0.0012407	4.0567
160	0.0003032	4.0109	0.0003061	4.0533

Table 5.3: Grid refinement study for the Stokes interface problem with $\Delta t = 0.01$ on the 80×80 mesh. The columns represent the error in the area at t=0.1 and t=1, correspondingly.

Table 5.3 shows the refinement study for $T = 0.1$ and $T = 1$. As we can see, the area is preserved with second-order accuracy using IIM FEM.

We also consider the behavior of IIM FEM over longer period of time. Define the smallest and the greatest distances from the origin to the interface at time t^n, r^n_{min} and r^n_{max} respectively

$$r^n_{min} = \min_{1\le k\le N_{int}} \sqrt{(X^n_k)^2 + (Y^n_k)^2} \qquad r^n_{max} = \max_{1\le k\le N_{int}} \sqrt{(X^n_k)^2 + (Y^n_k)^2}$$

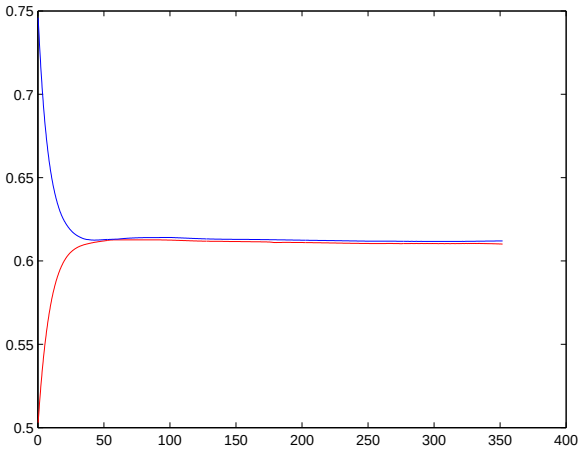

Figure 5.4: The plot shows the behavior of r^n_{max} (upper curve) and r^n_{min} (lower curve) with time. Clearly they converge towards the equilibrium radius r_e. This results are obtained with the 100×100 mesh with 100 points on the interface and $\Delta t = 0.25$.

As we can see from Figure 5.4 both distances converge towards the equilibrium radius r_e. This is the expected behavior since the interface should eventually obtain the equilibrium circular shape with radius r_e and thus we expect $r^n_{min} \to r_e$ and $r^n_{min} \to r_e$ as $n \to \infty$. Similar behavior was shown in [32] and [9]. Figure 5.5 shows the error in the area.

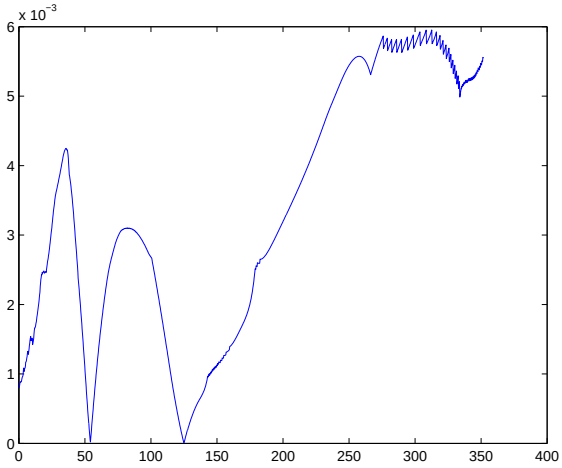

Figure 5.5: The error in the mass conservation. This results are obtained with the 100×100 mesh with 100 points on the interface and $\Delta t = 0.25$.

Chapter 6

Conclusions and future work

In this thesis, we have presented a new finite element based method for the solution of the one and two-dimensional elliptic interface problems. The advantages of using distributions in terms of treatment of the singular forces and discontinuous coefficients have been pointed out. The use of distributions leads naturally to the weak form of the equations. This fact together with the thorough theoretical basis have motivated our choice of using the finite element method for the discretization of the problems.

The interface jump conditions associated with the discontinuities in the coefficients and singularities of the forces have been derived and used to appropriately modify the basis functions such that the jump conditions are satisfied either exactly or approximately. This modification of the basis function resulted in a non-conforming finite element space whose approximation capabilities were numerically studied.

The numerical experiments have been made to confirm that the modified approach can handle well both one and two-dimensional elliptic problems with severe discontinuities in the coefficients and singularities represented by the delta functional and its derivatives. For the considered test problems our approach proved to be superior to the standard finite element method and exhibited second order convergence in the L^2 norm. In addition, we should remind that all the results are obtained on the grids that are not aligned with the interface. That allows us to to avoid the difficulties and additional time consumption associated with the generation of the body fitted meshes for the interface problems. This property of our method is even more desirable for the moving interface problems where the body fitted grid has to be generated at each time step.

As an example of the moving interface problem, we considered an incompressible Stokes flow with the immersed elastic boundary. The numerical results obtained with our method show good agreement with the results found in the literature. In addition, our approach provides very good mass conservation. We should also note that, using the proposed method, we can handle much more severe singularities that those appearing in the Stokes problem. Although we have presented our method mainly in the context of two dimensional problems, the ideas extend to the three space dimensions as well.

Future work points in several directions from the current stand. One is the theoretical investigation of the introduced non-conforming finite element method. The other is the extension and improvement of the method itself. Finally, it is intriguing to apply our method to some more realistic applications.

The thorough theoretical investigation of the approximation capabilities of the introduced non-conforming finite element method can help us to improve the performance of our approach. In addition, a rigorous investigation of the interplay between the approximation

of the flow and the interface should be done. The primary focus for the extension of the method should be the incorporation of the density and viscosity jumps in the interface Stokes flows, such that more realistic interface fluid models can be considered. That should not be a problem since similar elliptic model problems have already been considered in this thesis. An improved approximation of the interface should be added as well. It might be also interesting to couple our approach with some different interface representation techniques, for example a level-set method.

Chapter 7

Appendix

Appendix A

In this appendix we present the exact solution for the test problem 1 from Chapter 4. Consider

$$\beta u_{xx} + ku = 1 + \delta_\alpha$$
$$u(0) = u(\pi/(2\gamma_+) = 0$$

with $x \in [0, \pi/(2\gamma_+)]$, $k = 1$, $\alpha = \pi/(6\gamma_+)$ and

$$\beta(x) = \begin{cases} \beta_-, & \text{if} \quad x \geq \alpha \\ \beta_+, & \text{if} \quad x < \alpha \end{cases}$$

where $\gamma_+ = \sqrt{k/\beta_+}$ and $\gamma_- = \sqrt{k/\beta_-}$. The exact solution in this case is

$$u(x) = \begin{cases} C_1 \cos(x\gamma_-) + C_2 \sin(x\gamma_-) + 1/k, & \text{if} \quad 0 \leq x < \alpha \\ C_3 \cos(x\gamma_+) + C_4 \sin(x\gamma_+) + 1/k, & \text{if} \quad \alpha \leq x \leq \pi/(2\gamma_+). \end{cases}$$

where

$$C_1 = C_4 = -1/k,$$
$$C_3 = \frac{(\sin(\gamma_+) - \cos(\gamma_-))/k + C_2 \sin(\gamma_-))}{\cos(\gamma_+)}$$
$$C_4 = \frac{1 + \sqrt{\beta_+/k}(\cos(\gamma_+) + (\sin(\gamma_+) - \cos(\gamma_-)) \tan(\gamma_+)) + \sqrt{\beta_-/k} \sin(\gamma_-)}{\sqrt{k\beta_-} \cos(\gamma_-) + \sqrt{k\beta_+} \sin(\gamma_-) \tan(\gamma_+)}$$

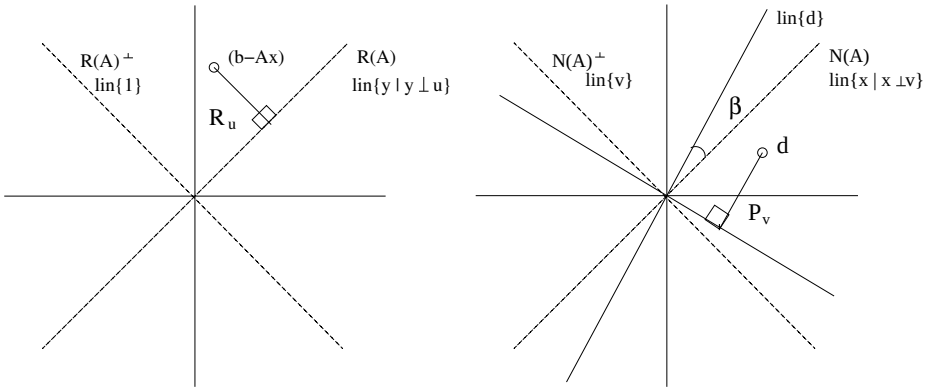

(a) STEP1 (b) STEP3

Figure 7.1: Projection method

Appendix B

Model problems 2 and 4 lead to the standard Neumann problems whose discretisation yields the linear system

$$Ax = b$$

with one-dimensional null-space of the system matrix A. In order to solve this discrete system we apply an approach proposed by Stewart in [9]. Let u and v be left and right null vectors of A (i.e. $u^T A = Av = 0$) and assume that $\|v\| = \|u\| = 1$. Define orthogonal projections $P_u := I - uu^T$, $P_v := I - vv^T$ such that P_u projects onto $\mathcal{R}(A)$ and P_v onto $\mathcal{R}(A^T)$. The solution x is the unique vector satisfying

$$\begin{aligned} P_u A P_v x &= P_u b \\ P_v x &= x \end{aligned} \tag{7.1}$$

Equivalently, we obtain the solution through the following iterative procedure

Algorithm Let x_0 be given with $P_v x_0 = x_0$

Step 1. $r = P_u(b - Ax_i)$

Step 2. $d = A^{-1}r$

Step 3. $x_{i+1} = x_i + P_v d$

There are two factors affecting the performance: the errors made in calculating the residual $(b - Ax)$ and the errors done in solving the almost singular system $Ad = r$. By use of P_u (Fig. 7.1(a)) and P_v (Fig. 7.1(b)) we are projecting out the roundoff errors, which are due to the matrix singularity. At this point several remarks should be made:

Remark 24.

- *Under reasonable conditions, few iterations should be sufficient [**9**].*
- *For a given vector y, the product $P_v y$ can be computed as follows:*

$$P_v y = (I - vv^T)y = y - v(v^T y) = y - \gamma V$$

where $\gamma = v^T y = (v, y)$ is an Euclidean scalar product.

- *The left and right null vectors are obtained by a variant of the inverse power method*
  - $A\hat{v}_{i+1} = u_i$
  - $v_{i+1} = \hat{v}_{i+1}/\|\hat{v}_{i+1}\|$
  - $A\hat{u}_{i+1} = v_i$
  - $u_{i+1} = \hat{u}_{i+1}/\|\hat{u}_{i+1}\|$
- *The angle β , between null-space of A and the space spanned by vectors d (Fig. 7.1(b)), is the measure of how much the error will be projected out. Thus the closer β is to 0^o the better is the expected performance. When β is close to 90^o the performance is the worst.*

Bibliography

[1] S.Manservisi A.Aulisa and R. Scardovelli. A mixed markers and volume-of-fluid method for reconstruction and advection of interfaces in two-phase and free-boundary flows. *J.Comput.Phys.*, 188:611–639, 2003.

[2] A.L.Fogelson and J.P.Keener. Immersed interface methods for neumann and related problems in two and three dimensions. *SIAM J.Sci.Comput.*, 22:1630–1654, 2000.

[3] A.M.Roma. A multilevel self adaptive version of the immersed boundary method. *PhD thesis, New York University*, 1996.

[4] A.Wiegmann and K.P.Bube. The immersed interface method for nonlinear differential equations with discontinuous coefficients and singular forces. *SIAM J.Numer. Anal.*, 35(1):177–200, 1998.

[5] B.D.Nichols and C.W.Hirt. Methods for calculating multidimensional, transient free surface flows past bodies. *Proc.First Intern.Conf.Num.Ship Hydrodynamics, Gaithersburg,ML*, 1975.

[6] C.Pozrikidis. Interfacial dynamics for stokes flow. *J.Comput. Phys.*, 169:250–301, 2001.

[7] C.S.Peskin. The immersed boundary method. *Acta Numerica*, pages 1–39, 2002.

[8] C.S.Peskin and D.M.McQueen. Modelling prosthetic heart valves for numerical analysis of blood in the heart. *J.Comput.Phys.*, 37:113–132, 1980.

[9] C.Tu and C.S.Peskin. Stability and instability in the computation of flows with moving immersed boundaries: a comparison of three methods. *SIAM J.Sci. Stat. Comput.*, 13:1361–1376, 1992.

[10] C.W.Hirt and B.D.Nichols. Volume of fluid (vof) method for the dynamics of free boundaries. *J.Comput. VOLUME=*.

[11] C.Zhang. Immersed interface method for hyperbolic systems of partial differential equations with discontinuous coefficients. *PhD thesis, University of Washington*, 1996.

[12] D.Calhoun. A cartesian grid method for solving the stream function vorticity equations in irregular geometries. *PhD thesis, University of Washington*, 1999.

[13] J.Fetziger D.Enright, R.Fedkiw and I.Mitchell. A hybrid particle level set method for improved interface capturing. *J.Comput.Phys.*, 183:83–116, 2002.

[14] D.H.Griffel. Applied functional analysis. *Ellis Horwood Limited*, 1981.

[15] G.B.McFadden D.M.Anderson and A.A.Wheelr. Diffuse-interface methods in fluid mechanics. *Ann.Rev.Fluid Mech.*, 30:139–165, 1998.

[16] F.H.Harlow and J.E.Welch. The mac method: a computing technique for solving viscous, incompressible, transient fluid flow problems involving free surface. *J.Phys. Fluids*, 8:2182–2189, 1965.

[17] A.Esmaeeli D.Juric-N.Al-Rawahi W.Tauber J.Han S.Nas G.Tryggvason, B.Bunner and Y.-J. Jan. A front-tracking method for the computations of multiphase flow. *J.Comput.Phys.*, 169:708–759, 2001.

[18] G.W.Stewart. On the implicit deflation of nearly singular systems of linear equations. *SIAM J.Sci. Stat. Comput.*, 2:136–140, 1981.

[19] H.Huang and Z.Li. Convergence analysis of the immersed interface method. *SIAM J.Numer. Anal.*, 19:583–608, 1999.

[20] I.Stakgold. Green's functions and boundary value problems. *Willey*, 1979.

[21] J.Bramble and J.King. A finite element method for interface problems in domains with smooth boundaries and interfaces. *Advances in Comput. Math.*, 6:109–138, 1996.

[22] J.Chorin. Numerical solution of the navier-stokes equations. *Math. Comput.*, 22:745–762, 1968.

[23] X.L.Li K.-M.Shyue-Q.Zhang J.Glimm, J.W.Grove and Y.Zeng. Three-dimensional front tracking. *SIAM J.Sci.Comput*, 19:703–727, 1998.

[24] L.M.Adams. A multigrid algorithm for immersed interface problems. *Technical report 95-02, Department of Applied Mathematics, University of Washington*, 1995.

[25] J.S. Lowengrub and L. Truskinovky. Quasi-incompressible cahn-hilliard fluids and topological transitions. *Prov.R.Soc.Lond*, A 454:2617–2654, 1998.

[26] L.Rosehead. The formation of vortices from a surface of discontinuity. *Proc.R.Soc.Lond.*, A 134:170–192, 1932.

[27] M.Sussman. A second order coupled level-set and volume-of-fluid method for computing growth and collapse of vapor bubbles. *J.Comput.Phys.*, 187:110–136, 2003.

[28] M.Sussman and G.E.Puckett. A coupled level set and volume-of-fluid method for computing 3d and axisymmetric incompressible two-phase flows. *J.Comput.Phys.*, 162:301–337, 2000.

[29] P.Smereka M.Sussman and S.Osher. A level set approach for computing solutions to incompressible two-phase flow. *J.Comput.Phys.*, 114:146–159, 1994.

[30] R.D.Richtmyer and K.M.Morton. Difference methods for initial-value problems. *Interscience, New York*, 1967.

[31] R.J.LeVeque and Z.Li. The immersed interface method for elliptic equations with discontinous coefficients and singular sources. *SIAM J.Numer. Anal.*, 31:1019–1044, 1994.

[32] R.J.LeVeque and Z.Li. Immersed interface method for stokes flow with elastic boundaries or surface tension. *SIAM J. Sci Comput.*, 18:709–735, 1997.

[33] R.LeVeque and C.Zhang. The immersed interface method for acoustic wave equations with discontineous coefficients. *Wave Motion*, 25(3):237–263, 1997.

[34] R.LeVeque and D.Calhoun. A cartesian grid finite-volume method for the advection diffusion equation in irregular geometries. *Submitted to JCP*, 1998.

[35] R.P.Beyer and R.J.LeVeque. Analysis of a one-dimensional model for the immersed boundary method. *SIAM J.Numer. Anal.*, 29:332–364, 1992.

[36] R.Scardovelli and S.Zaleski. Direct numerical simulation of free-surface and interfacial flow. *Annu. Rev. Fluid Mech*, 31:567–603, 1999.

[37] S.J.Osher and J.A.Sethian. Fronts propagating with curvature dependent speed: algorithms based on hamilton-jacobi formulations. *J.Comput.Phys.*, 79:12–49, 1988.

[38] S.O.Unverdi and G.Tryggvason. A front tracking method for viscous, incompressible, multi-fluid flows. *J.Comput.Phys.*, 100:25–37, 1992.

[39] H.Zhao T.Y.Hou, Z.Li and S.Osher. A hybrid method for moving interface problems with application to hele-shaw flow. *J. Comput. Phys.*, 134(2):1997, 236-252.

[40] J.S.Lowengrub T.Y.Hou and M.J.Shelley. Boundary integral methods for multicomponent fluids and multiphase materials. *J.Comput.Phys.*, 169:302–362, 2001.

[41] B.Merriman Y.C.Chang, T.Y.Hou and S.Osher. A level set formulation of eulerian interface capturing methods for incompressible fluid flows. *J.Comput.Phys.*, 124:449–464, 1996.

[42] Z.Chen and J.Zou. Finite element methods and their convergence for elliptic and parabolic interface problems. *Numer. Math.*, 79:175–202, 1998.

[43] Z.Li. The immersed interface method - a numerical approach to partial differential equations with interfaces. *PhD thesis, University of Washington*, 1994.

[44] Z.Li. Immersed interface method for moving interface problems. *Numerical Algorithms*, 14(4):269–293, 1997.

[45] Z.Li. A fast iterative algorithm for elliptic interface problems. *SIAM J.Numer. Anal.*, 35(1):230–254, 1998.

[46] Z.Li. The immersed interface method using a finite element formulation. *Appl. Num. Math.*, 27:253–267, 1998.

[47] Z.Li and B.Soni. Fast and accurate numerical approaches for stefan problems and crystal growth. *Numerical Heat Transfer*, 1999.

[48] Z.Li and K.Ito. Maximum principle preserving schemes for interface problems with discontinuous coefficients. *SIAM J.Sci.Comput.*, 23:1225–1242, 2001.

[49] H.Zhao Z.Li and H.Gao. A numerical study of electron-migration voiding by evolving level set function on a fixed cartesian grid. *J. Comput. Phys.*, 152 (1):281–304, 1999.

[50] T.Lin Z.Li and X.Wu. New cartesian grid methods for interface problems using finite element formulation. *NSCU CRSC-TR99-5*, 1999.